
Thomas Schietinger

Regeneration of Neutral K Mesons in
Carbon at Energies Below 1 GeV

BASEL, JUNE 1998

**Regeneration neutraler K Mesonen in Kohlenstoff bei Energien von
weniger als 1 GeV**

(Regeneration of Neutral K Mesons in Carbon at Energies Below 1 GeV)

Inauguraldissertation

zur
Erlangung der Würde eines Doktors der Philosophie
vorgelegt der
Philosophisch-Naturwissenschaftlichen Fakultät
der Universität Basel
von

Thomas Schietinger

aus Basel

Basel, Juni 1998

Genehmigt von der Philosophisch-Naturwissenschaftlichen Fakultät auf Antrag von
Herrn Professor Dr. Ludwig Tauscher und von Herrn Privatdozent Dr. René Rickenbach.

Basel, den 30. Juni 1998

Prof. Dr. Thomas A. Bickle
Dekan

Thou, nature, art my goddess; to thy law
My services are bound.

William Shakespeare, *King Lear*

CONTENTS

1	Introduction	3
1.1	<i>Symmetries in physics</i>	3
1.2	<i>The strange world of (neutral) kaons</i>	4
1.3	<i>CPLEAR and regeneration</i>	4
1.4	<i>Thesis outline</i>	5
2	The neutral kaon system	6
2.1	<i>The effective Hamiltonian</i>	6
2.2	<i>CP violation</i>	9
2.2.1	CP violation in the mixing	10
2.2.2	CP violation in the decay (“direct” CP violation)	10
2.2.3	CP violation in the interference between mixing and decay	11
2.3	<i>CPT violation</i>	11
3	Regeneration of neutral kaons	13
3.1	<i>Types of regeneration</i>	13
3.2	<i>Coherent (transmission) regeneration</i>	14
3.2.1	Coherent scattering and complex index of refraction	15
3.2.2	The effective Hamiltonian in matter and the regeneration parameter	16
3.2.3	Time development of a general state in matter	18
3.2.4	Two pion decay after penetration of a regenerator	19
3.3	<i>Incoherent regeneration</i>	21
3.3.1	Phenomenology	22
3.3.2	Contribution to the measured two pion decay rate	22
3.3.3	Numerical computation for $\pi^+\pi^-$ decays at CPLEAR	24
4	The CPLEAR experiment	26
4.1	<i>Low energy antiprotons at CERN</i>	26
4.2	<i>The CPLEAR detector</i>	26
4.2.1	The beam-target system	27
4.2.2	The tracking detectors	27
4.2.3	The particle identification detector	27
4.2.4	The electromagnetic calorimeter	29
4.2.5	The magnet	29
4.2.6	The trigger system	29
4.2.7	Data acquisition	30
4.2.8	Event display	30
4.3	<i>Regeneration effects and their correction</i>	30
5	The CPLEAR regeneration experiment	33
5.1	<i>Design and installation of the regenerator</i>	33
5.2	<i>The carbon regenerator</i>	34
5.3	<i>Measurement of the regenerator position</i>	35
5.3.1	Surveyor measurement	35
5.3.2	Photon conversion analysis	37
5.3.3	Comparison and final values	38
5.4	<i>Further utilization of the regenerator</i>	39
6	The regeneration measurement	40
6.1	<i>Overview of the method</i>	40
6.1.1	Decay rate asymmetry in vacuum	40
6.1.2	Decay rate asymmetry in the presence of a regenerator	40
6.1.3	Comparison of the two asymmetries	40
6.2	<i>Data selection</i>	41
6.2.1	Offline selection of “golden events”	41

6.2.2	Selection of four track events	41
6.2.3	Filtering of $\pi^+\pi^-$ decays	41
6.2.4	Micro data summary tapes for $\pi^+\pi^-$ events	42
6.2.5	Selection of regeneration events	42
6.3	<i>Determination of the regeneration amplitudes</i>	43
6.4	<i>Systematic uncertainties</i>	44
6.4.1	K^0/\bar{K}^0 rate normalization	44
6.4.2	Regenerator position	44
6.4.3	Compatibility of the two data sets	44
6.4.4	Incoherent regeneration	46
6.4.5	Limitations of the asymmetry method	46
6.4.6	Further consistency checks	47
6.5	<i>Additional constraints on $Im \Delta f$ from other experiments</i>	47
6.6	<i>Final results</i>	47
6.7	<i>Application to the measurement of η_{+-}</i>	47
7	A dispersion relation analysis of the regeneration amplitude	51
7.1	<i>Selection and treatment of data</i>	51
7.2	<i>The dispersion relation and its parameterization</i>	52
7.3	<i>Fit results and discussion</i>	53
7.4	<i>Determining the regeneration phase from a dispersion relation: the example of E731/E773</i> .	55
8	Summary and conclusion	57
A	Phase conventions in the neutral kaon system	58
	References	60
	Acknowledgements	63
	Curriculum vitae	64
	Zusammenfassung	64

1 INTRODUCTION

The subject of this thesis is a measurement of the difference of the forward scattering amplitudes of K^0 and \bar{K}^0 , also called regeneration amplitude, in carbon at laboratory momenta between 250 and 750 MeV/c. I could not blame anyone for asking whether the knowledge of these amplitudes is a blessing for the human race and therefore I deem a few words of introduction appropriate.

In this Section I briefly explain how our measurement of scattering amplitudes helps us improve our measurement of the violation of so-called CP symmetry, a mysterious phenomenon which is probably related to the imbalance of matter and antimatter in the universe. Thus the study of CP violation, to which this work represents an important albeit small contribution, may bring us closer to understanding why at all there are stars, planets and human beings crawling on them. I cannot think of a greater incentive!

1.1 Symmetries in physics

Symmetry has always inspired humanity: from Egyptian pyramids to modern skyscrapers, symmetry represents harmony and perfection. Moreover, it simplifies planning and construction. In physics, the beauty and usefulness of symmetries was not immediately realized: the differential equations of Newton and Maxwell favoured an analytical approach rather than an algebraic. It was not before the revolutions of relativity and quantum mechanics that the concept of symmetry became the backbone of theoretical physics. At the end of the 20th century, symmetries are still the guiding principle in physics and the 21st may well see the discovery of a new fundamental symmetry of nature, so-called supersymmetry relating bosons and fermions.

A physical system is said to have a symmetry if the underlying equations are invariant under a transformation. Such a transformation may depend continuously on some parameters, for instance displacement vector and rotation angles for the well known examples of space translations and rotations. A fundamental theorem due to Emmy Noether assigns an additive conserved quantity to each continuous symmetry. In our examples, these are linear and angular momentum, respectively. The transformation defining the symmetry may also be discrete, in which case there are only a finite (or denumerably infinite) number of different ways to carry out the symmetry operation. Examples of discrete transformations are permutations or spatial reflections. Discrete symmetries are associated with multiplicative conserved quantities.

Three discrete symmetry transformations play a central role in particle physics and are intimately connected by an important theorem:

1. **Charge conjugation (C):** transforms particles into their anti-particles, for instance $e^- \rightarrow e^+$, $p \rightarrow \bar{p}$, $K^0 \rightarrow \bar{K}^0$, etc. Thus positive charges—electrical or generalized ones like flavour, baryon number, etc.—become negative and vice versa. The corresponding conserved quantity is called C-parity.
2. **Parity inversion (P):** the reflection of space coordinates at the origin, $(x, y, z) \rightarrow (-x, -y, -z)$. Common mirror reflections are combinations of a parity inversion and a rotation. The parity operator changes the “handedness” (chirality) of objects: left-handed is transformed into right-handed and vice versa. “Parity” is also the name of the associated conserved quantum number.
3. **Time reversal (T):** the analogous reflection of the time coordinate: $t \rightarrow -t$. After time reversal, physical processes proceed backwards in time like in a film that is run backwards from the end to the beginning. T is a special case in so far as it is not a unitary operator (it is anti-unitary) and therefore can never commute with the Hamiltonian. For this reason it is not possible to assign a conserved quantum number, there is no such thing as “T-parity”!

The fundamental interactions behave differently under these symmetry operations: in the domains of the electromagnetic and the strong interactions C, P, and T are (according to the current experimental status) exact symmetries, whereas the weak force maximally violates C and P, a fact that is demonstrated most dramatically through the non-existence of neither right-handed neutrinos nor left-handed anti-neutrinos. Violation of the product symmetry CP, however, only occurs in very few (weak) reactions; so far it has been observed exclusively in the decays of one particle, the K_L meson. All experimental observations are compatible with the hypothesis that the combination of all three symmetries, CPT (or any other permu-

tation), is an exact symmetry in nature. There is a very strong theoretical argument for this hypothesis, the so-called CPT theorem. Found in the early fifties by Lüders and Schwinger and thoroughly analyzed thereupon by Pauli and Jost, the theorem states that it is not possible to construct a Lorentz-invariant local field theory obeying the spin-statistics relation in which CPT is violated.

The framework of present-day particle physics, the seemingly unimpeachable Standard Model, fulfils all conditions of the CPT theorem. Therefore any evidence for CPT violation would point beyond the Standard Model, to the eagerly awaited “new physics.” Indeed many of the hypothetical extensions of the Standard Model that are discussed today, in particular theories based on strings, no longer comply with all conditions of the CPT theorem and allow CPT violation at some level. Likewise there are hints from the theory of gravity that the incorporation of this fourth fundamental force into our picture of particle physics will not come about without giving up CPT symmetry.

1.2 The strange world of (neutral) kaons

The discovery of strange particles in cosmic rays in the 1940s marked the beginning of particle physics as we know it today. It became clear that the constituents of atoms: protons, neutrons and electrons, were not the only form of matter. This at first puzzling fact paved the way towards a much deeper understanding of elementary particles and their interactions crystallizing into the quark model of hadrons, put forward by Gell-Mann and Zweig in 1964. Today the quark model is, in slightly modified form, one of the main ingredients of the widely accepted Standard Model of particle physics. We now know that strange particles contain at least one s quark (the letter stands for strange) which only reluctantly decays into the first generation u quark by emitting a heavy W boson (weak interaction with Cabibbo suppression). This explains the strangely long lifetimes of these particles.

The quark structure of matter was not the only physics revolution triggered by strange particles. In 1956, the observed decay modes of the K^+ meson into 2π and 3π , two final states of different parity, lead Lee and Yang to the conclusion that parity is a violated symmetry in nature. Experimental confirmation of this hypothesis followed in the same year and came simultaneously from the realms of nuclear and particle physics: The predicted asymmetries were found by Wu et al. in β decays of polarized ^{60}Co nuclei and by groups led by Lederman and Telegdi in the study of the decay sequence $\pi^+ \rightarrow \mu^+ \rightarrow e^+$. The latter experiments also demonstrated a violation of C symmetry.

The next surprise from the world of strangeness was due to the most peculiar of all strange particles, the neutral kaons. Similar to the K^+ decay it was observed that also the long-lived version of the neutral kaons, the K_L , could decay to 2π as well as to 3π (Christenson et al., 1964). In this case, however, the final states are different eigenstates of the combined CP operator, and the implication is that CP too is violated in nature.

Apart from CP violation, neutral kaons exhibit two other bizarre phenomena which for a long time were exclusively seen with these particles: particle–antiparticle oscillations and regeneration of one species from the other in the presence of matter, as a result of forward scattering off of nuclei. These effects will be described in more detail along with CP violation in Sections 2 and 3.

Despite the ongoing efforts to measure the parameters of the neutral kaon system, it is generally believed today that the answers to the current questions in particle physics—such as why are there three generations of particles, how does mass arise, what is the role of gravity?—will come from the study of heavier particles like B mesons and Higgs bosons. Nevertheless, thanks to their sensitivity to new phenomena and easy experimental accessibility the neutral kaons remain one of the most promising roads towards new physics.

1.3 CPLEAR and regeneration

The CPLEAR experiment at CERN pursues a novel approach to “get a look at the neutral kaon system from all sides” (James Cronin). The method of observing asymmetries between decay rates of initial K^0 and \bar{K}^0 , which will be detailed in Section 4, indeed exhibits the oscillatory behaviour of this system in a most beautiful way and has yielded the best measurements for many of the parameters describing it, most notably η_{+-} .

As mentioned in the previous Subsection, neutral kaons oscillate, violate CP and when in matter,

they also regenerate. One of the main experimental difficulties when studying these phenomena is the fact that they always occur simultaneously, i.e. we cannot turn off two effects to better measure the third. The result of a measurement of the phase of the CP violating 2π decay, for instance, is always correlated with the oscillation frequency Δm and in addition depends on the regeneration probabilities of the neutral kaons along their paths in the detector.

Therefore the outcome of such a measurement can only be interpreted correctly if the other effects are under control. In the case of regeneration this requires good knowledge of the properties and distributions of the various materials used in the detector. (Of course a measurement in vacuum would eliminate all regeneration effects but particle detection necessitates some sort of interaction with matter!)

In the CPLEAR experiment the main contribution to the regeneration uncertainty was due to our ignorance of the neutral kaon scattering amplitudes in the detector material. With the very large number of neutral kaon decays accumulated by CPLEAR—a total of nearly 10^8 —this systematic uncertainty would dominate the statistical error on important CP violation parameters such as the above-mentioned phase.

To remedy this unsatisfying situation, it was decided to dedicate the 1996 run periods—the last before the shutdown of the LEAR decelerator, the experiment's particle supply—to the measurement of neutral kaon regeneration amplitudes in carbon. The strategy adopted for this supplementary experiment is rather straightforward: we let the neutral kaons cross an additional 2.5 cm of carbon and study the effect of the carbon on the decay rates, i.e. we intentionally enlarge the unwanted effect to learn more about its significance. Carbon was chosen for its similarity with most of the detector material, its relatively high density, easy handling and various other properties.

One can easily imagine that measuring regeneration amplitudes with a detector that is designed primarily for the study of CP violation poses an experimental challenge. The task may be compared with a spacecraft that has been built to fly by Jupiter and after a successful primary mission is redirected to explore Saturn: the instruments on board are not optimized for the new encounter taking place under different circumstances, and compromises as well as a bit of improvisation will be needed here and there, but it is certainly a lot of fun to have a look at another planet!

The execution of this experiment and the results gained from it are the subject of this thesis.

1.4 Thesis outline

Section 2 will give a more formal introduction to the phenomenology of neutral kaons and CP and CPT symmetry in this system will be further examined. In Section 3, the phenomenology of coherent and incoherent regeneration is developed, particular attention being given to the peculiar experimental situation at CPLEAR. In Sections 4 and 5, the CPLEAR detector and its modification for the regeneration measurement are described. Section 6 explains the analysis of the regeneration data and lists the results obtained. Finally, a dispersion relation analysis of all regeneration data available for carbon is presented in Section 7. Section 8 briefly summarizes and concludes the work of this thesis.

2 THE NEUTRAL KAON SYSTEM

The K mesons, or kaons, are the lightest hadrons containing strangeness. A strange quark s can combine with a \bar{u} antiquark to form a K^- or with a \bar{d} to give a \bar{K}^0 state. K^+ and K^0 are the respective antiparticles, built from \bar{s} quarks.

The *neutral* kaons only differ by their isospin and strangeness quantum numbers. As the weak interaction conserves neither of them, transitions between the two states are possible and have actually been observed. One consequence of these remarkable particle–antiparticle transitions is that K^0 and \bar{K}^0 are not physical states with well-defined masses and lifetimes. Instead, these parts are played by two linear combinations (mixtures) of K^0 and \bar{K}^0 . The two particles are distinguished by their decay modes: one decays predominantly into two pions whereas the other prefers to decay into three pions. Both also decay at essentially equal rates into the semileptonic final state $\pi^\pm \ell^\mp \nu$ where ℓ stands for electron or muon. The vast difference in phase space available for two or three pions accounts for the very distinct lifetimes of the two particles: the short-lived species, appropriately called $K_{S(\text{HORT})}$, has a mean life of 89 ps (corresponding to some 2.7 cm) while the long-lived one, the $K_{L(\text{ONG})}$, holds out for 52 ns (15.5 m) on average.

K_L and K_S also differ in mass: the tiny mass difference of $3.5 \mu\text{eV}$ is deduced from the measured K^0 – \bar{K}^0 oscillation frequency of 5.3 GHz. It is one of the great successes of the weak interaction theory that this value can be reproduced by way of calculation if the contributions from heavy quarks are taken into account [1].

The different decay modes of K_L and K_S are interpreted as a manifestation of the fact that the former mainly consists of a CP odd and the latter mainly of a CP even state. We write “mainly” because a small admixture of the “wrong” CP eigenstate in K_L has been found experimentally through detection of its $\pi^+\pi^-$ decay and later verified in other decay channels. Thus K_L cannot be regarded as a pure CP eigenstate and CP is not a good symmetry in the neutral kaon system.

In historical retrospect it was the K_S which was first identified in cosmic rays by Rochester and Butler in 1947 [2]. The K_L was predicted in 1954 by Gell-Mann and Pais in their prescient analysis of the neutral kaon system advocating the particle mixture hypothesis [3] and found shortly after by Lederman and his collaborators [4]. A decade later, in 1964, Christenson, Cronin, Fitch, and Turlay identified the CP violating two pion decay of the K_L [5], triggering a series of neutral kaon experiments continuing to this day.

2.1 The effective Hamiltonian

In the analysis of the neutral kaon system it is customary to work in a two-dimensional Hilbert space spanned by the two basis vectors of definite strangeness, K^0 and \bar{K}^0 , and to incorporate the effects of decays into some *effective Hamiltonian* instead of expanding the Hilbert space to include all final states. Clearly, this effective Hamiltonian \mathbf{H} will not conserve probability and therefore cannot be Hermitian. It may, however, like any quadratic matrix be decomposed into a Hermitian and an anti-Hermitian matrix, physically corresponding to a dispersive and an absorptive part:

$$\mathbf{H} = \mathbf{M} - \frac{i}{2}\mathbf{\Gamma} \quad (2.1)$$

where the *mass matrix* \mathbf{M} and the *decay matrix* $\mathbf{\Gamma}$ are defined as

$$\mathbf{M} = \frac{1}{2}(\mathbf{H} + \mathbf{H}^\dagger) \quad \text{and} \quad \mathbf{\Gamma} = i(\mathbf{H} - \mathbf{H}^\dagger).$$

Both are Hermitian 2×2 matrices by definition. The time evolution of a general state ψ is governed by the time-dependent Schrödinger equation

$$i \frac{d\psi}{dt} = \mathbf{H}\psi. \quad (2.2)$$

This treatment of unstable particles is named after Weisskopf and Wigner, who introduced the formalism to calculate light emission curves of atoms and harmonic oscillators [6], and was first applied to the neutral kaon system by Lee, Oehme and Yang [7].

For our purposes it proves useful to expand \mathbf{H} in the Hermitian basis $\mathbb{1}, \sigma_1, \sigma_2, \sigma_3$ where the σ_i denote the Pauli matrices [8]:

$$\begin{aligned} \mathbf{M} - \frac{i}{2}\Gamma &= D\mathbb{1} + \mathbf{E} \cdot \boldsymbol{\sigma} \\ &= \begin{pmatrix} D + E_3 & E_1 - iE_2 \\ E_1 + iE_2 & D - E_3 \end{pmatrix} \end{aligned} \quad (2.3)$$

D and $\mathbf{E} = (E_1, E_2, E_3)$ are a complex number and a complex vector, respectively. The physical meaning of the coefficients is quite obvious [9, 10]:

- D does not mix K^0 and \bar{K}^0 ,
- E_1 mixes them in a CP conserving way,
- E_2 violates T but not CPT,
- E_3 violates CPT but not T.

The eigenvalues of \mathbf{H} are found to be

$$\lambda_{L,S} = D \pm \sqrt{E_1^2 + E_2^2 + E_3^2} \equiv D \pm E, \quad (2.4)$$

corresponding to the eigenvectors $|K_L\rangle$ and $|K_S\rangle$:

$$\mathbf{H}|K_{L,S}\rangle = \lambda_{L,S}|K_{L,S}\rangle \quad (2.5)$$

These are the physical states with definite masses $m_{L,S}$ and lifetimes $\tau_{L,S} = 1/\Gamma_{L,S}$ accounting for the real and imaginary parts of the eigenvalues

$$\lambda_L = m_L - \frac{i}{2}\Gamma_L, \quad (2.6a)$$

$$\lambda_S = m_S - \frac{i}{2}\Gamma_S, \quad (2.6b)$$

so that the time evolution of the two eigenstates is given by

$$K_L(\tau) = K_L(0)e^{-i\lambda_L\tau} = K_L(0)e^{-im_L\tau}e^{-(\Gamma_L/2)\tau}, \quad (2.7a)$$

$$K_S(\tau) = K_S(0)e^{-i\lambda_S\tau} = K_S(0)e^{-im_S\tau}e^{-(\Gamma_S/2)\tau}, \quad (2.7b)$$

where τ denotes proper time. (In order to simplify our notation we omit the kets around the kaon states in most equations.) Writing K_L and K_S as linear combinations of K^0 and \bar{K}^0 ,

$$K_L = \frac{1}{\sqrt{|p_L|^2 + |q_L|^2}}[p_L K^0 + q_L \bar{K}^0], \quad (2.8a)$$

$$K_S = \frac{1}{\sqrt{|p_S|^2 + |q_S|^2}}[p_S K^0 + q_S \bar{K}^0], \quad (2.8b)$$

and inserting (2.3) into the eigenvalue equation (2.5) we obtain the following relations for the coefficients:

$$\frac{q_{L,S}}{p_{L,S}} = \frac{\pm E - E_3}{E_1 \pm iE_2} \quad (2.9)$$

Since we know that CP violation and a possible violation of CPT are small, we introduce the small complex quantities ϵ_L and ϵ_S that fulfil

$$\frac{q_{L,S}}{p_{L,S}} = \pm \frac{1 - \epsilon_{L,S}}{1 + \epsilon_{L,S}} \quad (2.10)$$

and rewrite (2.8) as

$$K_L = \frac{1}{\sqrt{2(1 + |\epsilon_L|^2)}} [(1 + \epsilon_L)K^0 + (1 - \epsilon_L)\bar{K}^0],$$

$$K_S = \frac{1}{\sqrt{2(1 + |\epsilon_S|^2)}} [(1 + \epsilon_S)K^0 - (1 - \epsilon_S)\bar{K}^0].$$

Note that by choosing the signs (and assuming small ϵ parameters) we fix the relative phase¹ between K^0 and \bar{K}^0 . Expressing ϵ_L and ϵ_S in terms of the coefficients E_i reveals that their sum is a measure of T violation whereas a nonzero difference would imply a violation of CPT:

$$\begin{aligned} \text{us } \left. \begin{aligned} \epsilon_S &= \epsilon + \delta \\ \epsilon_L &= \epsilon - \delta \end{aligned} \right\} \epsilon = \frac{\epsilon_S + \epsilon_L}{2} \end{aligned} \quad \epsilon_T \equiv \frac{\epsilon_L + \epsilon_S}{2} = \frac{-iE_2}{E + E_1} \quad (2.11)$$

$$\delta_{\text{CPT}} \equiv \frac{\epsilon_L - \epsilon_S}{2} = \frac{E_3}{E + E_1} \quad (2.12)$$

These mixing parameters depend on our choice of the phase between the two kaon states of definite strangeness. It can be shown, however, that δ_{CPT} and the real part of ϵ_T are to first order not affected by a change of phase whereas the imaginary part of ϵ_T is phase convention dependent to all orders [11].

We summarize the different eigenstates of the neutral kaon system.

- The eigenstates of the strong and electromagnetic part of the Hamiltonian are the states with definite strangeness given by the strange valence quark:

$$K^0 = d\bar{s} \quad (S = +1) \quad (2.13a)$$

$$\bar{K}^0 = \bar{d}s \quad (S = -1) \quad (2.13b)$$

With the usual convention for the quark phases, namely $Cq = +\bar{q}$, we have $CPK^0 = -\bar{K}^0$ (because the quark and the antiquark have opposite intrinsic parity).

- The CP eigenstates are then given by

$$K_1 = \frac{1}{\sqrt{2}} [K^0 + \bar{K}^0] \quad (CP = -1), \quad (2.14a)$$

$$K_2 = \frac{1}{\sqrt{2}} [K^0 - \bar{K}^0] \quad (CP = +1). \quad (2.14b)$$

- The eigenstates of the most general Hamiltonian (2.3) are

$$K_L = \frac{1}{\sqrt{2(1 + |\epsilon_T + \delta_{\text{CPT}}|^2)}} [(1 + \epsilon_T + \delta_{\text{CPT}})K^0 + (1 - \epsilon_T - \delta_{\text{CPT}})\bar{K}^0], \quad (2.15a)$$

$$K_S = \frac{1}{\sqrt{2(1 + |\epsilon_T - \delta_{\text{CPT}}|^2)}} [(1 + \epsilon_T - \delta_{\text{CPT}})K^0 - (1 - \epsilon_T + \delta_{\text{CPT}})\bar{K}^0], \quad (2.15b)$$

where $\epsilon_T \neq 0$ and $\delta_{\text{CPT}} \neq 0$ indicate violation of T and CPT, respectively. For the overlap of the two states we find (to first order in ϵ_T and δ_{CPT})

$$\langle K_S | K_L \rangle \approx 2(\text{Re } \epsilon_T - i \text{Im } \delta_{\text{CPT}}). \quad (2.16)$$

The states are only orthogonal if both T and CPT invariance hold.

Before including regeneration effects into our effective Hamiltonian in the next Section, we will first set out on a brief tour of the CP and CPT symmetries in the neutral kaon system.

1. For a detailed account on our phase convention see Appendix A.

2.2 CP violation

In the Standard Model, CP violation is a natural consequence of the fact that there are three quark generations. This leads to a non-trivial phase in the Cabibbo–Kobayashi–Maskawa (CKM) quark mixing matrix, the one parameter that describes CP violation in the Standard Model [12]. The only puzzle is the apparent absence of CP violation in the sector of strong interactions.

But even though it can be well accommodated in the Standard Model, CP violation remains one of the most active fields of both experimental and theoretical particle physics, mainly for two reasons: The CKM matrix is one of the weakest (and least tested) features of the Standard Model. After all it is just a bunch of parameters summarizing our experimental knowledge on flavour-changing decays, but does not really explain why such decays can occur let alone why there are flavours at all. Perhaps the study of CP violation which seems to be related to the numbers of generations will shed some light on one of the deepest mysteries in modern physics: why we live in a world with three generations. Secondly, almost any extension of the Standard Model bears new CP violating effects. CP violation therefore constitutes a promising window to look for “new physics”.

In this Subsection we give a brief overview of the appearances of CP violation in the neutral kaon system *within the framework of the Standard Model*. To this end we first introduce some notation that is commonly used in the context of neutral meson systems.

In the Standard Model, CPT is a conserved symmetry and we may rewrite (2.8) with $p_S = p_L$ and $q_S = -q_L$ as

$$K_L = pK^0 + q\bar{K}^0, \quad (2.17a)$$

$$K_S = pK^0 - q\bar{K}^0, \quad (2.17b)$$

where we have omitted a common normalization factor. For the decay amplitudes into the various final states f we write

$$A_f = A(K^0 \rightarrow f) \equiv \langle f | \mathcal{H}_{\text{wk}} | K^0 \rangle \quad \text{and} \quad (2.18a)$$

$$\bar{A}_f = A(\bar{K}^0 \rightarrow f) \equiv \langle f | \mathcal{H}_{\text{wk}} | \bar{K}^0 \rangle \quad (2.18b)$$

where \mathcal{H}_{wk} is the weak transition operator underlying the effective Hamiltonian of the last Subsection. The interference parameter λ is defined as

$$\lambda_f = \left(\frac{q}{p} \right) \left(\frac{\bar{A}_f}{A_f} \right). \quad (2.19)$$

Note that $|q/p|$, $|A_f/\bar{A}_f|$ and λ_f are *phase convention independent* quantities.

For decays into two pions we further abbreviate

$$A_I = |A_I| e^{i(\theta_I + \delta_I)} \equiv A(K^0 \rightarrow (\pi\pi)_I) \quad (2.20)$$

where $I = 0$ or 2 denotes the isospin of the two pions and θ_I and δ_I are the phases arising from weak and strong interactions, respectively (i.e. the δ_I are the strong interaction $\pi\pi$ s-wave phase shifts). Using CPT invariance it can be shown that

$$\bar{A}_I \equiv A(\bar{K}^0 \rightarrow (\pi\pi)_I) = |A_I| e^{i(-\theta_I + \delta_I + \pi)}. \quad (2.21)$$

There are four amplitudes describing the transitions from the kaon mass eigenstates K_L and K_S to the two pion states with isospin $I = 0$ and $I = 2$. It is customary to normalize them with respect to the largest amplitude and to define the three amplitude ratios [13]

$$\epsilon \equiv \frac{A(K_L \rightarrow (\pi\pi)_{I=0})}{A(K_S \rightarrow (\pi\pi)_{I=0})}, \quad \epsilon_2 \equiv \frac{A(K_L \rightarrow (\pi\pi)_{I=2})}{A(K_S \rightarrow (\pi\pi)_{I=0})} \quad \text{and} \quad \omega \equiv \frac{A(K_S \rightarrow (\pi\pi)_{I=2})}{A(K_S \rightarrow (\pi\pi)_{I=0})}. \quad (2.22)$$

The phases of ϵ_2 and ω depend on the arbitrary phase we choose between the $\pi\pi$ states with $I = 0$ and $I = 2$. We employ the natural phase implied by real Clebsch–Gordan coefficients. The parameter ϵ

evidently is a measure of CP violation. It is therefore closely related to our mixing parameter ϵ_T but *not identical* to it. The relation between the two parameters is

$$\epsilon = \frac{\epsilon_T + i \tan \theta_0}{1 + \epsilon_T i \tan \theta_0} \quad (2.23)$$

(see Appendix) and shows clearly that the *mixing* parameter ϵ_T depends on what phase we choose for A_0 (or, equivalently, between K^0 and \bar{K}^0) whereas the *decay* parameter ϵ , as we have defined it, is independent of any phase convention. Unfortunately, many authors fail to properly distinguish the two parameters which leads to deplorable inconsistencies.²

In the Standard Model, CP violation with neutral kaons comes in three forms:

2.2.1 CP violation in the mixing

We have seen in the last Subsection that if p and q differ by more than just a phase, the mass eigenstates are not CP eigenstates and CP symmetry is violated:

$$\left| \frac{q}{p} \right| \neq 1 \quad \Longleftrightarrow \quad \text{CP VIOLATION IN THE MIXING}$$

This is the only experimentally confirmed type of CP violation to date. It has been observed in the semileptonic decay $K_L \rightarrow \pi^\mp \ell^\pm \nu$ and in the nonleptonic decays $K_L \rightarrow 2\pi$ and $K_L \rightarrow \pi^+ \pi^- \gamma$. The experimentally measured parameters are [15]

$$\delta \equiv \frac{\Gamma(K_L \rightarrow \pi^- \ell^+ \nu) - \Gamma(K_L \rightarrow \pi^+ \ell^- \bar{\nu})}{\Gamma(K_L \rightarrow \pi^- \ell^+ \nu) + \Gamma(K_L \rightarrow \pi^+ \ell^- \bar{\nu})}, \quad (2.24)$$

$$\eta_{+-} = |\eta_{+-}| e^{i\phi_{+-}} \equiv \frac{A(K_L \rightarrow \pi^+ \pi^-)}{A(K_S \rightarrow \pi^+ \pi^-)}, \quad (2.25)$$

$$\eta_{00} = |\eta_{00}| e^{i\phi_{00}} \equiv \frac{A(K_L \rightarrow \pi^0 \pi^0)}{A(K_S \rightarrow \pi^0 \pi^0)}, \quad (2.26)$$

$$\eta_{+-\gamma} = |\eta_{+-\gamma}| e^{i\phi_{+-\gamma}} \equiv \frac{A(K_L \rightarrow \pi^+ \pi^- \gamma, \text{CP violating})}{A(K_S \rightarrow \pi^+ \pi^- \gamma)}. \quad (2.27)$$

(The CPLEAR collaboration has also measured the parameter $A_T \approx 4 \text{Re } \epsilon_T / (1 + |\epsilon_T|^2)$ in semileptonic decays [16], but has not yet published its result.) If the mixing of the mass eigenstates is the only source of CP violation then there is just one parameter describing it, the ϵ of Eq. 2.22. Its relations to the above experimental parameters are then

$$\delta = \frac{2 \text{Re } \epsilon}{1 + |\epsilon|^2} \quad \text{and} \quad \eta_{+-} = \eta_{00} = \eta_{+-\gamma} = \epsilon. \quad (2.28)$$

2.2.2 CP violation in the decay (“direct” CP violation)

CP symmetry is also violated if the direct decay amplitude for $K^0 \rightarrow f$ and the one for $\bar{K}^0 \rightarrow f$ are not of the same magnitude (“direct” decay means without mixing effects):

$$\left| \frac{\bar{A}_f}{A_f} \right| \neq 1 \quad \Longleftrightarrow \quad \text{CP VIOLATION IN THE DECAY}$$

The condition requires at least two amplitudes contributing to A_f to interfere which occurs only if they have both different weak and strong phases [17]. Such a situation is possible in the two pion decay of the K_L where the $I = 0$ and $I = 2$ amplitudes can interfere to give the final states $\pi^+ \pi^-$ and $\pi^0 \pi^0$. We know from various scattering and decay experiments [18] that the strong phases δ_0 and δ_2 differ by about

2. Probably the best example of such an inconsistency is given by L. Wolfenstein and T. Trippel in Ref. 14: In their Eq. 4 they have ϵ essentially equal to the observables η_{+-} and η_{00} . Already in the following sentence they then claim that the imaginary part of ϵ could be set to zero by a suitable phase convention!

45° so that any difference in the weak phases θ_0 and θ_2 would signal direct CP violation. The effect is usually parameterized by

$$\epsilon' \equiv \frac{i}{\sqrt{2}} \operatorname{Im} \left(\frac{A_2}{A_0} \right) e^{i(\delta_2 - \delta_0)} \approx \frac{1}{\sqrt{2}} (\epsilon_2 - \epsilon\omega) \quad (2.29)$$

which has the phase $\phi_{\epsilon'} = \delta_2 - \delta_0 + \pi/2$ and a magnitude proportional to $\sin(\theta_2 - \theta_0)$. For the experimental parameters we get, after some isospin algebra,

$$\eta_{+-} = \epsilon + \frac{\epsilon'}{1 + \omega/\sqrt{2}} \approx \epsilon + \epsilon', \quad (2.30)$$

$$\eta_{00} = \epsilon - \frac{2\epsilon'}{1 - \sqrt{2}\omega} \approx \epsilon - 2\epsilon', \quad (2.31)$$

where the approximation consists in using the experimental fact that $|\omega| \approx 1/22 \ll 1$ ($\Delta I = 1/2$ rule). By pure coincidence the phases of ϵ and ϵ' are nearly equal. Thus we may as well take $\operatorname{Re}(\epsilon'/\epsilon)$ as a measure for direct CP violation. This quantity is experimentally accessible via

$$\left| \frac{\eta_{+-}}{\eta_{00}} \right|^2 \approx 1 - 6 \operatorname{Re} \left(\frac{\epsilon'}{\epsilon} \right). \quad (2.32)$$

No unambiguous experimental evidence for direct CP violation exists to date. Predictions in the Standard Model are notoriously difficult. Present estimates for $\operatorname{Re}(\epsilon'/\epsilon)$ are of the order 10^{-4} but do not exclude vanishing or even small negative values [19]. Three experiments are currently taking data (KTeV at Fermilab and NA48 at CERN) or in preparation (KLOE at Frascati) with the goal of measuring $\operatorname{Re}(\epsilon'/\epsilon)$ to a precision of 10^{-4} .

2.2.3 CP violation in the interference between mixing and decay

Even if $|q/p| = 1$ and $|\bar{A}_f/A_f| = 1$, the Standard Model still gives us a chance to see CP violation: in the interference between mixing and decay amplitudes. All we need is a nontrivial relative phase in the interference term of the decay to a CP eigenstate:

$$\lambda_{fCP} \neq 1 \iff \text{CP VIOLATION IN THE MIXING-DECAY INTERFERENCE}$$

The prime example where this effect dominates is the truly golden decay of the Standard Model, $K_L \rightarrow \pi^0 \nu \bar{\nu}$ [20]. Unfortunately it has a very small predicted branching ratio of the order of 10^{-12} . Nevertheless, a recently approved experiment at Brookhaven (BNL-926) is setting out to tackle this formidable experimental challenge. In the B system the same part is played by the decay $B^0(\bar{B}^0) \rightarrow J/\psi K_S$, to be studied soon at B factories at SLAC and KEK. Both decays are expected to provide us with extraordinarily clean information on the CKM parameters and are therefore very sensitive probes for new physics.

In our brief overview of CP violation in the neutral kaon system we have only mentioned K_L decays. Of course we expect very similar CP violating effects in the decays of K_S , but they are much harder to observe.

2.3 CPT violation

CPT invariance is firmly rooted in quantum field theory, the very foundation of the Standard Model (cf. Section 1.1). Thus any experimental evidence for CPT being violated would profoundly change our understanding of physics.

CPT violating effects, wherever they may occur, are very likely to be proportional to CP violating effects in the same system [21]. It is therefore natural to look for CPT violation where CP has shown or is expected to be violated, namely in the neutral meson systems. Among these, the neutral kaon system offers by far the most favourable experimental conditions: macroscopic decay lengths and a

fantastically small mass difference allowing very precise interference measurements. Indisputably, it is the most promising place to test CPT invariance. Most of the tests fall into two classes.

The first class consists of *phase comparisons*. Thanks to the fortunate coincidence of ϵ and ϵ' being nearly parallel we know that ϵ' may split the magnitudes of the amplitude ratios η_{+-} and η_{00} but not (or hardly) their phases. Any difference between ϕ_{+-} and ϕ_{00} exceeding the range allowed by our experimental knowledge on ϵ' would signal a violation of CPT. Today's world average, $\phi_{+-} - \phi_{00} = -0.2^\circ \pm 0.8^\circ$ [15] is well in accordance with CPT symmetry, but the situation has not always been that satisfactory [22]. According to (2.30) the phase of ϵ lies between ϕ_{+-} and ϕ_{00} so that the comparison of ϕ_ϵ and the experimentally relatively easily accessible ϕ_{+-} would be an even better test of CPT. Unfortunately, there is no way to measure ϕ_ϵ (because we cannot isolate a final state of definite isospin) but under certain assumptions it can be shown [23] that ϕ_ϵ is very nearly equal to the so-called "superweak" phase defined as

$$\phi_{\text{sw}} \equiv \arctan \frac{2(m_L - m_S)}{\Gamma_S - \Gamma_L} = 43.49^\circ \pm 0.08^\circ \quad (2.33)$$

where we have inserted the experimental values from Ref. 15. The assumptions to be made here are negligibly small violations of the $\Delta S = \Delta Q$ rule in the semileptonic decay mode and of CP symmetry in the decay to three pions. Both conditions are well fulfilled in the Standard Model, but it is not so clear whether one should rely on them when testing anything as fundamental as CPT invariance. Therefore the comparison between ϕ_{+-} and the superweak phase should be considered a test of the Standard Model rather than of CPT invariance [23].

A much more fundamental test of CPT is obtained when simply considering the conservation of probability in the neutral kaon system. For any particle with wave function ψ , the decrease of its norm must be compensated by its decay probability:

$$\frac{d}{d\tau} |\psi|^2 = - \sum_f |\langle f | \mathcal{H}_{\text{wk}} | \psi \rangle|^2 \quad (2.34)$$

where the summation is over all possible final states f . When we insert an arbitrary kaon state $|\psi\rangle = \alpha_L |K_L\rangle + \alpha_S |K_S\rangle$ and carry out the multiplications, the terms proportional to $|\alpha_L|^2$ and $|\alpha_S|^2$ yield simple unitarity relations for K_L and K_S . The mixed terms proportional to $\alpha_L \alpha_S^*$ and $\alpha_L^* \alpha_S$, however, reveal a highly nontrivial relation:

$$\frac{d}{d\tau} \langle K_S | K_L \rangle = - \sum_f \langle K_S | \mathcal{H}_{\text{wk}} | f \rangle \langle f | \mathcal{H}_{\text{wk}} | K_L \rangle$$

For the left hand side we have from (2.7) and (2.16)

$$\begin{aligned} \frac{d}{d\tau} \langle K_S | K_L \rangle &= -i(\lambda_L - \lambda_S^*) \langle K_S | K_L \rangle \\ &= (2i[m_L - m_S] + \Gamma_L + \Gamma_S) (\text{Re } \epsilon_T - i \text{Im } \delta_{\text{CPT}}) \end{aligned}$$

and therefore

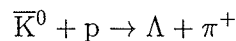
$$\text{Re } \epsilon_T - i \text{Im } \delta_{\text{CPT}} = \frac{\sum_f A^*(K_S \rightarrow f) A(K_L \rightarrow f)}{2i(m_L - m_S) + \Gamma_L + \Gamma_S}. \quad (2.35)$$

This important result was first derived by Bell and Steinberger in a classic proceedings paper [13] and has henceforth become known as the Bell–Steinberger relation. It allows us not only to obtain an experimental estimate of $\text{Re } \epsilon_T \approx \text{Re } \epsilon$ which is completely independent of the direct semileptonic measurement (2.24 and 2.28) but also to test CPT invariance by evaluating the imaginary part of the left hand side of (2.35). Again all experimental data are in agreement with CPT invariance. Currently the test is limited by the precision of CP violation measurements in the decay to three pions.

3 REGENERATION OF NEUTRAL KAONS

Before diving into the (somewhat lengthy) formalism of neutral kaon regeneration, let us first elucidate the physical essence of this important phenomenon in simple terms. We emphasize that regeneration a priori has nothing to do with CP violation. Therefore this irrelevant complication will be ignored in the following introductory remarks.

Let us imagine the production of a neutral kaon beam, for instance by protons impinging on a target. If we further assume that the kaons leave the target at a momentum of a few GeV then the short-lived K_S component will have decayed after a few metres and we are left with a pure K_L beam. (Actually this separation of the two mass eigenstates is a great experimental boon!) Now we send this K_L beam through another block of matter, carbon for instance. The strongly interacting carbon nuclei “see” the incoming K_L as a superposition of the strangeness states K^0 and \bar{K}^0 . These two components will interact very differently in matter: \bar{K}^0 mesons are effectively absorbed through hyperon production processes such as



whereas K^0 mesons can only scatter elastically or undergo charge exchange. Let f and \bar{f} denote the amplitudes of K^0 and \bar{K}^0 scattering off a nucleus. The scattering will transform the $K_L = \frac{1}{\sqrt{2}}(K^0 + \bar{K}^0)$ state into

$$\frac{1}{\sqrt{2}}(fK^0 + \bar{f}\bar{K}^0) = \frac{1}{2}f(K_L + K_S) + \frac{1}{2}\bar{f}(K_L - K_S) = \frac{1}{2}(f + \bar{f})K_L + \frac{1}{2}(f - \bar{f})K_S.$$

Hence, a K_S component is *regenerated* with an amplitude proportional to $f - \bar{f}$.

This at first baffling result is quite comprehensible if K^0 and \bar{K}^0 are envisaged as orthogonal basis vectors in a two-dimensional plane in which K_L and K_S form an equivalent basis, rotated by an angle of 45° . The decay of the K_S component corresponds to a projection of the state onto the K_L axis. Inside the absorbing material, the \bar{K}^0 component (or a large fraction of it) is projected out of the K_L state, leaving behind a state with predominant K^0 content. This state must contain a K_S component. Simple analogies involving linearly polarized light or atoms in a Stern–Gerlach type experiment can be found in various textbooks [24, 25].

Although the name *regeneration* clearly comes from the reappearance of K_S decays from a pure K_L beam outlined above, we will use it as a generic term to describe any transition between the mass eigenstates. Because of the non-zero mass difference, such transitions can only occur in the presence of matter (in contrast to strangeness oscillations).

The regeneration phenomenon was predicted by Pais and Piccioni [26] in 1955, shortly after Gell-Mann and Pais had published their particle mixture hypothesis [3], and still before the discovery of the K_L . In the following years the theoretical aspects of the “Pais–Piccioni experiment,” as regeneration was called in those days, were thoroughly analysed by Case [27] and Good [28]. The experimental search for regeneration succeeded in 1961 when R.H. Good and co-workers reported the first observation of K_S decays behind iron and lead plates exposed in a K_L beam [29].

3.1 Types of regeneration

According to the different ways of kaon scattering in condensed matter one generally distinguishes three classes of regeneration [30, 31]:

Coherent (transmission) regeneration: elastic scattering on nuclei in the forward direction where the scatterers act coherently over an extended region of several centimetres length.

Incoherent (diffraction) regeneration: elastic diffractive scattering off individual nuclei in any direction (including forward). Incoherent addition of intensities from different nuclei, but coherent action of the nucleons inside the nucleus.

Inelastic regeneration: inelastic scattering with large momentum transfer. Excitation or disintegration of the nucleus.

All three types of regeneration were observed, for the first time by R.H. Good et al. [29].

CLEAR, being an interference experiment, is most susceptible to coherent regeneration. Only coherently regenerated kaons can produce additional interference terms and significantly disturb the measurement. The main effect of the incoherently regenerated kaons is to produce some additional two pion decays which may be treated as a further source of (asymmetric) background. It is in most cases negligible. Inelastic regeneration is completely negligible at energies available to CLEAR as the corresponding cross-sections are one or two orders of magnitude smaller than their elastic counterparts.

In the following Subsection we present in detail the phenomenology of coherent regeneration for arbitrary mixtures of K^0 and \bar{K}^0 states.³ Ever since the pioneering work of Case [27] and Good [28] this topic has not received much attention because most experiments involving neutral kaon regeneration send a pure K_L beam through a regenerator. For these measurements it is sufficient to know the K_S amplitude after the regenerator. For experiments employing pure K^0 and \bar{K}^0 beams like CLEAR or detectors at ϕ -factories, however, a K_L - K_S symmetric approach taking into account all possible interference terms is imperative. In Section 3.3 we will turn to the effects of incoherent regeneration, again working with arbitrary mixtures of K^0 and \bar{K}^0 .

3.2 Coherent (transmission) regeneration

Coherent regeneration is a further example of how the tiny mass difference $\Delta m = m_L - m_S$ between K_L and K_S gives rise to phenomena involving macroscopic distances, in this case a coherence length of several centimetres. To see this⁴ let us consider the momentum transfer in a forward scattering reaction of the type $K_L + \text{nucleus} \rightarrow K_S + \text{nucleus}$. The incoming K_L has energy and momentum (four-momentum) (E_L, \mathbf{p}_L) before interacting with a nucleus of mass M at rest. After the scattering we have an outgoing K_S with (E_S, \mathbf{p}_S) and a nucleus carrying the transferred energy and momentum,

$$\begin{pmatrix} E' \\ \mathbf{p}' \end{pmatrix} = \begin{pmatrix} M + E_L - E_S \\ \mathbf{p}_L - \mathbf{p}_S \end{pmatrix}.$$

Energy and momentum conservation further require

$$\begin{aligned} (E_L - E_S)^2 - (p_L^2 - p_S^2)^2 &= (E' - M)^2 - p'^2 \\ &= 2M^2 - 2ME' \\ &= 2M(E_L - E_S). \end{aligned}$$

Solving for the energy difference $(E_L - E_S)$ we find that it vanishes provided that $M^2 \gg (p_L - p_S)^2$. Considering the minute momentum transfer needed to turn a K_L into a K_S without changing the direction of flight we may certainly consider this assumption to be valid. Thus we have $E_L = E_S$ and may write

$$p_L^2 + m_L^2 = p_S^2 + m_S^2$$

from which we deduce

$$p_S - p_L = \Delta m \frac{m_{K^0}}{p_{K^0}} \quad (3.1)$$

where the K^0 -subscript denotes the mean mass and momentum. Now imagine a second scatterer, some distance d further down the neutral kaon flight path. Our K_L may as well choose to regenerate into a K_S at this nucleus instead of the first, bringing about a second K_S amplitude. Will there be interference between the two amplitudes (i.e. will the two scatterers act coherently)? The amplitude regenerated at the first nucleus will have acquired an additional phase $p_S d$ when arriving at the second nucleus. The amplitude to be regenerated at the second nucleus travels the distance d as a K_L and therefore its phase will change by $p_L d$. (Both phases are equally affected by the regeneration process itself.) The K_S intensity will be proportional to

$$|e^{ip_S d} + e^{ip_L d}|^2 = 2 + 2 \cos((p_S - p_L)d),$$

3. Part of this work has been published in Ref. 32.

4. Our derivation of the coherence conditions essentially follows Ref. 30.

so the coherence condition reads

$$(p_S - p_L)d \lesssim 1. \quad (3.2)$$

Inserting (3.1) we see that for low kaon momenta ($p_{K^0} \approx m_{K^0}$) the maximum separation of two nuclei still acting coherently on the neutral kaon is given by the inverse of the mass difference Δm :

$$d_{\max} \approx \frac{1}{\Delta m} \approx 6 \text{ cm}, \quad (3.3)$$

and even larger at higher momenta. This result reflects the well known (and much lamented) fact that the resolution achievable in a scattering experiment is inversely proportional to the momentum transfer occurring in the reaction, usually denoted by q : we build stronger and stronger accelerators to study matter at smaller and smaller distances. Here, however, we find ourselves at the very opposite end of the spectrum: the momentum transfer needed to change a K_L into a K_S is so small, of the order of $\Delta m \approx 3.5 \mu\text{eV}$, that in this (very peculiar) scattering experiment we do not resolve structures smaller than several centimetres! Over such distances we cannot tell where the scattering took place. This means that a neutral kaon undergoing coherent regeneration in a solid plate of a few centimetres thickness interacts with the plate *as a whole*.⁵ In a formal treatment of coherent regeneration it is therefore most appropriate to describe the scatterer by a macroscopic variable, namely an *index of refraction* (see the following Subsection).

The maximum scattering angle θ_{\max} at which coherent regeneration is still possible is also found by considering the phase difference of the K_S amplitudes arising from two scattering centres. If the K_S is emitted under an angle θ with respect to the K_L beam axis then the phase difference in (3.2) decreases to

$$(p_S \cos \theta - p_L)d \approx \left[(p_S - p_L) - p_S \frac{\theta^2}{2} \right] d.$$

The additional term due to the finite scattering angle θ must be smaller than the original phase shift in order not to significantly disturb the coherence condition (3.2):

$$p_S \frac{\theta^2}{2} \lesssim p_S - p_L$$

This gives

$$\theta_{\max}^2 \approx 2 \frac{p_S - p_L}{p_{K^0}}, \quad (3.4)$$

or $\theta_{\max} \approx 10^{-7}$ for low momenta and less for higher momenta.

3.2.1 Coherent scattering and complex index of refraction

We treat the regenerating medium as a distribution of scatterers. An incident coherent wave of wave number (momentum) k will have a different wave number k' inside the medium because of the interaction with the scatterers. For randomly distributed scatterers the difference between the incident coherent field and the effective field inside the medium may be neglected and the relation between the wave numbers is given by [33]

$$(k')^2 = k^2 + 4\pi N f_{k'}(0) \quad (3.5)$$

where N is the density of scattering centres and $f_{k'}(0)$ is the elastic forward scattering amplitude evaluated at k' . Assuming that the additional term in (3.5) is very small we can calculate the index of refraction of the medium as

$$n = \frac{k'}{k} = 1 + \frac{2\pi N}{k^2} f_k(0). \quad (3.6)$$

It should be kept in mind that the above formula rests on two assumptions: firstly the scattering centres (i.e. the nuclei) are distributed completely at random and secondly $|n - 1| \ll 1$ so that we may set $f_{k'}(0) = f_k(0)$ and hence linearize in $(n - 1)$.

5. Coherent regeneration is sometimes called "regeneration by a plate" [29].

3.2.2 The effective Hamiltonian in matter and the regeneration parameter

Here we carry on our investigation of neutral kaon dynamics governed by an effective Hamiltonian from Section 2.1 and will extend it to incorporate the effects of a strongly interacting medium. For this phenomenological analysis of regeneration we assume CPT invariance but not T invariance, so that *in vacuum* we are dealing with an effective Hamiltonian of the form

$$\mathbf{H} = D\mathbb{1} + E_1\sigma_1 + E_2\sigma_2 \quad (3.7)$$

and its eigenstates

$$K_L = \frac{1}{\sqrt{2(1+|\epsilon_T|^2)}}[(1+\epsilon_T)K^0 + (1-\epsilon_T)\bar{K}^0], \quad (3.8a)$$

$$K_S = \frac{1}{\sqrt{2(1+|\epsilon_T|^2)}}[(1+\epsilon_T)K^0 - (1-\epsilon_T)\bar{K}^0], \quad (3.8b)$$

which we will call mass eigenstates. A general state ψ can be written as a linear combination of any pair of eigenstates:

$$\psi(\tau) = \alpha(\tau)K^0 + \bar{\alpha}(\tau)\bar{K}^0 = \alpha_L(\tau)K_L + \alpha_S(\tau)K_S \quad (3.9)$$

$\alpha_L(\tau)$ and $\alpha_S(\tau)$ are the amplitudes for finding the state as a K_L or a K_S , respectively. From (3.8) we get the following relations for the amplitudes:

$$\alpha = \frac{1+\epsilon}{\sqrt{1+|\epsilon|^2}} \frac{\alpha_L + \alpha_S}{\sqrt{2}} \quad (3.10a)$$

$$\bar{\alpha} = \frac{1-\epsilon}{\sqrt{1+|\epsilon|^2}} \frac{\alpha_L - \alpha_S}{\sqrt{2}} \quad (3.10b)$$

Now to accommodate for the strong interaction of the kaons with the nuclei of the surrounding medium we have to add to the effective Hamiltonian (3.7) a nuclear term that will be diagonal in the $K^0-\bar{K}^0$ basis:

$$\mathbf{H}' = \mathbf{H} + \mathbf{H}_{\text{nuc}} \quad (3.11)$$

The nuclear contribution to the rate of change of a general state ψ (3.9) is given by the indices of refraction for K^0 and \bar{K}^0 , defined in the last Paragraph:

$$\left(\frac{d\psi}{dz}\right)_{\text{nuc}} = ik \begin{pmatrix} n-1 & 0 \\ 0 & \bar{n}-1 \end{pmatrix} \psi$$

We transform into the particle's rest frame and insert (3.6):

$$i \left(\frac{d\psi}{d\tau}\right)_{\text{nuc}} = -\frac{2\pi N}{m} \begin{pmatrix} f & 0 \\ 0 & \bar{f} \end{pmatrix} \psi \quad (3.12)$$

Comparing with Schrödinger's equation for the time evolution we find

$$\mathbf{H}_{\text{nuc}} = \begin{pmatrix} \varkappa & 0 \\ 0 & \bar{\varkappa} \end{pmatrix} \quad (3.13)$$

with

$$\varkappa = -\frac{2\pi N}{m}f \quad \text{and} \quad \bar{\varkappa} = -\frac{2\pi N}{m}\bar{f}, \quad (3.14)$$

defined in analogy to the eigenvalues of the free Hamiltonian λ_L and λ_S . The interaction with matter leads to a term proportional to σ_3 in the effective Hamiltonian, mimicking a violation of CPT. (This comes as no surprise as our regenerating medium consists solely of matter and not antimatter.) To obtain the

eigenvalues and eigenvectors of \mathbf{H}' we can therefore simply apply the general formulae from Section 2.1. Writing

$$\mathbf{H}' = D' \mathbb{1} + \mathbf{E}' \cdot \boldsymbol{\sigma} \quad (3.15)$$

we find that

$$D' = D + \frac{\kappa + \bar{\kappa}}{2}, \quad E'_3 = \frac{\kappa - \bar{\kappa}}{2}. \quad (3.16)$$

Our expression for the index of refraction (3.6) is linearized in κ . Consequently, we must drop terms proportional to E'_3 and set $E' = E$. The eigenvalues of the new effective Hamiltonian are then

$$\lambda'_{L,S} = D' \pm E = \lambda_{L,S} + \frac{\kappa + \bar{\kappa}}{2}. \quad (3.17)$$

For the eigenstates we employ expressions (2.15) with δ_{CPT} replaced by

$$\delta' = \frac{E'_3}{E + E_1}. \quad (3.18)$$

δ' is, to first order in ϵ_T , equal to the *regeneration parameter* r defined as

$$r := \frac{\Delta\kappa}{2\Delta\lambda} = -\frac{\pi N}{m} \frac{\Delta f}{\Delta m - (i/2)\Delta\Gamma}. \quad (3.19)$$

(In all our equations $\Delta x \equiv x_L - x_S$ for quantities referring to the mass eigenstates and $\Delta y \equiv y - \bar{y}$ for variables associated with strangeness.) The parameter r is sometimes expressed in terms of the mean life τ_S and the mean decay length $\Lambda_S = \gamma v \tau_S$ of the K_S as

$$r = i\pi \frac{f - \bar{f}}{p} \frac{N\Lambda_S}{\frac{1}{2} - i\Delta m \tau_S} \quad (3.20)$$

where $p = \gamma v m$ is the particle's momentum, v its velocity relative to the regenerator, $\gamma = (1 - v^2)^{-1/2}$ the usual Lorentz factor and Γ_L is neglected with respect to Γ_S [34]. The magnitude of r is typically of the order of 10^{-2} for condensed matter, i.e. regeneration effects are fairly small in most materials. The eigenstates in matter may now be written as

$$K'_L = \frac{1}{\sqrt{2(1 + |\epsilon_T + r|^2)}} [(1 + \epsilon_T + r)K^0 + (1 - \epsilon_T - r)\bar{K}^0], \quad (3.21a)$$

$$K'_S = \frac{1}{\sqrt{2(1 + |\epsilon_T + r|^2)}} [(1 + \epsilon_T - r)K^0 - (1 - \epsilon_T + r)\bar{K}^0]. \quad (3.21b)$$

Neglecting furthermore quadratic terms in r we arrive at

$$\begin{aligned} K'_L &= \frac{1}{\sqrt{2}} [(1 + \epsilon_T)K^0 + (1 - \epsilon_T)\bar{K}^0 + r(K^0 - \bar{K}^0)] \\ &= K_L + rK_S, \end{aligned} \quad (3.22a)$$

$$K'_S = K_S - rK_L. \quad (3.22b)$$

Having found the eigenstates and eigenvalues of the effective Hamiltonian, the time development in matter is readily computed for a general state

$$\psi(\tau) = \alpha_L(\tau)K_L + \alpha_S(\tau)K_S = \alpha'_L(\tau)K'_L + \alpha'_S(\tau)K'_S.$$

Using (3.22) and (3.17) we have (always to first order in ϵ_T and r)

$$\begin{aligned} \alpha_L(\tau) &= \alpha'_L(0)e^{-i\lambda'_L\tau} - r\alpha'_S(0)e^{-i\lambda'_S\tau} \\ &= e^{-\frac{i}{2}(\kappa + \bar{\kappa})\tau} \left[\alpha_L(0)e^{-i\lambda_L\tau} + r\alpha_S(0) \left(e^{-i\lambda_L\tau} - e^{-i\lambda_S\tau} \right) \right] \\ &= e^{-\frac{i}{2}(\kappa + \bar{\kappa})\tau} e^{-i\lambda_L\tau} (\alpha_L(0) + \rho\alpha_S(0)) \end{aligned} \quad (3.23a)$$

and similarly

$$\alpha_S(\tau) = e^{-\frac{i}{2}(\kappa+\bar{\kappa})\tau} e^{-i\lambda_S\tau} \left(\alpha_S(0) + \varrho\alpha_L(0)e^{-i\Delta\lambda\tau} \right), \quad (3.23b)$$

where we define the *geometry-dependent regeneration parameter* $\varrho(L)$ as the fraction of K_S in an initially pure K_L beam after penetrating a regenerator of thickness $L = \gamma v\tau$:

$$\varrho(L) \equiv \frac{\alpha_S(L)}{\alpha_L(L)} \quad \text{for} \quad \alpha_L(0) = 1 \quad \text{and} \quad \alpha_S(0) = 0. \quad (3.24)$$

This ratio is—to first order in r —equal to r times a geometrical factor in accordance with (3.23) (see also Eq. 3.33 in the following Paragraph):

$$\varrho(L) = r \left[1 - \exp\left(i\Delta\lambda\frac{L}{\gamma v}\right) \right] \quad (3.25)$$

In the notation of Eq. 3.20 this reads [30]

$$\varrho(L) = i\pi \frac{f - \bar{f}}{p} N\Lambda_S \frac{1 - \exp\left[\left(i\Delta m\tau_S - \frac{1}{2}\right)\frac{L}{\Lambda_S}\right]}{\frac{1}{2} - i\Delta m\tau_S}. \quad (3.26)$$

3.2.3 Time development of a general state in matter

The simple formulae for the time development of a general state in matter obtained in the last Paragraph only hold in first order of ϵ_T and r . To derive exact expressions it is more convenient to directly solve the Schrödinger equation

$$i\frac{d\psi}{d\tau} = \mathbf{H}'\psi = (\mathbf{H} + \mathbf{H}_{\text{nuc}})\psi \quad (3.27)$$

as was first done by Case [27] and Good [28]. The eigenvalues and eigenvectors of either part of the Hamiltonian are well known and their respective contributions to the change of the state ψ with respect to proper time τ are given by

$$i\left(\frac{d\psi}{d\tau}\right)_{\text{vac}} = \lambda_L\alpha_L K_L + \lambda_S\alpha_S K_S, \quad (3.28)$$

$$i\left(\frac{d\psi}{d\tau}\right)_{\text{nuc}} = \kappa\alpha K^0 + \bar{\kappa}\bar{\alpha}\bar{K}^0. \quad (3.29)$$

Applying (3.10) we express the sum in the basis of the mass eigenstates and obtain Good's equations in the particle's rest frame:

$$i\frac{d\alpha_L}{d\tau} = \lambda_L\alpha_L + \left(\frac{\kappa + \bar{\kappa}}{2}\right)\alpha_L + \left(\frac{\kappa - \bar{\kappa}}{2}\right)\alpha_S \quad (3.30a)$$

$$i\frac{d\alpha_S}{d\tau} = \lambda_S\alpha_S + \left(\frac{\kappa + \bar{\kappa}}{2}\right)\alpha_S + \left(\frac{\kappa - \bar{\kappa}}{2}\right)\alpha_L \quad (3.30b)$$

CP violation does not manifest itself in the equations, a fact pointed out by Good already. The solution of (3.30) may be written as⁶

$$\alpha_L(\tau) = e^{-i\Sigma\cdot\tau} \left[\alpha_L^0 \cos(\Omega\tau) - \frac{i}{2\Omega}(\Delta\lambda\alpha_L^0 + \Delta\kappa\alpha_S^0) \sin(\Omega\tau) \right], \quad (3.31a)$$

$$\alpha_S(\tau) = e^{-i\Sigma\cdot\tau} \left[\alpha_S^0 \cos(\Omega\tau) + \frac{i}{2\Omega}(\Delta\lambda\alpha_S^0 - \Delta\kappa\alpha_L^0) \sin(\Omega\tau) \right], \quad (3.31b)$$

6. The general solution of the system

$$\dot{\mathbf{x}}(t) = \mathbf{A}\mathbf{x}(t) \quad \Leftrightarrow \quad \begin{aligned} \dot{x}_1(t) &= a_{11}x_1(t) + a_{12}x_2(t) \\ \dot{x}_2(t) &= a_{21}x_1(t) + a_{22}x_2(t) \end{aligned}$$

with constants

$$\Omega = \frac{1}{2} \sqrt{\Delta\lambda^2 + \Delta\kappa^2}, \quad \Sigma = \frac{1}{2}(\lambda_L + \lambda_S + \kappa + \bar{\kappa}).$$

α_L^0 and α_S^0 are the initial amplitudes for $\tau = 0$. The factor $e^{-i\Sigma\tau}$ appearing in both amplitudes describes the decay of the mass eigenstates as well as the absorption of the strangeness eigenstates:

$$|e^{-i\Sigma\tau}|^2 = e^{-\frac{1}{2}(\Gamma_L + \Gamma_S)\tau} e^{-\frac{N}{2}(\sigma_T + \bar{\sigma}_T)\gamma v \tau}$$

where σ_T and $\bar{\sigma}_T$ are the total cross sections for K^0 and \bar{K}^0 , respectively, and we have used the optical theorem. In terms of the regeneration parameter⁷ r defined in the preceding Paragraph, (3.31) reads

$$\alpha_L(\tau) = e^{-i\Sigma\tau} \left[\alpha_L^0 \cos\left(\frac{\Delta\lambda}{2} \sqrt{1 + 4r^2\tau}\right) - i \frac{\alpha_L^0 + 2r\alpha_S^0}{\sqrt{1 + 4r^2}} \sin\left(\frac{\Delta\lambda}{2} \sqrt{1 + 4r^2\tau}\right) \right], \quad (3.32a)$$

$$\alpha_S(\tau) = e^{-i\Sigma\tau} \left[\alpha_S^0 \cos\left(\frac{\Delta\lambda}{2} \sqrt{1 + 4r^2\tau}\right) + i \frac{\alpha_S^0 - 2r\alpha_L^0}{\sqrt{1 + 4r^2}} \sin\left(\frac{\Delta\lambda}{2} \sqrt{1 + 4r^2\tau}\right) \right]. \quad (3.32b)$$

In (3.31) and (3.32) quadratic terms in κ , $\bar{\kappa}$ and $\Delta\lambda/\lambda$ are neglected but no approximations concerning the smallness of ϵ_T and r have been made so far. For the calculation of the following Paragraph, however, we do take advantage of the fact that $r \ll 1$ and limit the discussion to first or second order processes. Expanding (3.32) up to second order in r we get

$$\alpha_L(\tau) = e^{-\frac{i}{2}(\kappa + \bar{\kappa})\tau} \left\{ \alpha_L^0 e^{-i\lambda_L\tau} + r\alpha_S^0 \left[e^{-i\lambda_L\tau} - e^{-i\lambda_S\tau} \right] - r^2\alpha_L^0 \left[e^{-i\lambda_L\tau} - e^{-i\lambda_S\tau} + i\Delta\lambda\tau e^{-i\lambda_L\tau} \right] \right\}, \quad (3.33a)$$

$$\alpha_S(\tau) = e^{-\frac{i}{2}(\kappa + \bar{\kappa})\tau} \left\{ \alpha_S^0 e^{-i\lambda_S\tau} + r\alpha_L^0 \left[e^{-i\lambda_L\tau} - e^{-i\lambda_S\tau} \right] + r^2\alpha_S^0 \left[e^{-i\lambda_L\tau} - e^{-i\lambda_S\tau} + i\Delta\lambda\tau e^{-i\lambda_S\tau} \right] \right\}. \quad (3.33b)$$

It is easily verified that the first order approximation reduces to (3.23).

3.2.4 Two pion decay after penetration of a regenerator

Let us consider a neutral kaon which, at $\tau = 0$, is in an arbitrary state and approaches a regenerator of thickness L with relative velocity v . It enters the regenerator at proper time $\tau_1 \geq 0$ and leaves it again at

$$\tau_2 = \tau_1 + L/\gamma v \equiv \tau_1 + \delta\tau$$

(see Fig. 1). Before entering the regenerator the two mass components evolve separately according to is given by

$$\begin{aligned} x_1(t) &= C_{11}e^{\lambda_1 t} + C_{12}e^{\lambda_2 t}, \\ x_2(t) &= C_{21}e^{\lambda_1 t} + C_{22}e^{\lambda_2 t}, \end{aligned}$$

where λ_1 and λ_2 are the eigenvalues of \mathbf{A} , $\lambda_{1,2} = a^\pm \pm \Delta$ with $a^\pm := \frac{1}{2}(a_{11} \pm a_{22})$ and $\Delta := \sqrt{(a^-)^2 + a_{12}a_{21}}$. We express the solution in the basis of the hyperbolic functions,

$$\begin{aligned} x_1(t) &= e^{a^+ t} [C_c \cosh(\Delta \cdot t) + C_s \sinh(\Delta \cdot t)], \\ x_2(t) &= e^{a^+ t} [C'_c \cosh(\Delta \cdot t) + C'_s \sinh(\Delta \cdot t)], \end{aligned}$$

and determine the constants from the initial values at $t = 0$:

$$\begin{aligned} C_c &= x_1(0) & C_s &= \Delta^{-1}[a^- x_1(0) + a_{12}x_2(0)] \\ C'_c &= x_2(0) & C'_s &= \Delta^{-1}[a_{21}x_1(0) - a^- x_2(0)] \end{aligned}$$

7. Our parameter r is essentially equal to the coefficient $R/(1 - R^2)$ in Good's solution of the differential equations.

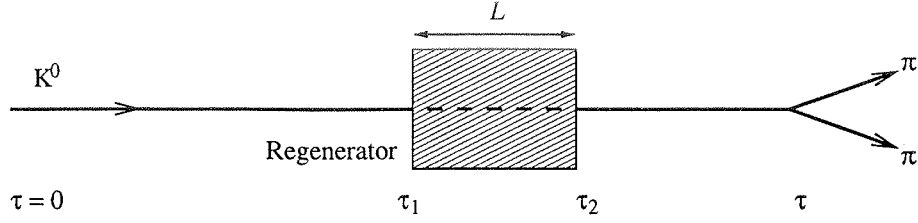


Figure 1: Neutral kaon traversing a regenerator before decaying into two pions.

(3.28):

$$\alpha_{L,S}(\tau_1) = e^{-i\lambda_{L,S}\tau_1} \alpha_{L,S}^0,$$

whereas inside the regenerator the components mix as described by (3.33):

$$\alpha_{L,S}(\tau_2) = e^{-\frac{i}{2}(\kappa+\bar{\kappa})\tau} \left\{ \alpha_{L,S}(\tau_1) e^{-i\lambda_{L,S}\delta\tau} + r\alpha_{S,L}(\tau_1) \left[e^{-i\lambda_L\delta\tau} - e^{-i\lambda_S\delta\tau} \right] \right. \\ \left. \mp r^2 \alpha_{L,S}(\tau_1) \left[e^{-i\lambda_L\delta\tau} - e^{-i\lambda_S\delta\tau} + i\Delta\lambda\delta\tau e^{-i\lambda_{L,S}\delta\tau} \right] \right\}.$$

Afterwards the wave propagates through vacuum again, so that for life times $\tau \geq \tau_2$ we have

$$\alpha_{L,S}(\tau) = e^{-i\lambda_{L,S}(\tau-\tau_2)} \alpha_{L,S}(\tau_2).$$

The two pion decay rate of a general state (3.9) can be reduced to the corresponding time-independent decay rate R_S of the K_S eigenstate:

$$R(\tau) = R_S |\alpha_S(\tau) + \eta\alpha_L(\tau)|^2 \quad (3.34)$$

where η is the ratio of the CP violating to the CP conserving decay amplitude as defined in (2.25–2.27). Inserting the above recursive formulae for the amplitudes into (3.34) we arrive at

$$R(\tau) = R_S e^{-\frac{N}{2}(\sigma_T+\bar{\sigma}_T)L} \left(e^{-\Gamma_S\tau} \mathcal{S} + 2|\eta|e^{-\frac{1}{2}(\Gamma_L+\Gamma_S)\tau} \mathcal{M} + |\eta|^2 e^{-\Gamma_L\tau} \mathcal{L} \right), \quad (3.35)$$

with

$$\mathcal{L}, \mathcal{S} = |\alpha_{L,S}^0|^2 \\ \pm 2|r||\alpha_L^0||\alpha_S^0| \left[e^{\pm\frac{1}{2}\Delta\Gamma\tau_1} \cos(\Delta m\tau_1 \pm \varphi_r - \Delta\varphi^0) \right. \\ \left. - e^{\pm\frac{1}{2}\Delta\Gamma\tau_2} \cos(\Delta m\tau_2 \pm \varphi_r - \Delta\varphi^0) \right] \\ + |r|^2 |\alpha_{S,L}^0|^2 \left[e^{\pm\Delta\Gamma\tau_1} + e^{\pm\Delta\Gamma\tau_2} - 2e^{\pm\frac{1}{2}\Delta\Gamma(\tau_1+\tau_2)} \cos(\Delta m\delta\tau) \right] \\ + 2|r|^2 |\alpha_{L,S}^0|^2 \left[e^{\pm\frac{1}{2}\Delta\Gamma\delta\tau} \cos(\Delta m\delta\tau \pm 2\varphi_r) \right. \\ \left. - \left(1 \pm \frac{1}{2}\Delta\Gamma\delta\tau \right) \cos(2\varphi_r) \pm \Delta m\delta\tau \sin(2\varphi_r) \right]$$

and

$$\mathcal{M} = |\alpha_L^0||\alpha_S^0| \cos(\Delta m\tau - \phi - \Delta\varphi^0) + \mathcal{M}_1 + \mathcal{M}_2,$$

$$\begin{aligned}
\mathcal{M}_{1,2} = & \pm |r| |\alpha_{S,L}^0|^2 \left[e^{\pm \frac{1}{2} \Delta \Gamma \tau_1} \cos(\Delta m(\tau - \tau_1) - \phi \mp \varphi_r) \right. \\
& \left. - e^{\pm \frac{1}{2} \Delta \Gamma \tau_2} \cos(\Delta m(\tau - \tau_2) - \phi \mp \varphi_r) \right] \\
& + |r|^2 |\alpha_L^0| |\alpha_S^0| \left[e^{\pm \frac{1}{2} \Delta \Gamma \delta \tau} \cos(\Delta m(\tau - \tau_1 - \tau_2) - \phi + \Delta \varphi^0) \right. \\
& - \cos(\Delta m(\tau - 2\tau_{1,2}) - \phi + \Delta \varphi^0) \\
& + e^{\pm \frac{1}{2} \Delta \Gamma \delta \tau} \cos(\Delta m(\tau - \delta \tau) - \phi \mp 2\varphi_r - \Delta \varphi^0) \\
& - (1 \pm \frac{1}{2} \Delta \Gamma \delta \tau) \cos(\Delta m \tau - \phi \mp 2\varphi_r - \Delta \varphi^0) \\
& \left. - \Delta m \delta \tau \sin(\Delta m \tau - \phi \mp 2\varphi_r - \Delta \varphi^0) \right],
\end{aligned}$$

where φ_r is the phase of r and $\Delta \varphi^0$ is defined as

$$\Delta \varphi^0 = \varphi_L^0 - \varphi_S^0 = \arg(\alpha_L^0) - \arg(\alpha_S^0).$$

The general formulae can easily be adapted to the physically relevant cases of initial eigenstates of definite strangeness as produced in strong interactions. For K^0 and \bar{K}^0 as initial states we have from (3.8)

$$|\alpha_L^0|^2 = |\alpha_S^0|^2 = |\alpha_L^0| |\alpha_S^0| \approx \begin{cases} \frac{1}{2} - \text{Re } \epsilon_T & \text{for } K^0 \\ \frac{1}{2} + \text{Re } \epsilon_T & \text{for } \bar{K}^0 \end{cases}$$

and

$$\Delta \varphi^0 = \begin{cases} 0 & \text{for } K^0 \\ \pi & \text{for } \bar{K}^0, \end{cases}$$

i.e. for an initial \bar{K}^0 the terms containing $\Delta \varphi^0$ in the cosine argument change their signs. Hence the measurement of the time-dependent decay rate (3.35) for initial K^0 and \bar{K}^0 allows the determination of the magnitude and the phase of the regeneration parameter r and so, via (3.19), of the regeneration amplitude Δf .

The terms of lowest order in r may be rewritten by use of the geometry-dependent regeneration parameter $\varrho (L = \gamma v \delta \tau)$, yielding

$$\mathcal{L}, \mathcal{S} = |\alpha_{L,S}^0|^2 + 2|\varrho| |\alpha_L^0| |\alpha_S^0| e^{\pm \frac{1}{2} \Delta \Gamma \tau_{1,2}} \cos(\Delta m \tau_{1,2} \pm \varphi_\varrho - \Delta \varphi^0)$$

and

$$\begin{aligned}
\mathcal{M} = & |\alpha_L^0| |\alpha_S^0| \cos(\Delta m \tau - \phi - \Delta \varphi^0) \\
& + |\varrho| |\alpha_S^0|^2 e^{\frac{1}{2} \Delta \Gamma \tau_1} \cos(\Delta m(\tau - \tau_1) - \phi - \varphi_\varrho) \\
& + |\varrho| |\alpha_L^0|^2 e^{-\frac{1}{2} \Delta \Gamma \tau_2} \cos(\Delta m(\tau - \tau_2) - \phi + \varphi_\varrho)
\end{aligned}$$

as lowest order approximations.

It is noteworthy that the decay rates for initial K^0 or \bar{K}^0 exhibit a substantial *linear* dependence on the regeneration parameter r whereas for initial K_L or K_S only terms proportional to r^2 or ηr remain. Conventional regeneration experiments dealing with K_L beams are therefore only sensitive to the second order of r [30]. We have included second order effects in our calculations so that Eq. 3.35 applies to all possible experimental situations.

3.3 Incoherent regeneration

For scattering angles greater than 10^{-7} the neutral kaon amplitudes scattered by two separate nuclei are no longer in phase and therefore add up *incoherently* (cf. the discussion at the beginning of the preceding Subsection). The K_S amplitude regenerated in this way does not interfere with the inherent

K_S component of the incoming beam which is why this type of regeneration plays a minor role in the CPLEAR experiment. Nevertheless we must assess its influence on our measurement.

Our phenomenological approach is based on the analysis of Good [28] but presented in the modernized notation introduced in the previous Subsection. We then examine the effect of incoherent regeneration for the specific case of the measurement of $\pi^+\pi^-$ decay rates with CPLEAR.

3.3.1 Phenomenology

We describe the scattering of K^0 and \bar{K}^0 at an angle θ by the amplitudes $f(\theta)$ and $\bar{f}(\theta)$. Since in our phase convention⁸ $K_S = \frac{1}{\sqrt{2}}(K^0 - \bar{K}^0)$ the differential cross section for the scattering of the state ψ (see Eq. 3.9) into the final state K_S is given by

$$\frac{d\sigma_{\psi \rightarrow K_S}}{d\Omega}(\theta) = \left| \frac{\alpha f(\theta) - \bar{\alpha} \bar{f}(\theta)}{\sqrt{2}} \right|^2 = \left| \frac{\alpha_L[f(\theta) - \bar{f}(\theta)] + \alpha_S[f(\theta) + \bar{f}(\theta)]}{2} \right|^2 \quad (3.36a)$$

where the α coefficients are evaluated at the scattering point according to (3.31). By analogy we also get

$$\frac{d\sigma_{\psi \rightarrow K_L}}{d\Omega}(\theta) = \left| \frac{\alpha f(\theta) + \bar{\alpha} \bar{f}(\theta)}{\sqrt{2}} \right|^2 = \left| \frac{\alpha_L[f(\theta) + \bar{f}(\theta)] + \alpha_S[f(\theta) - \bar{f}(\theta)]}{2} \right|^2. \quad (3.36b)$$

To obtain the number of K_S (K_L) scattered at θ into a solid angle $d\Omega$ and originating from a regenerator slice of thickness dx at position x we multiply by Ndx , the area density of scattering centres in dx :

$$\begin{aligned} dn_S(x, \theta) &= \frac{1}{4} |\alpha_L(x)[f(\theta) - \bar{f}(\theta)] + \alpha_S(x)[f(\theta) + \bar{f}(\theta)]|^2 N dx d\Omega \\ dn_L(x, \theta) &= \frac{1}{4} |\alpha_L(x)[f(\theta) + \bar{f}(\theta)] + \alpha_S(x)[f(\theta) - \bar{f}(\theta)]|^2 N dx d\Omega \end{aligned}$$

We integrate over the solid angle $d\Omega = 2\pi\theta d\theta$ and replace distance by proper time according to $dx = \gamma v d\tau$ to arrive at

$$\begin{aligned} dn_S(\tau_{sc}) &= \frac{\pi}{2} \gamma v N d\tau_{sc} \int d\theta \theta \varepsilon(\theta) |\alpha_L(\tau_{sc})[f(\theta) - \bar{f}(\theta)] + \alpha_S(\tau_{sc})[f(\theta) + \bar{f}(\theta)]|^2, \\ dn_L(\tau_{sc}) &= \frac{\pi}{2} \gamma v N d\tau_{sc} \int d\theta \theta \varepsilon(\theta) |\alpha_L(\tau_{sc})[f(\theta) + \bar{f}(\theta)] + \alpha_S(\tau_{sc})[f(\theta) - \bar{f}(\theta)]|^2, \end{aligned}$$

where τ_{sc} stands for the time of the scattering and $\varepsilon(\theta)$ is the overall detection efficiency as a function of the deflection angle θ . Any K_S or K_L emerging from such a scattering process is subject to further incoherent or coherent scattering as well as absorption or decay. For our purpose, thanks to the modest size and density of the regenerator installed in the CPLEAR detector ($2.5 \text{ cm} \times 1.85 \text{ g/cm}^3$ carbon, see Section 5), we may neglect multiple scattering (i.e. further incoherent regeneration) [35]. This applies all the more to scattering in the detector walls, of course. The remaining three processes, coherent scattering, absorption and decay, are well described in the framework of coherent regeneration.

3.3.2 Contribution to the measured two pion decay rate

Let us assume, as in Paragraph 3.2.4, that the kaons perpendicularly penetrate a regenerator of finite thickness L (Fig. 1). For a given momentum $p = \gamma v m$ they will enter the medium at proper time τ_1 and leave it again at τ_2 . We are interested in the number of additional two pion decays at some proper time $\tau \geq \tau_2$ caused by incoherent regeneration. This contribution to two pion decays is given by the number of particles times their two-pionic decay rate. For K_S incoherently produced at τ_{sc} for instance, the (normalized) contribution at τ is

$$dn_S(\tau_{sc}) R_{2\pi}^{(S)}(\tau; \tau_{sc}, \tau_2)$$

8. CP violation may be ignored at this point as it cancels anyway in the right hand side of Eq. 3.36.

where

$$R_{2\pi}^{(S)}(\tau; \tau_{\text{sc}}, \tau_2) = \left| \alpha_S^{(S)}(\tau) + \eta \alpha_L^{(S)}(\tau) \right|^2$$

and the superscripts of the amplitudes α indicate that they are evaluated according to (3.31) for a K_S at the scattering time τ_{sc} : Starting from

$$\alpha_S^{(S)}(\tau_{\text{sc}}) = 1 \quad \text{and} \quad \alpha_L^{(S)}(\tau_{\text{sc}}) = 0$$

we get, if we neglect the additional path length inside the medium resulting from the scattering angle,

$$\begin{aligned} \alpha_S^{(S)}(\tau_2) &= e^{-i\Sigma \cdot (\tau_2 - \tau_{\text{sc}})} \left[\cos(\Omega(\tau_2 - \tau_{\text{sc}})) + \frac{i\Delta\lambda}{2\Omega} \sin(\Omega(\tau_2 - \tau_{\text{sc}})) \right], \\ \alpha_L^{(S)}(\tau_2) &= -e^{-i\Sigma \cdot (\tau_2 - \tau_{\text{sc}})} \left[\frac{i\Delta\kappa}{2\Omega} \sin(\Omega(\tau_2 - \tau_{\text{sc}})) \right] \end{aligned}$$

and simply

$$\begin{aligned} \alpha_S^{(S)}(\tau) &= e^{-i\lambda_S(\tau - \tau_2)} \alpha_S^{(S)}(\tau_2), \\ \alpha_L^{(S)}(\tau) &= e^{-i\lambda_L(\tau - \tau_2)} \alpha_L^{(S)}(\tau_2) \end{aligned}$$

for the trajectory after the regenerator. To avoid any confusion in the final result we reserve the Greek letter α for the amplitudes of the unscattered (i.e. only coherently regenerated) beam and rename the amplitudes of the scattered particles in the following manner:

$$\begin{aligned} a_{LL} &:= \alpha_L^{(L)} & a_{LS} &:= \alpha_L^{(S)} \\ a_{SL} &:= \alpha_S^{(L)} & a_{SS} &:= \alpha_S^{(S)} \end{aligned}$$

The total number of two pion decays from incoherently regenerated kaons is given by the sum of the contributions from K_S and K_L integrated over the thickness of the regenerator. The final result is

$$R_{2\pi}^{\text{inc}}(\tau) = \frac{\pi}{2} \gamma v N \int_{\tau_1}^{\tau_2} d\tau_{\text{sc}} \left(R_{2\pi}^{(L)}(\tau; \tau_{\text{sc}}, \tau_2) I_L(\tau_1, \tau_{\text{sc}}) + R_{2\pi}^{(S)}(\tau; \tau_{\text{sc}}, \tau_2) I_S(\tau_1, \tau_{\text{sc}}) \right) \quad (3.37)$$

with

$$\begin{aligned} R_{2\pi}^{(L)}(\tau; \tau_{\text{sc}}, \tau_2) &= |a_{SL}(\tau; \tau_{\text{sc}}, \tau_2) + \eta a_{LL}(\tau; \tau_{\text{sc}}, \tau_2)|^2, \\ R_{2\pi}^{(S)}(\tau; \tau_{\text{sc}}, \tau_2) &= |a_{SS}(\tau; \tau_{\text{sc}}, \tau_2) + \eta a_{LS}(\tau; \tau_{\text{sc}}, \tau_2)|^2, \end{aligned}$$

$$I_{L,S}(\tau_1, \tau_{\text{sc}}) = \int d\theta \theta \varepsilon(\theta) \left| \alpha_{L,S}(\tau_{\text{sc}}) [f(\theta) + \bar{f}(\theta)] + \alpha_{S,L}(\tau_{\text{sc}}) [f(\theta) - \bar{f}(\theta)] \right|^2 \quad (3.38)$$

and

$$\begin{aligned} a_{LL}(\tau; \tau_{\text{sc}}, \tau_2) &= e^{-i\lambda_L(\tau - \tau_2)} e^{-i\Sigma \cdot (\tau_2 - \tau_{\text{sc}})} \left[\cos(\Omega(\tau_2 - \tau_{\text{sc}})) - \frac{i\Delta\lambda}{2\Omega} \sin(\Omega(\tau_2 - \tau_{\text{sc}})) \right], \\ a_{LS}(\tau; \tau_{\text{sc}}, \tau_2) &= -e^{-i\lambda_L(\tau - \tau_2)} e^{-i\Sigma \cdot (\tau_2 - \tau_{\text{sc}})} \frac{i\Delta\kappa}{2\Omega} \sin(\Omega(\tau_2 - \tau_{\text{sc}})), \\ a_{SL}(\tau; \tau_{\text{sc}}, \tau_2) &= -e^{-i\lambda_S(\tau - \tau_2)} e^{-i\Sigma \cdot (\tau_2 - \tau_{\text{sc}})} \frac{i\Delta\kappa}{2\Omega} \sin(\Omega(\tau_2 - \tau_{\text{sc}})), \\ a_{SS}(\tau; \tau_{\text{sc}}, \tau_2) &= e^{-i\lambda_S(\tau - \tau_2)} e^{-i\Sigma \cdot (\tau_2 - \tau_{\text{sc}})} \left[\cos(\Omega(\tau_2 - \tau_{\text{sc}})) + \frac{i\Delta\lambda}{2\Omega} \sin(\Omega(\tau_2 - \tau_{\text{sc}})) \right]. \end{aligned}$$

$\alpha_L(\tau_{sc})$ and $\alpha_S(\tau_{sc})$ are the coherently regenerated (unscattered) amplitudes at the time of the scattering τ_{sc} , recursively calculated with (3.31) as

$$\begin{aligned}\alpha_L(\tau_{sc}) &= e^{-i\Sigma \cdot (\tau_{sc} - \tau_1)} \left[\alpha_L(\tau_1) \cos(\Omega(\tau_{sc} - \tau_1)) - \frac{i}{2\Omega} (\Delta\lambda\alpha_L(\tau_1) + \Delta\kappa\alpha_S(\tau_1)) \sin(\Omega(\tau_{sc} - \tau_1)) \right], \\ \alpha_S(\tau_{sc}) &= e^{-i\Sigma \cdot (\tau_{sc} - \tau_1)} \left[\alpha_S(\tau_1) \cos(\Omega(\tau_{sc} - \tau_1)) + \frac{i}{2\Omega} (\Delta\lambda\alpha_S(\tau_1) - \Delta\kappa\alpha_L(\tau_1)) \sin(\Omega(\tau_{sc} - \tau_1)) \right];\end{aligned}$$

$$\begin{aligned}\alpha_L(\tau_1) &= e^{-i\lambda_L\tau_1} \alpha_L(0), \\ \alpha_S(\tau_1) &= e^{-i\lambda_S\tau_1} \alpha_S(0),\end{aligned}$$

from the initial amplitudes $\alpha_L(0)$ and $\alpha_S(0)$ as given by (3.8) for initial K^0 and \bar{K}^0 . $R_{2\pi}^{inc}(\tau)$ is to be added to the decay rate after coherent regeneration, $R_{2\pi}^{coh}(\tau)$, to obtain the observed decay rate:

$$R_{2\pi}^{obs}(\tau) = R_{2\pi}^{coh}(\tau) + R_{2\pi}^{inc}(\tau) \quad (3.39)$$

For all practical purposes the contribution of K_L to the 2π decay rate may safely be neglected and (3.37) reduces to

$$R_{2\pi}^{inc}(\tau) = \frac{\pi}{2} \gamma v N \int_{\tau_1}^{\tau_2} d\tau_{sc} |a_{SS}(\tau; \tau_{sc}, \tau_2)|^2 I_S(\tau_1, \tau_{sc}). \quad (3.40)$$

3.3.3 Numerical computation for $\pi^+\pi^-$ decays at CPLEAR

In order to carry out the integration (3.40) we must know the angular variation of the scattering amplitudes $f(\theta)$, $\bar{f}(\theta)$ and the experimental detection efficiency $\varepsilon(\theta)$.

$f(\theta)$ and $\bar{f}(\theta)$ can be well reproduced by an optical model calculation which results in an integration over a weighted Bessel function. The weighing function to be applied is not the same for K^0 and \bar{K}^0 reflecting the different interaction length of the two states inside the nucleus and therefore $f(\theta)$ and $\bar{f}(\theta)$ have somewhat different slopes [36]. For our estimate, however, we do not take into account this rather small difference [37] and assume furthermore that only the magnitudes of the amplitudes are affected by the angular variation:

$$\frac{\bar{f}(\theta)}{\bar{f}(0)} \approx \frac{f(\theta)}{f(0)} \approx \frac{|f(\theta)|}{|f(0)|} =: F(\theta)$$

This last assumption is not valid in the vicinity of resonances, but the deviations will not significantly alter our conclusions. The θ integrations (3.38) then simplify to

$$I_{L,S}(\tau_1, \tau_{sc}) = |\alpha_{L,S}(\tau_{sc}) [f(0) + \bar{f}(0)] + \alpha_{S,L}(\tau_{sc}) [f(0) - \bar{f}(0)]|^2 I_\theta$$

with

$$I_\theta = \int d\theta \theta \varepsilon(\theta) |F(\theta)|^2. \quad (3.41)$$

For $f(0)$ and $\bar{f}(0)$ we take the theoretical results of Baldini and Michetti [38]. Their values are in agreement with the work of Eberhard and Uchiyama [39] who give the difference $f(0) - \bar{f}(0)$ only.

We then describe $|F(\theta)|^2$ by a Gauss function [30, 36],

$$|F(\theta)|^2 \approx \exp \left[-\frac{1}{2} \left(\frac{\theta}{\sigma_f} \right)^2 \right]. \quad (3.42)$$

We expect the half-width σ_f to be roughly inversely proportional to the momentum. Experimental data exist for K^\pm scattering on carbon nuclei at 800 MeV/c [37] and indicate $\sigma_f \approx 6.8^\circ$. For lower momenta, we use calculations of elastic K_L scattering [40] to estimate σ_f . At 500 MeV/c we find a value of $\approx 9.8^\circ$.

For $\pi^+\pi^-$ decays, our results depend only weakly on the exact angular behaviour of the scattering amplitudes because the integral I_θ is dominated by the detection efficiency.

The angular detection efficiency of neutral kaons decaying to $\pi^+\pi^-$ for the CPLEAR experiment, i.e. the probability for a scattered $K^0(\bar{K}^0)$ to survive all selection criteria including the constrained fit for $\pi^+\pi^-$ decays (9C-fit, see Section 6.2), was first studied by Ch. Yeche [41], and more recently and more thoroughly by Ph. Bloch [42]. The computed acceptance curves are fairly well approximated by the sum of two Gaussians,

$$\varepsilon(\theta) \approx \alpha \exp \left[-\frac{1}{2} \left(\frac{\theta}{\sigma_1} \right)^2 \right] + (1 - \alpha) \exp \left[-\frac{1}{2} \left(\frac{\theta}{\sigma_2} \right)^2 \right], \quad (3.43)$$

where the values of the parameters α , σ_1 and σ_2 depend on the radius at which the scattering occurs. For a scatterer at a distance of about 10 cm for instance we find $\alpha \approx 0.8$, $\sigma_1 \approx 1.7^\circ$ and $\sigma_2 \approx 3.5^\circ$; a smaller distance leads to smaller widths.

Inserting the numbers for various energies and scattering radii into (3.42) and (3.43) yields values for the θ integration (3.41) between 1 and 2.5×10^{-3} [43]. For the carbon regenerator used in our experiment we find an average of

$$I_\theta \approx 1.35 \times 10^{-3}. \quad (3.44)$$

Having made these simplifications it is a straightforward (albeit time consuming) task to compute the number of additional $\pi^+\pi^-$ decays caused by incoherent regeneration for any geometry as long as we can compute the time the particle spends inside the regenerator.

4 THE CPLEAR EXPERIMENT

When in 1982 physicists congregated to Erice to discuss the experimental programme of the new Low Energy Antiproton Ring (LEAR) under construction at CERN, Gabathuler and Pavlopoulos presented their proposal [44] to turn the antiproton factory into a neutral kaon factory. The antiprotons would be used to separately produce K^0 and \bar{K}^0 particles in large amounts in order to study CP, T and CPT symmetry: the CPLEAR idea was born!

The whole idea is based on the fact that $p\bar{p}$ annihilation at rest not only results in multi-pion final states but can also produce strange particles. With a probability of about 0.5%, a charged and a neutral kaon are produced, together with a charged pion to balance charge [45]:

$$(p\bar{p})_{\text{rest}} \rightarrow K^0 K^- \pi^+ \quad \text{or} \quad (p\bar{p})_{\text{rest}} \rightarrow \bar{K}^0 K^+ \pi^- \quad (4.1)$$

The neutral kaon must compensate for the strangeness of the charged kaon. Therefore, if we can identify the charged kaon and measure the sign of its charge, we know with certainty the strangeness of the neutral kaon at the time of production. We can then separately study the decays of K^0 and \bar{K}^0 —any difference in the way they decay will be a clear signal of CP (or perhaps even CPT) violation. For a quantitative analysis, it is most useful to form time dependent asymmetries for the decays into different final states f :

$$A_f(\tau) = \frac{R(\bar{K}^0 \rightarrow f)(\tau) - R(K^0 \rightarrow f)(\tau)}{R(\bar{K}^0 \rightarrow f)(\tau) + R(K^0 \rightarrow f)(\tau)} \quad (4.2)$$

The physics of Eqs. 4.1 and 4.2 constrain the design of the experiment: Selecting the “golden” annihilation channel (4.1) from the many multi-pion channels requires fast identification of the charged kaon. For the precise measurement of the asymmetries (4.2) a large quantity of statistics is needed, to be achieved through a high \bar{p} rate, an efficient triggering system and a large geometrical coverage. To measure the asymmetries as a function of time, the detector must provide accurate information on the positions of production and decay vertices as well as the momenta of the final state particles. The detector should also be capable of distinguishing between the various neutral kaon decay modes. Furthermore the detector volume must be large enough in order to cover the K_L – K_S interference and contain as little material as possible to minimize regeneration effects.

The requirements are met by a set of sub-detectors working in cooperation with a sophisticated trigger system, and a high rate, low energy antiproton source. In the following two Subsections we briefly describe the antiproton source used by CPLEAR and give an overview of the detector and its various elements.

4.1 Low energy antiprotons at CERN

At CERN, antiprotons are produced by shooting 26 GeV/c protons coming from the Proton Synchrotron (PS) onto a copper target. The emerging antiprotons have typical momenta between 3 and 4 GeV/c. They are accumulated and stochastically cooled in the antiproton accumulator complex from where they are transferred back to the PS for redistribution to the Sp \bar{p} S and LEAR accelerators⁹ [46]. Antiprotons bound for LEAR are decelerated in the PS to 609 MeV/c. Inside LEAR the momentum is reduced to 310 MeV/c by stochastic cooling and further to 200 and 105 MeV/c by electron cooling.¹⁰ CPLEAR (experiment PS195) receives antiprotons of 200 MeV/c with a momentum spread $\Delta p/p$ of 0.05% at a rate of 600–800 kHz in spills of 60–90 min extraction length [48]. After a spill is delivered it takes about 15 min to refill the stack.

4.2 The CPLEAR detector

Although there is a fixed target, the CPLEAR detector has the onion-like structure typical of detectors at colliders. This is because the antiproton annihilations are observed at rest and the produced particles are distributed isotropically.

9. After the shutdown of the Sp \bar{p} S ring in 1990 LEAR was the only antiproton user at CERN.

10. For a nice and readable account on stochastic and electron cooling see Ref. 47.

Figures 2a and b show the profile and a cross section of the detector, respectively. We briefly describe each detector component going from the centre outwards. For a comprehensive presentation of the CPLEAR detector see Ref. 49.

4.2.1 The beam-target system

The antiproton beam coming from LEAR is centred on the detector by two vertical and two horizontal bending magnets (dipoles) followed by a quadrupole doublet. Before hitting the hydrogen target, the antiprotons penetrate a beam monitoring system consisting of three parts:

1. Two multi-wire proportional chambers (MWPCs) measure the beam shape perpendicular to its (nominal) axis. The output is used by a beam centring system to automatically correct for deviations by changing the bending power of the dipole magnets.
2. A beryllium degrader reduces the antiproton momentum to about 80 MeV/c. It is adjustable via its inclination to control the \bar{p} stopping distribution along the beam axis.
3. The beam scintillator just in front of the target signals the arrival of an antiproton and starts the trigger sequence.

A detailed description of these apparatus is given in Ref. 50. The target has the shape of a cylinder (12 mm radius, 120 mm length) and is filled with gaseous hydrogen of 27 bar pressure. It is surrounded by a small proportional chamber (15.3 mm radius at the wires) containing 96 axially placed anode wires and 100 helical cathode strips in a gas mixture of 80% carbon tetrafluoride and 20% isobutane. This chamber was installed in 1995 as a detector upgrade and named PC0 because of its position inside the two existing proportional chambers. It is used for background rejection at an early trigger stage (see Paragraph 4.2.6). Unfortunately, it cannot be used for event reconstruction since it is mounted on the beam monitor support structure and has no sufficiently rigid connection with the other tracking devices.

4.2.2 The tracking detectors

The tracking of charged particles is performed by two proportional chambers (PC1 and PC2), six drift chambers (DC1 to DC6) and two layers of streamer tubes (ST1 and ST2).

The proportional chambers provide the trigger with a hit pattern which allows the determination of the event multiplicity and the classification of a track as “primary” or “secondary.” A track is regarded (online) as “secondary” if there is no hit associated with it in either PC. Since both PCs together are 99.9% efficient, such a track is very unlikely to originate from the annihilation vertex and is therefore disregarded by the trigger. The two chambers are equipped with axially placed anode wires and helical cathode strips at angles of 19.5° (PC1) and 27.9° (PC2) with respect to the detector axis. The gas mixture used is 79.5% argon, 20% isobutane and 0.5% freon (by volume) [51] at a high voltage of 2700 V.

The six radially equidistant drift chambers supply the main tracking information [52]. Their features are characterized by the high event-rates: The drift-cell size is limited to 5 mm to keep the drift time below 120 ns, and a double sense-wire technique is used to solve the left-right ambiguity without time-consuming software reconstruction. The anode wires are parallel to the detector axis, the cathode strips helical at angles between 11.6° (DC1) and 25.4° (DC6). The strips of four chambers (1, 2, 4 and 6) are read out to obtain an offline measurement of the longitudinal position z of a track (3 mm resolution). The chambers are operated at 2450 V with a 50:50 mixture of argon and ethane (by volume).

Two layers of 192 streamer tubes each complete the tracking system. Their principle task is to deliver a fast readout of the z coordinate of a track to the trigger. At a voltage of 4000 V, the tubes are operated in the limited streamer mode, i.e. a penetrating particle sets off a fast rising charge pulse on the anode wire. The pulse reaches the two ends of a tube with a certain time difference which is translated to a z coordinate. The resolution obtained is 2 cm online and 1.5 cm offline. The gas mixture comprises isobutane, argon and methylal (50%, 46% and 4%, respectively).

4.2.3 The particle identification detector

The Particle Identification Detector (PID), one of the cornerstones of the experiment, performs the essential task of identifying the charged kaon in reaction (4.1). This is achieved with a Čerenkov detector, the properties of which are optimised to produce light (no light) when penetrated by a charged

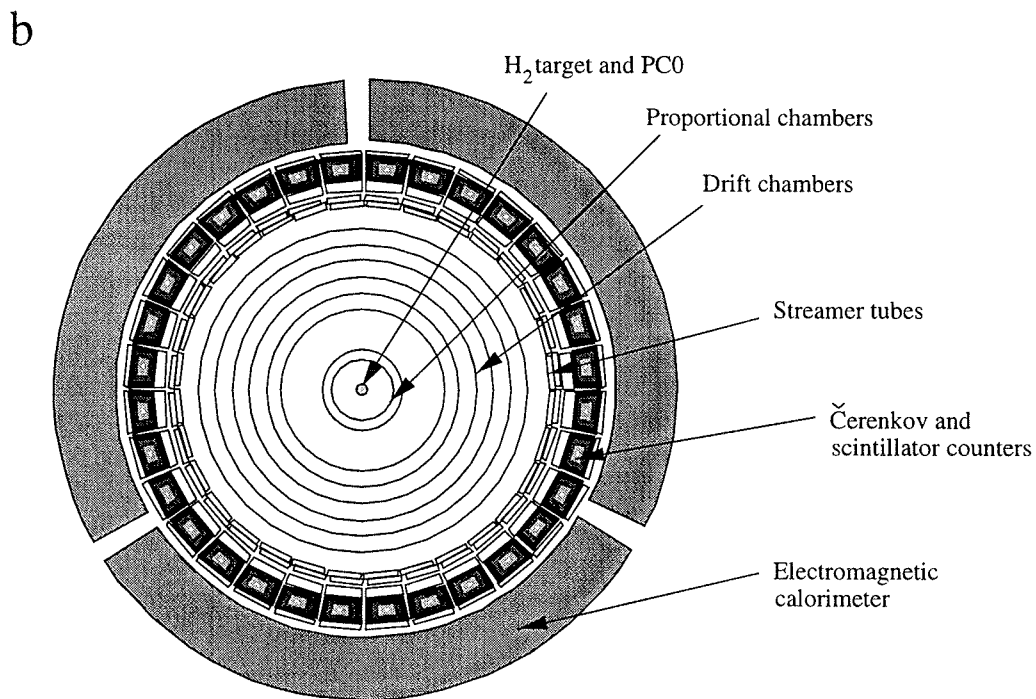
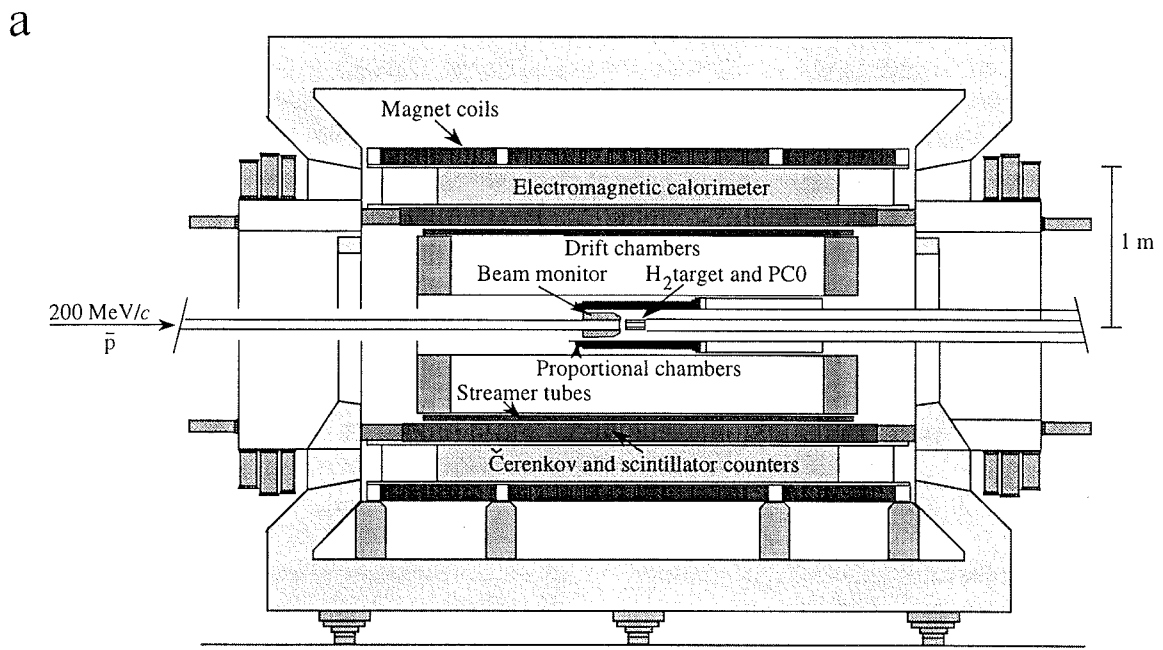


Figure 2: Profile (a) and cross section (b) of the CPLEAR detector (before installation of the carbon regenerator).

pion (charged kaon). To come as close as possible to the ideal threshold of $\beta = 0.84$ (0.81 if energy loss is taken into account) imposed by the kinematics of (4.1), the detector is filled with the liquid radiator C_6F_{14} which has a refractive index of 1.25, very low dispersion and good transparency [53]. A wavelength shifter (2,5-diphenyl Oxazole, PPO) is added to improve the photon-electron yield.

The Čerenkov detector is arranged in 32 sectors surrounding the cylindrical tracking detectors. Each sector is sandwiched between two plastic scintillators which ensure that a charged kaon candidate traverses the Čerenkov detector. In addition to their role as a trigger hodoscope the scintillator signals are used, both offline and online, to identify particles by their energy loss and time of flight.

Further details on the PID can be found in Ref. 54.

4.2.4 The electromagnetic calorimeter

To study final states containing neutral pions, CPLEAR uses a highly granular lead-gas sampling calorimeter, designed to detect photons with energies above 50 MeV. A comprehensive description of this sub-detector can be found in Ref. 55. The electromagnetic calorimeter was not used for the regeneration measurement.

4.2.5 The magnet

All sub-detectors are situated in a solenoidal magnet which provides a magnetic field of 0.44 T. The field polarity is changed approximately three times per day to avoid biases due to geometrical imperfections. The magnet was formerly used in an e^+e^- collider experiment at Orsay (DM2).

4.2.6 The trigger system

To select reaction (4.1) from the very large background of useless annihilations, CPLEAR uses a multilevel hardwired processor system, the backbone of this experiment.

The first level (early decision logic) looks for a kaon candidate, defined by the telltale signal from one of the Čerenkov sandwiches, i.e. a signal from both scintillators but no Čerenkov response ($S\bar{C}S$). The kaon candidate must be accompanied by at least one additional charged track identified as a hit in the inner scintillator of any of the other sectors. Furthermore, the early decision logic demands exactly two clusters in the innermost proportional chamber (PC0). This eliminates a large fraction of unwanted multi-pionic and multi-kaonic annihilation backgrounds like $KK\pi\pi$. The early decision logic takes 60 ns to execute and reduces the event rate by a factor of 15.

The second trigger stage uses the drift chamber information of the sector where the kaon candidate has been found to obtain an estimate of the transverse momentum of the associated track. A p_t cut at about 270 MeV/c (minimum value) is applied to remove false kaon candidates feigned by slow pions. This requires 400 ns and achieves a further rate reduction by a factor of about 2.6.

At the following level, called intermediate decision logic, the tracks are counted and classified as “primary” or “secondary” which takes about 80 ns. No events are rejected at this level.¹¹

At the configuration stage, the full tracking information is available. The tracks are entirely reconstructed and parameterized within 1900 ns. Again, no event selection is made.

The register control files the tracks according to their sign and identity (kaon, pion) for further processing (500 ns, no rate reduction).

The event is now passed on to two processes running in parallel: a kinematical cut is made on the total momentum of the primary $K\pi$ pair, $|\mathbf{p}_K| + |\mathbf{p}_\pi| > 700$ MeV/c (500 ns, rate reduction 2.2) while an additional hardwired processor performs a more accurate particle identification based on energy loss and time of flight measurements obtained with the inner scintillator, and the number of photoelectrons in the Čerenkov detector. Events not compatible with the values expected from “golden” events (4.1) are rejected (1900 ns, rate reduction 24).

In the case of only two primary and no secondary tracks, a dedicated hardwired processor calculates the number of showers seen by the electromagnetic calorimeter (not used during the regeneration run).

11. The description for the data runs relevant for this work is given. In earlier data runs, specially before the installation of the PC0, rate reductions were also performed at the intermediate decision logic, configuration and register control levels.

The total rate reduction achieved is around 2000 and events are read out after $34 \mu\text{s}$.

4.2.7 Data acquisition

For each sub-detector, there is a dedicated readout system, called valet+, collecting the data from the front-end electronics. The data are then passed on to an additional valet+ which combines the information of one event (“event builder”) and transfers it via a data distribution system to two IBM 3480 cartridge drives. A small fraction of the events is directed to a VAX cluster for online monitoring.

One event typically takes up about 2500 bytes. The read out rate during the regeneration run was between 200 and 300 Hz.

4.2.8 Event display

Figure 3 shows the hit pattern of a typical “golden” event. The primary kaon’s $\overline{S\overline{C}S}$ signature in the particle identification detector is clearly visible. The neutral kaon, invisible in the detector, decays after about 15 cm into two charged pions, the tracks of which are reconstructed from their drift chamber hits.

4.3 Regeneration effects and their correction

With our measurement of the forward scattering amplitudes we want to improve the accuracy of the regeneration correction applied to the observed decay rates. The correction factor is calculated for each event individually. From the coordinates of the annihilation and the decay vertex we find out the detector components that the neutral kaon has crossed and, taking into account its momentum, how much time it spent in each of them. Then we subject the two-dimensional kaon amplitude—known at the time of production from strangeness tagging—to a series of matrices along the lines of (3.31), each matrix corresponding to a material layer penetrated by the particle. Where necessary, a correction for incoherent regeneration is computed according to (3.40) and added to the decay rate. This small adjustment is only required for the $\pi^+\pi^-$ analysis, owing to the high statistical precision.

It is obvious that the regeneration amplitudes of the various materials represent only part of the input to this correction procedure. Just as important is the knowledge of the size, the atomic composition and the location of each of the relevant detector elements. Therefore we carefully compiled all the essential parameters on each detector part to input them into our correction code. In Tables 1 and 2 we list this information for reference.

Before the results of our measurement of the regeneration amplitudes became available the optical model calculations by Eberhard and Uchiyama [39] were used as input to the correction code. This gave a correction of about 2.5° on ϕ_{+-} . In view of the complete lack of any kind of error estimate in the publication of Eberhard and Uchiyama (and their firm refusal to comment on this matter) we investigated ourselves the quality of their K -nucleon input data and the uncertainties associated with the extrapolation to heavier nuclei. The study came to the conclusion that one should reckon with an average uncertainty of $\pm 13\%$ on the magnitudes and $\pm 9^\circ$ on the phases of the calculated amplitudes [56]. Variation of the amplitudes within these limits changes ϕ_{+-} by $\pm 0.6^\circ$ —roughly the size of the statistical error to be expected after the analysis of the full CPLEAR data set. To provide a solid experimental footing for the regeneration correction and to reduce the systematic error on ϕ_{+-} due to this correction to a level significantly below the statistical error are the aims of our regeneration experiment, the subject of the next Section.

on new target

Table 1: Materials used in the inner part of the CPLEAR detector which contribute to regeneration effects.

material	chemical composition	density [g/cm ³]
kevlar	C ₁₄ H ₁₀ O ₂ N ₂	1.40
kapton	C ₂₂ H ₁₀ O ₅ N ₂	1.42
araldite	64.4% C, 19.6% O, 8% H, 4.9% N, 3% Si, 0.1% Cl	1.10
rohacell	C ₈ H ₁₁ O ₂ N	0.05
mylar	C ₅ H ₄ O ₂	1.39
hydrogen (30 bar)	H ₂	2.47 × 10 ⁻³
air	78% N, 21% O, 1% Ar	1.21 × 10 ⁻³
gas mixture PC0	80% CF ₄ , 20% CH(CH ₃) ₃	3.65 × 10 ⁻³
gas mixture PCs	89.5% Ar, 20% CH(CH ₃) ₃ , 0.5% CF ₃ Br	1.96 × 10 ⁻³
gas mixture DCs	50% Ar, 50% (CH ₃) ₂	1.57 × 10 ⁻³

Table 2: The inner (cylindrical) layers of the CPLEAR detector. Some of the radii are approximate only. Most relevant for the regeneration correction are the thicknesses of the solid layers.

component	radius [cm]	thickness [μm]	material	component	radius [cm]	thickness [μm]	material
target (old)	0.0	11300	hydrogen 70% (2.8 mg/cm ²)	PC2	12.4	13.8	araldite
	1.13	550	kevlar 800 (80 mg/cm ²)		12.4	25	kapton
	1.185	1350	air		12.4	6000	gas mixture
	1.32	100	kapton		13.0	25	kapton
PC0	1.33	4000	gas mixture		13.0	13.8	araldite
	1.73	100	kapton		13.0	1920	rohacell
	1.74	72850	air		13.2	13.8	araldite
	9.025	25	kapton		13.2	25	kapton
	9.025	13.8	araldite		13.2	68000	air
	9.025	1920	rohacell	DC shell	20.0	25	mylar
	9.225	13.8	araldite		20.0	11000	rohacell
	9.225	25	kapton		21.1	25	mylar
PC1	9.225	6000	gas mixture		21.1	39000	gas mixture
	9.825	25	kapton		25.0	50	mylar
	9.825	13.8	araldite	DC1	25.0	10000	gas mixture
	9.825	1920	rohacell		26.0	50	mylar
	10.025	13.8	araldite		26.0	40000	gas mixture
	10.025	25	kapton		20 + 5n	50	mylar
	10.025	21750	air	DCn	20 + 5n	10000	gas mixture
	12.2	25	kapton	(n ≤ 6)	21 + 5n	50	mylar
	12.2	13.8	araldite		21 + 5n	40000	gas mixture
	12.2	1920	rohacell				

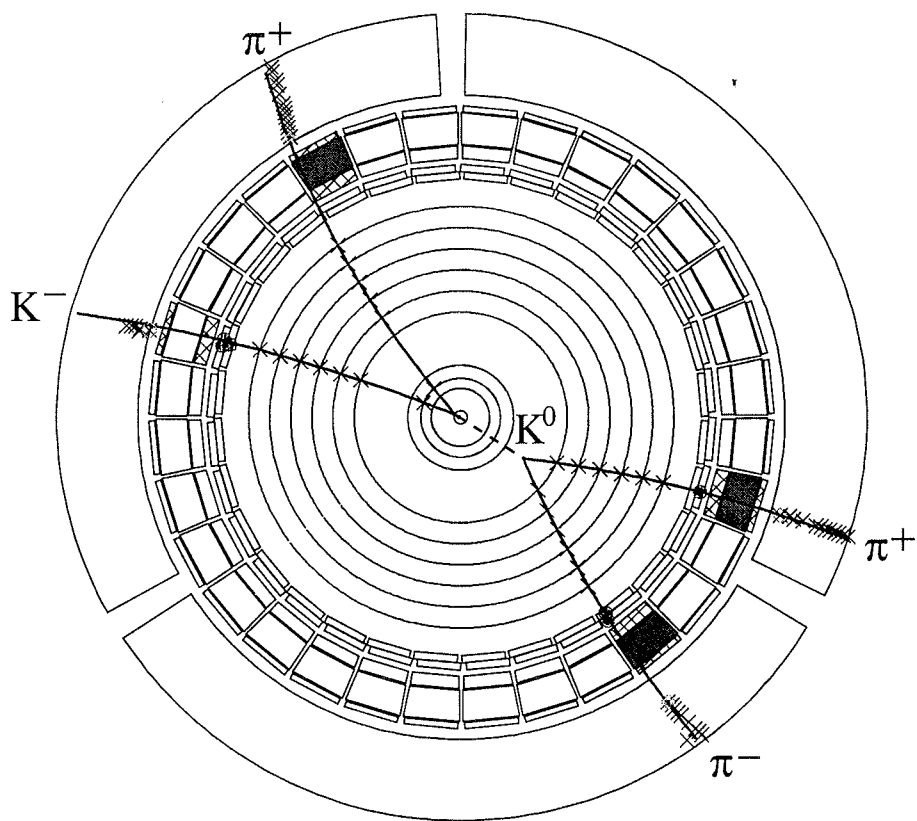


Figure 3: Graphical representation of a typical $K^0 \rightarrow \pi^+\pi^-$ event as recorded by the CPLEAR detector.

5 THE CPLEAR REGENERATION EXPERIMENT

The measurement of regeneration amplitudes with CPLEAR is based on the well-proven method of time dependent decay rate asymmetries $A_f(\tau)$ (4.2). Clearly, a layer of regenerating medium in the decay path of the neutral kaons has an influence on the measured asymmetry of all final states f . We choose $f = \pi^+\pi^-$ for various reasons: First of all, the regeneration effect is very large in this channel (hence the need to measure it!) owing to the interference between the inherent and regenerated K_S amplitudes. Further advantages are the large branching ratio ensuring good statistics and the simple event topology (see Fig. 3) allowing straightforward reconstruction with minimal background.

Our choice of the two pion final state and the geometry of the existing detector lead to several constraints in the design of the regenerator, which will be discussed in the following Subsection.

5.1 Design and installation of the regenerator

As was briefly outlined in Section 1.3 we want to let the neutral kaons cross a solid regenerator before recording their decays into two pions. It is not obvious how to realize this simple idea in a 4π detector. We decided to adapt the regenerator design to the cylindrical detector geometry by choosing the shape of a tube segment. The partial angular coverage allows the selection of events with neutral kaons regenerated in the carbon but no charged primary tracks crossing it.

Apart from the trivial (linear) effects of the density and the thickness of the regenerator, there is one more important parameter to be considered for the experimental arrangement, the distance of the regenerator from the $K^0(\bar{K}^0)$ production point. Fig. 4 shows the two pion decay rate asymmetry for the same regenerator, set up at different distances (without the complications arising from oblique particle tracks). It can be seen that the effect is largest for a regenerator distance of about five K_S decay lengths.

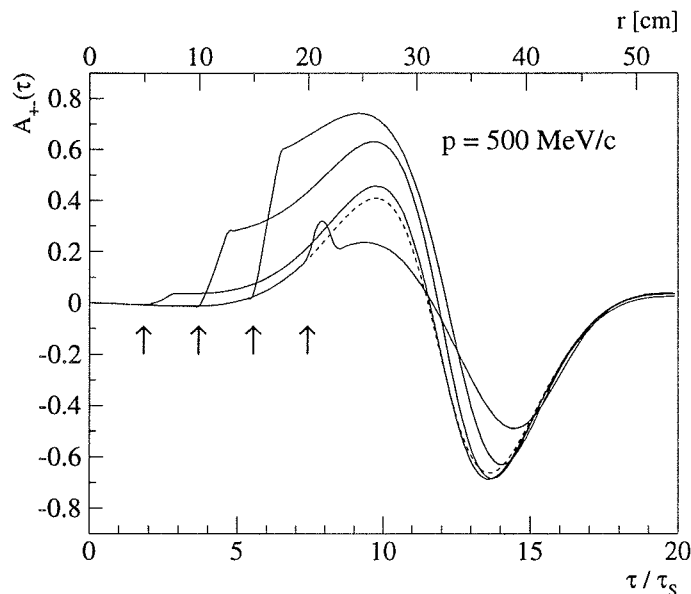


Figure 4: Two pion decay rate asymmetries $A_{+-}(\tau)$ for mono-energetic neutral kaons of 500 MeV/c momentum with a 2.5 cm carbon regenerator set up at 5, 10, 15 and 20 cm (arrows). The vacuum asymmetry is marked as a dashed line.

For the highest neutral kaon momentum available through reaction (4.1), 750 MeV/c, this translates to a regenerator distance of 20 cm, roughly the location of the inner shell of the first drift chamber. Therefore a regenerator distance of around 10–15 cm would be ideal for measurements in the momentum range between 200 and 750 MeV/c (below 200 MeV/c the number of events becomes very small). However, the need for high statistics and good reconstruction quality favors a regenerator closer to the target. The compromise made consists in placing the regenerator as close as possible to the inner shell of the first proportional chamber (PC1). That way we still obtain a distinct step in the measured asymmetry at high

momenta whilst having available reasonable statistics at low momenta and the essential reconstruction efficiency provided by the proportional chambers.

Having found the optimal position for the regenerator, there remains the question of how to install it there. The lack of time and manpower before the start of the regeneration run precluded the option of opening the end-cap of the detector and mounting the regenerator like a wire chamber. Instead the regenerator had to be inserted into the detector through the opening left for the incoming antiproton beam. Attached to the end of the beam pipe (together with the beam monitor) it was brought into position in the central detector region. Owing to the small diameter of the insertion tube, the regenerator could reach its final radial position only once it was inside the detector. A pneumatic device, operated by remote control under video surveillance, was designed specially to perform this movement. It took a supreme effort on the part of the CERN technicians to complete this delicate construction on time.

Figure 5 shows a cross section of the inner detector with the regenerator in position.

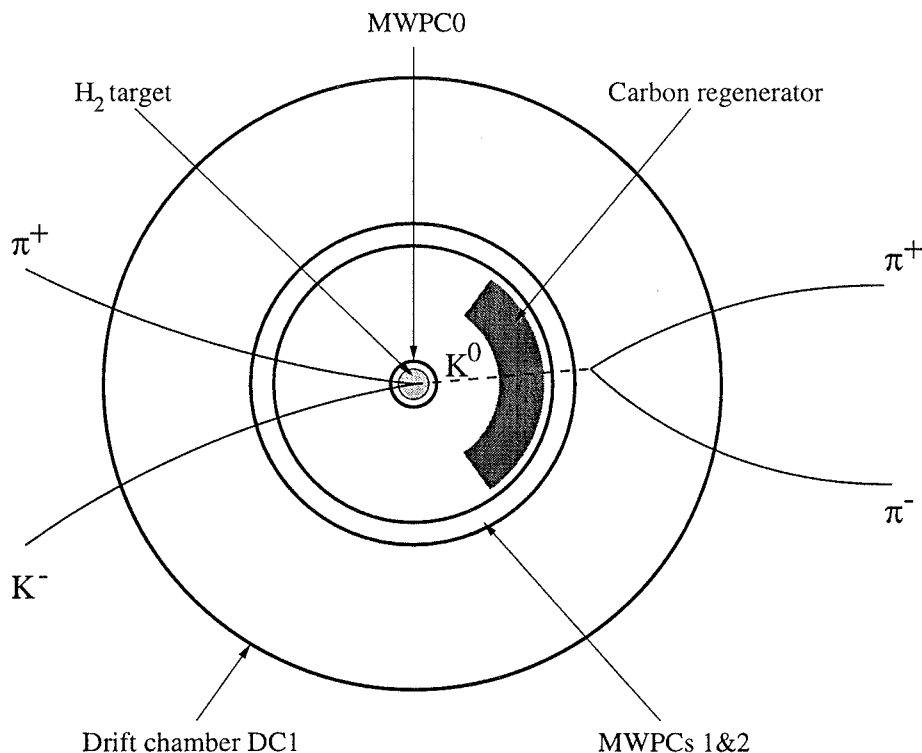


Figure 5: Expanded view of the inner detector with the carbon regenerator in position. The diagram of a typical regeneration event is overlaid.

5.2 The carbon regenerator

We use carbon (^{12}C) as the regenerating medium because the atomic compositions of most of the relevant detector materials are dominated by this element (see Section 4.3). Measurements with a pure chemical element moreover facilitate the comparison with theory and other experiments. In this respect, the ^{12}C nucleus is a particularly handy one thanks to its isosymmetry (equal number of protons and neutrons).

The carbon from which the regenerator was made was manufactured by Le Carbone SA, Bern. Their grade 2120 graphite material (very fine grain structure) has a density of 1.85 g/cm^3 , an open porosity of 8%, a shore hardness of D-75 and an ash content of less than 0.1%. Higher density graphite ("pyrocarbon") was not available for our geometry.

The regenerator has the shape of a segment of a hollow cylinder with the following dimensions: inner radius 5.8 cm, outer radius 8.3 cm, length 25.5 cm and opening angle 115° . This results in a thickness of 2.5 cm and a total weight of 1.67 kg. Deviations from these desired values were found to be completely negligible for our measurement.

Another important prerequisite for our measurement is that the density of the carbon be constant over the entire volume. This was checked by subjecting the regenerator to a computerized tomographic imaging analysis [57], performed at the Institute of Biomedical Engineering and Medical Informatics at ETH Zurich. The relative local density variations found do not exceed 0.8%.

5.3 Measurement of the regenerator position

It can be seen from Fig. 4 that the distance of the regenerator from the $K^0(\bar{K}^0)$ production point has a very sizable influence on the measured decay rate asymmetry. In our situation—regenerator distance between 1.5 and $5\tau_S$ —the effects of an increased distance and a larger regeneration amplitude are almost indistinguishable. Thus good knowledge of the position of the carbon regenerator relative to the tracking chambers is of utmost importance for our measurement.

A priori this position is known to only a few millimetres, corresponding to variations in the regeneration amplitude of the order of 10–20%. The large uncertainty arises from the fact that the regenerator is mounted on the movable beam pipe (cf. Section 5.1) which has no rigid connection with the fixed parts of the detector such as the tracking chambers.

Two methods were applied to determine the position of the regenerator inside the detector: a conventional survey and a photon conversion analysis. Before comparing the results of the two measurements we must choose a suitable parameterization of the position and orientation of the regenerator inside the detector.

Three numbers are needed to describe the position of the regenerator in the plane perpendicular to the detector axis, two coordinates and an angle. For practical reasons we work with the coordinates (x_m, y_m) of the cylinder axis and the angles φ_- and φ_+ under which the edges of the regenerator are seen from the coordinate origin. The second angle can be calculated from the known angular size of the carbon piece (115°) so that its measurement serves as a cross check.

In our experimental setup with the regenerator on the positive x -side (Fig. 6) the regenerator distance is almost entirely determined by the value of x_m (if the regenerator is not too badly misaligned). x_m is therefore by far the most significant position parameter to be measured. In contrast to x_m errors on y_m practically cancel in the total decay rate asymmetry if the detector is φ -symmetric. Although this requirement unfortunately is not fully met by the CPLEAR detector, y_m is still much less important than x_m . The precision on the angles φ_+ and φ_- finally is not relevant as long as we apply safe cuts on φ when selecting our kaon sample.

To fully describe the regenerator's position in three dimensions accounting for a possible misalignment with respect to the detector axis we define the inclinations $\Delta x/\Delta z$ and $\Delta y/\Delta z$ of the regenerator axis in the x - and y -projections, respectively. These parameters are not very significant for the regeneration measurement because, similarly to y_m , their errors tend to cancel in the decay rate asymmetry.

5.3.1 Surveyor measurement

The CERN surveyors measured the x - y -positions of two marks fixed to the downstream end of the regenerator immediately after data taking had been completed. Such positions are measured relative to some reference axis through the detector with a claimed accuracy of 0.03 cm in both dimensions. To relate this reference axis to the origin of the CPLEAR coordinate system as used in the offline analysis we compare the surveyors' measurement of the beam monitor with the beam position we see in the data. Analysis of the last ten minimum bias trigger tapes¹² written yields the following coordinates for the position of the antiproton beam (B):

$$\begin{aligned}x_B &= 0.08 \pm 0.02 \text{ cm,} \\y_B &= -0.06 \pm 0.05 \text{ cm,}\end{aligned}$$

where the given errors are simply the standard deviations of the ten measurements. The large error in the vertical (y) coordinate reflects the significant difference between the positions for the two magnetic

12. The minimum bias trigger requires one charged track to be found in the detector. Minimum bias events are recorded for calibration purposes after each change of the magnetic field polarity.

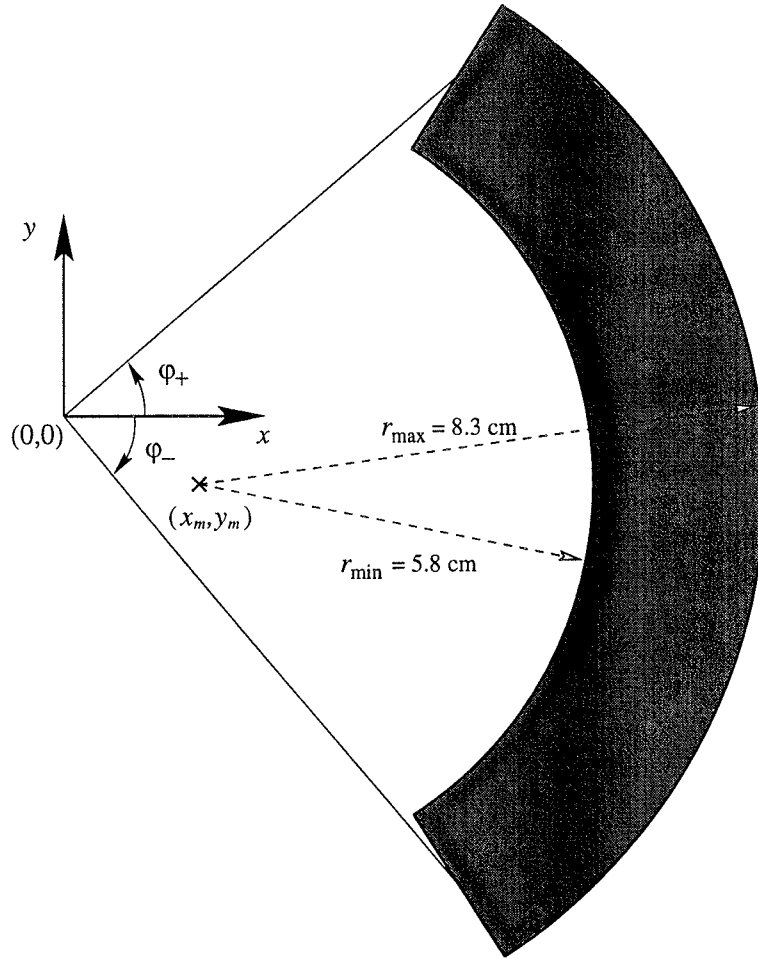


Figure 6: Parameters used to describe the position of the regenerator in the transverse detector plane (not to scale).

field polarities (M1 and M2) which is not well understood. During that period the beam was not aimed at the centre of the beam monitor but to a point with coordinates $(-0.05, -0.07)$ in an attempt to avoid annihilations in the target window.

The measured coordinates of the two marks glued on the regenerator can easily be transformed to the four desired parameters. For the position of the centre relative to the beam monitor (BM) we get

$$\begin{aligned} x_m - x_{\text{BM}} &= 0.15 \pm 0.04 \text{ cm}, \\ y_m - y_{\text{BM}} &= -0.15 \pm 0.04 \text{ cm}, \end{aligned}$$

where an error in the positioning of the stickers of the same order of magnitude as the surveying error has been taken into account.

Combining this with the offline data on the beam position and working out the angles we arrive at the final result of the surveyors' measurement which gives the following values for the downstream end of the regenerator ($z = +12.75$ cm):

$$\begin{aligned} x_m &= 0.28 \pm 0.05 \text{ cm} & \varphi_- &= -54.0^\circ \pm 0.4^\circ \\ y_m &= -0.14 \pm 0.07 \text{ cm} & \varphi_+ &= 56.7^\circ \pm 0.4^\circ \end{aligned} \quad (5.1)$$

The regenerator's opening angle derived from these data is $\alpha = 114.7^\circ \pm 0.5^\circ$, in remarkable agreement with the expected value of 115° .

The inclination of the regenerator could not be measured by the surveyors while it was still installed. Later attempts to ascertain the inclination relative to the support structure lead to inconclusive results—apparently the support structure was significantly disturbed during the removal procedure.

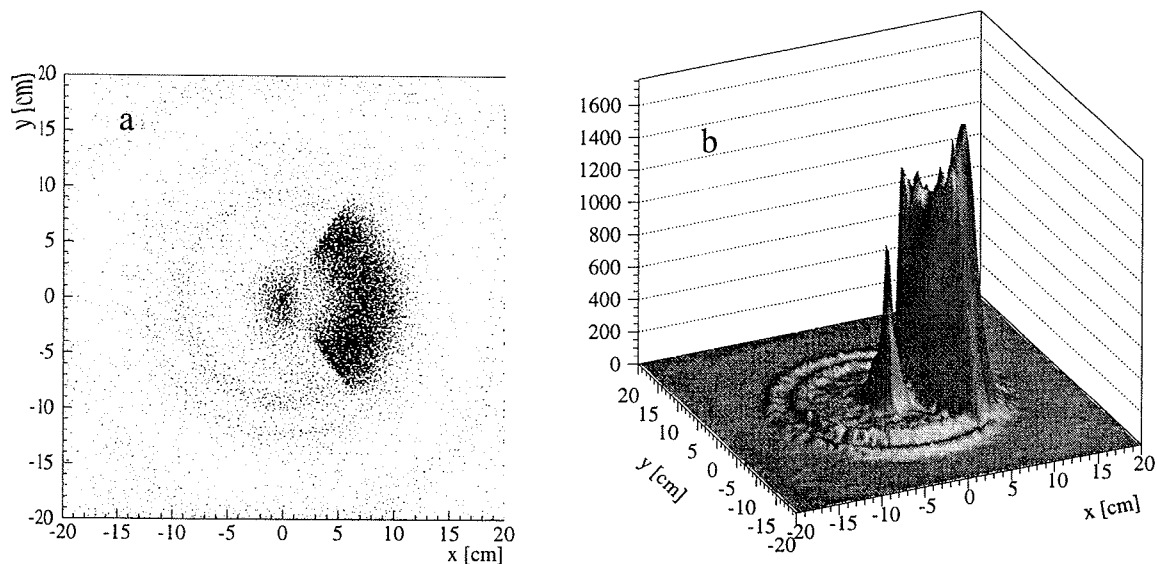


Figure 7: Scatter plot (a) of reconstructed photon conversions in the inner part of the detector and the same information as a surface plot (b) in which height stands for density of conversions (arbitrary units). The carbon regenerator appears as a “mountain range” to the right of the centre. The peaks in the lower half of the plot are higher because of the better detector efficiency in this sector. The two “craters” are due to the proportional chambers and the central peak represents conversions inside the hydrogen target. The latter appears somewhat asymmetric owing to the screening effect of the regenerator (e^+e^- pairs escaping identification after undergoing multiple scattering inside the carbon).

5.3.2 Photon conversion analysis

The process $\gamma \rightarrow e^+e^-$ (photon conversion) is only possible in matter and therefore the measured density of such conversions roughly maps the distribution of matter in the detector similar to an X-ray image.

To map the cross section of the regenerator, photon conversions were selected according to the method described in Ref. 58 (see also Section 6.2.3). Fig. 7 shows the integrated distribution of conversion vertices in the x - y plane recorded in about fifty net hours of data taking, spread over the regeneration run. The regenerator as well as the proportional chambers and the rohacell shell in front of the drift chambers are clearly visible. The radial resolution for each vertex is very poor (about 1.5 cm) as a result of the collinearity of the e^+e^- pair. However, when taking into account the known circular shape of the regenerator, a rather precise measurement of its position can be obtained from the conversion statistics.

The data set used comprises nine subsets, each corresponding to five hours of data taking. The total number of selected conversion events is 656 961. The subsets were selected according to their recording date with approximately one calendar week in between. This allows one to search for systematic time dependent effects (for instance an increasing bend downwards caused by material fatigue in the support).

The extraction of the angles φ_- and φ_+ is straightforward: we project the r - φ -histogram of conversion vertices onto the φ -axis and fit a Gaussian box function

$$N(\varphi) = A \left[\operatorname{erf} \left(\frac{\varphi_+ - \varphi}{\sqrt{2}\sigma} \right) - \operatorname{erf} \left(\frac{\varphi_- - \varphi}{\sqrt{2}\sigma} \right) \right] + B = A' \int_{\varphi_-}^{\varphi_+} d\varphi' \exp \left(-\frac{(\varphi - \varphi')^2}{2\sigma^2} \right) + B \quad (5.2)$$

with free parameters A (A'), B , φ_- , φ_+ and σ to the resulting projection by minimizing

$$\chi^2 = \sum_k \frac{(N(\varphi_k) - N_k)^2}{N_k},$$

where N_k is the content of bin k . Despite the distortion due to the φ -asymmetry in the detection efficiency the fit yields very reasonable values for φ_- and φ_+ .

For determining x_m and y_m we parameterize the circular shape of the regenerator with the following function

$$r(\varphi) = x_m \cos \varphi + y_m \sin \varphi + \sqrt{(x_m \cos \varphi + y_m \sin \varphi)^2 - x_m^2 - y_m^2 + R^2} \quad (5.3)$$

describing a circle with centre (x_m, y_m) and radius R in the r - φ -plane. To extract experimental values for $r(\varphi)$ the r - φ -histogram of conversion points is divided into 12 φ -slices ranging from $\varphi = -54^\circ$ to $\varphi = +54^\circ$. These slices are then projected onto the r -axis. For the conversions in the slices we would expect a radial distribution similar to a Gaussian box (5.2) as in the angular projection. However, due to the relatively small radial size of the regenerator (2.5 cm) as compared to the radial resolution for a single conversion vertex (≈ 1.5 cm) no stable fit to a Gaussian box is possible and the data is much better described by a simple Gaussian:

$$N(r) = A \exp \left[-\frac{1}{2} \left(\frac{r - r_0}{\sigma} \right)^2 \right] - B \times \beta(r) \quad (5.4)$$

where $\beta(r)$ describes the shape of the background, i.e. conversions from the proportional chambers and the target, as determined from the regenerator-free sector. Function (5.4) was fitted to the r -projection of each slice with A , B , r_0 and σ as free parameters by minimizing

$$\chi^2 = \sum_k \frac{(N(r_k) - N_k)^2}{N_k}$$

where N_k again denotes the content of bin k . To avoid the background from conversions in the target and PC0 which is not correctly reproduced by the data from the regenerator-free sector owing to the screening effect of the regenerator, the fit is performed for $r > 3$ cm only. A circle (5.3) is then fitted to the resulting 12 points by minimizing

$$\chi^2 = \sum_i \frac{(r(\varphi_i) - r_i)^2}{\sigma_i^2}$$

where the σ_i are the errors on r_i from the first fit. Note that although we know the mean radius of the regenerator (7.05 cm) we cannot fix R to that value because the reconstruction efficiency is not constant along the radial direction but decreasing towards the inner edge of the regenerator owing to multiple scattering of the electrons and positrons inside the carbon.

The individual analyses of the nine subsets reveal no statistically significant trends in time for any of the parameters. Separation of the data according to magnetic field polarity gives no effects either. Hence we may perform the analysis on the combined set of all data. The result is

$$\begin{aligned} x_m &= 0.27 \pm 0.03 \text{ cm} & \varphi_- &= -53.9^\circ \pm 0.2^\circ \\ y_m &= -0.18 \pm 0.01 \text{ cm} & \varphi_+ &= 56.6^\circ \pm 0.2^\circ \end{aligned} \quad (5.5)$$

where the errors are purely statistical. These numbers describe the average position in a region around the middle of the regenerator ($z = 0$), exactly where the actual regeneration measurement was carried out. The derived opening angle is $\alpha = 114.1^\circ \pm 0.3^\circ$, somewhat too small, but not far off.

The distribution of conversions along z gives an upper limit of 2% on the inclination of the regenerator axis in the x direction. No information on the inclination in the y direction can be obtained.

5.3.3 Comparison and final values

Comparison of the opening angle α as derived from the measurements with the known value of 115° demonstrates the high degree of self-consistency of both methods. Furthermore the results for the position parameters obtained from the two very different and completely independent procedures agree

well within errors. The photon conversion method has the crucial advantage that its result is based on the same instrumentation and averaged over the same range in space and time as the actual regeneration measurement so that any systematic errors associated with absolute position, misalignment and movement cancel. Any residual systematic errors are essentially unknown but expected to be small. The surveyor measurement on the other hand locates only one end of the regenerator on the last day of data taking and the result has to be converted to offline coordinates, but the estimated uncertainties may be regarded as total errors.

Taking all facts into consideration we have more confidence in the photon conversion data but use the surveyor data as an excellent cross-check and to constrain the errors on the coordinates. Specifically we use the values for x_m and y_m from the photon conversion analysis and enlarge the error bars to ± 0.05 cm, now encompassing the surveyor results. For the angles we simply subtract a safety margin of one degree and round down to the next integer. Therefore the following values will be passed on to the regeneration analysis:

$$\begin{aligned} x_m &= 0.27 \pm 0.05 \text{ cm} & \varphi_- &> -53^\circ \\ y_m &= -0.18 \pm 0.05 \text{ cm} & \varphi_+ &< 55^\circ \end{aligned} \quad (5.6)$$

5.4 Further utilization of the regenerator

In addition to its intended role as a regenerator the carbon tube can also act as a strangeness identification device. The carbon nuclei make possible the charge exchange reactions $K^0 p \rightarrow K^+ n$ and $\bar{K}^0 n \rightarrow K^- p$ or the strangeness exchange reactions $\bar{K}^0 p \rightarrow \Lambda \pi^+$ and $\bar{K}^0 n \rightarrow \Lambda \{\pi^0 \text{ or } \pi^+ \pi^-\}$. The outgoing strange particle unambiguously identifies the strangeness of the neutral kaon at the time of the interaction in the regenerator, just as the lepton from a semileptonic decay tags the strangeness at the time of decay. Therefore such charge (strangeness) exchange events allow a measurement of the probability for a K^0 – \bar{K}^0 transition or vice versa between the creation point and the regenerator. Thanks to the rather broad momentum spectrum resulting from the production through reaction (4.1) and the cylindrical regenerator geometry this probability can be determined for a whole range of lifetimes. In this way a measurement of the oscillation frequency Δm is obtained which is free from correlation with ϕ_{+-} , similar to our Δm -measurement using semileptonic decays [59]. Preliminary results from this analysis look very promising [60].

In a more sophisticated variant of this experiment, carried out during a dedicated 10-day run following the regeneration run, the carbon regenerator was supplemented by a copper regenerator covering the remaining angle at 2 cm radius and the trigger setting was changed to collect $p\bar{p} \rightarrow K^0 \bar{K}^0$ events (PC0 in veto). Events were selected in which both kaons revealed their strangeness inside the regenerators through one of the processes enumerated above. Then the measured strangeness correlations were compared against the predictions obtained when assuming the non-separability of the $K^0 \bar{K}^0$ wave function as implied by Quantum Mechanics or a spontaneous wave-function factorisation at creation (Furry's hypothesis). The results, published in Ref. 61, are consistent with Quantum Mechanics. The measurement represents the first Einstein–Podolsky–Rosen-type experiment performed with neutral kaons.

6 THE REGENERATION MEASUREMENT

6.1 Overview of the method

We measure the impact of the regenerator on the $\pi^+\pi^-$ decay rate asymmetry to draw conclusions on the regeneration amplitudes. The regenerator effect is ascertained by comparing the decay rates recorded before and after the installation of the regenerator.

6.1.1 Decay rate asymmetry in vacuum

Inserting the K_L , K_S decay rates and $\eta_{+-} = A(K_L \rightarrow \pi^+\pi^-)/A(K_S \rightarrow \pi^+\pi^-)$ into the decay rate asymmetry (4.2) results in the following analytic expression:

$$A_{+-}(\tau) = \frac{\delta(e^{-\gamma_S\tau} + |\eta_{+-}|^2 e^{-\gamma_L\tau}) - 2|\eta_{+-}|e^{-\frac{1}{2}(\gamma_S+\gamma_L)\tau} \cos(\Delta m\tau - \phi_{+-})}{e^{-\gamma_S\tau} + |\eta_{+-}|^2 e^{-\gamma_L\tau} - 2\delta|\eta_{+-}|e^{-\frac{1}{2}(\gamma_S+\gamma_L)\tau} \cos(\Delta m\tau - \phi_{+-})} \quad (6.1)$$

with $\delta = 2 \operatorname{Re} \epsilon_T / (1 + |\epsilon_T|^2)$ (compare with (2.28)!). It is customary to accommodate the ϵ_T -terms in a normalization factor for the rates in order to obtain a simpler expression for the asymmetry. The definitions

$$\alpha := \frac{1 + \delta}{1 - \delta} = \frac{|1 + \epsilon_T|^2}{|1 - \epsilon_T|^2} \quad \text{and} \quad A'_{+-}(\tau) := \frac{\bar{R}(\tau) - \alpha R(\tau)}{\bar{R}(\tau) + \alpha R(\tau)}$$

(with \bar{R} and R being the decay rates for \bar{K}^0 and K^0 , respectively) yield the well-known formula [56]

$$A'_{+-}(\tau) = -2 \frac{|\eta_{+-}| e^{\frac{1}{2}(\gamma_S - \gamma_L)\tau} \cos(\Delta m\tau - \phi_{+-})}{1 + |\eta_{+-}|^2 e^{(\gamma_S - \gamma_L)\tau}}. \quad (6.2)$$

A simple fit to the measured asymmetry determines the parameters $|\eta_{+-}|$, ϕ_{+-} , Δm , and α . (Note that neither $\operatorname{Re} \epsilon_T$ nor $|\epsilon_T|$ but only α (or δ) is an observable quantity. It is only after presuming $|\epsilon_T|^2 \approx 0$ that $\alpha \approx 1 - 4 \operatorname{Re} \epsilon_T$ and $\operatorname{Re} \epsilon_T$ becomes measurable!)

6.1.2 Decay rate asymmetry in the presence of a regenerator

A regenerator in the decay path of the neutral kaons complicates the expression for $A_{+-}(\tau)$ or $A'_{+-}(\tau)$ beyond readability (cf. Eq. 3.35). We simply note here that regeneration leads to additional terms of the form $|\rho| \cos(\Delta m\tau - \phi_{+-} + \arg(\rho))$ which profoundly alter the A_{+-} oscillation pattern. This change can be regarded as an additional interference, between inherent and regenerated K_S amplitudes, or as an amplification of the asymmetry caused by the unequal interaction of K^0 and \bar{K}^0 in the medium. In our case the observed asymmetry is further modified due to the fact that the regenerator is cylindrical in shape: the effective distance and thickness of the regenerator as encountered by the neutral kaon vary from event to event depending on the kaon's emission angle relative to the detector axis. Moreover the neutral kaons are not mono-energetic but have a finite range of momenta. Therefore, instead of a sharp step at a certain decay time (Fig. 4), we observe a more or less smooth transition in the decay time range where the regenerator is encountered (see the data in Fig. 9).

6.1.3 Comparison of the two asymmetries

To separate the geometrical effects entering the regenerated asymmetry from the pure regeneration effect, we must know the spatial distribution of recorded $K^0(\bar{K}^0)$ decays in the regenerator sector of the detector. If we only had the regeneration data at our disposal we would need a Monte Carlo simulation to obtain this distribution. We are, however, in the fortunate position of having a large data set of $\pi^+\pi^-$ decays which was recorded under the same conditions but without the regenerator installed: the main CPLEAR data set from which the CP violation parameter η_{+-} is extracted! Hence we use two sets of data for the determination of the regeneration amplitudes:

1. the actual regeneration data taken in 1996 with the carbon regenerator installed as described in the previous Section and

2. a reference set containing data which was obtained in 1995 *without the regenerator*, i.e. with the original experimental set-up.

The two sets of data were taken under the same detector and trigger conditions, the only difference being the presence of the regenerator and they were also subject to exactly the same selection procedure. The comparison between the two sets isolates the interference terms arising from regeneration and minimizes systematic uncertainties in the measurement. The reference data set contains more than three times the number of events of the regeneration data set so that the statistical errors are almost entirely given by the statistics of the latter.

6.2 Data selection

For the regeneration measurement we use the standard selection of $K^0(\bar{K}^0) \rightarrow \pi^+\pi^-$ decays as used for the CP violation measurement (Paragraphs 6.2.1–6.2.4). On top of that a few additional cuts specific to the regeneration analysis are applied (Paragraph 6.2.5).

6.2.1 Offline selection of “golden events”

The raw data tapes contain the output of the sub-detectors for all events selected by the trigger. In a first step, this information is decoded and converted into meaningful physical variables. A pattern recognition program identifies track helices from the wire chamber hits. Only events with either two or four tracks are kept and passed to the initial filtering stages. The kaon filter (FILKA) requires at least one kaon candidate with a \overline{SCS} signature and a total momentum greater than 300 MeV/c. A track quality control routine demands at least three wire and two strip hits from the DCs as well as a non-zero longitudinal momentum for each track and classifies tracks as primary (at least one PC hit) or secondary (no PC hit). A good event must have at least two primary tracks and the charges of all tracks must add up to zero.

6.2.2 Selection of four track events

The events containing two and four tracks are passed through the filters ANA2T and ANA4T, respectively. Detailed track and vertex fits are performed at this level, the effects of energy loss and multiple scattering being taken into account. For tracks crossing the carbon regenerator these corrections are adapted accordingly. It is required that the number of fitted tracks equal the number of tracks found by the pattern recognition and that the total charge be zero. There must be a primary pion, i.e. a primary track which forms a vertex with the charged kaon candidate in the target and is of opposite charge. The four track filter additionally demands a secondary vertex to be found and that no track momentum exceed 1000 MeV/c.

6.2.3 Filtering of $\pi^+\pi^-$ decays

At the next stage the remaining events are divided into decay classes. There are four classes (filters) for the four track events: ANA2PI for $\pi^+\pi^-$ and semileptonic decay candidates, ANA3PI for $\pi^+\pi^-\pi^0$, ANAPPG for $\pi^+\pi^-\gamma$ and ANACON for events where the secondary pair is likely to come from a photon conversion ($\gamma \rightarrow e^+e^-$). Events of this last class are used to determine the regenerator position (Section 5.3).

The ANA2PI filter applies the following cuts: the momenta of the primary tracks must be greater than 60 MeV/c (to ensure they have reached the particle identification detectors); for both the primary and the secondary track pair the cosine of the spatial opening angle must exceed -0.98 ; and the fitted secondary vertex must be at a position inside the first hits of the secondary tracks. Furthermore a constrained fit analysis at the primary vertex is performed, the constraint being that the missing mass equals the neutral kaon mass (1C-fit). A χ^2 fit probability of more than 1% is demanded.

Events passing the ANA2PI filter are further tested for their compatibility with the $\pi^+\pi^-$ or the semileptonic hypothesis. $\pi^+\pi^-$ decay candidates are identified via a 5C-fit in which the four additional constraints ensure conservation of energy and momentum for the whole event (i.e. there is no neutral particle carrying away energy and momentum). To be flagged as a $\pi^+\pi^-$ candidate this fit must yield a

χ^2 probability greater than 2%. In the regeneration data set the tracks crossing the carbon are corrected for energy loss and their momentum errors are increased to allow for multiple scattering before applying the constrained fit. The energy loss correction is based on the Bethe–Bloch formula and was checked by comparing the $\pi^+\pi^-$ invariant mass from neutral kaon decays occurring before and after the regenerator.

All events that qualify for one of the decay candidate classes are then written to so-called MINRAW tapes. These tapes contain the data of the RAW tapes and further information from the filtering procedure.

6.2.4 Micro data summary tapes for $\pi^+\pi^-$ events

The MINRAW data format is rather unwieldy for physics analysis, in particular in the $\pi^+\pi^-$ case where a very large number of events has been accumulated. A further reduction of both the number of events and the size of each event is desirable to facilitate the analysis. The events are therefore subject to another filter which further improves the quality of the sample. Of the selected events, only the information relevant to the analysis is written out in a new format, called micro data summary tape (micro-DST). The extra cuts remove events where there are large uncertainties or ambiguities in the reconstruction of the tracks or vertices. They include a cut on the spatial opening angle of the track pairs—the cosine must be less than 0.99—to reject photon conversions.

The result of a 9C-fit is also written to the micro-DSTs but no cut on its probability is applied at this stage. The 9C-fit is an extension of the 5C-fit in which the additional four constraints require the intersections of the track helices at the primary (annihilation) and the secondary (decay) vertex, respectively, and the neutral kaon momentum to be collinear with the line joining the two vertices.

The overall efficiency of the selection procedure up to the micro-DST format (including all detector and trigger efficiencies) is about 2.5% for $K^0(\bar{K}^0) \rightarrow \pi^+\pi^-$ decays. It occurs, in particular at short lifetimes, that two configurations of the same event pass all selection cuts. In such cases the fitted variables for both configurations are written out.

6.2.5 Selection of regeneration events

The $\pi^+\pi^-$ micro-DSTs form the basis of the regeneration analysis. We first reject events in which more than one configuration meet all $\pi^+\pi^-$ selection criteria. Then the subset of events used for the regeneration analysis is defined according to the following requirements:

- A χ^2 probability for the 9C-fit of more than 5% is demanded.
- The primary vertex must lie inside the hydrogen target and the secondary vertex outside the cylinder described by the PCO.
- The reconstructed lifetime of the neutral kaon must be greater than $1 \tau_S$.
- The momentum of the neutral kaon as given by the 9C-fit must point into the regenerator sector of the detector: $-53^\circ < \varphi_{K^0} < 55^\circ$ (see Section 5.3 for the definition of the angle φ).
- The primary tracks must not cross the volume occupied by the regenerator.
- The neutral kaon momentum must be at least 250 MeV/c (see following Subsection).

These cuts are applied to both the regeneration data set and the reference data set in order to obtain two comparable event samples covering identical volumes in phase space. No distinction is made between neutral kaon decays occurring before, inside or after the regenerator. About two thirds of the events of the regeneration data set fall into the first category and thus yield no information on the regeneration amplitude (but are needed for normalization purposes, see Paragraph 6.4.1). The efficiency for these events is somewhat low because they are likely to contain a secondary pion that crosses the regenerator and which is subject to multiple scattering inside the carbon (Fig. 8). However, this screening effect of the carbon affects K^0 and \bar{K}^0 events in the same way and therefore cancels in the asymmetry (see also Paragraph 6.4.1). The same applies to the events of the second category (decay inside the regenerator), of course, which is why we make use of them in our analysis.

3 174 585 events of the regeneration data set satisfy all selection criteria, about 26% of all $\pi^+\pi^-$ events on micro-DST. 10 208 706 events of the reference data set remain after applying identical selection cuts.

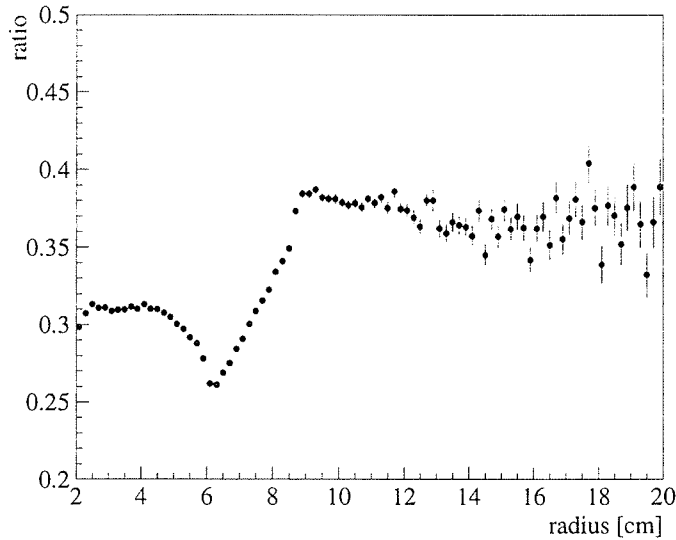


Figure 8: The ratio of the number of events in the regeneration data set and in the reference data set as a function of the (cylindrical) radius of the neutral kaon decay vertex. The screening effect of the regenerator results in a lower ratio for decays before the regenerator with a pronounced minimum at the inner radius of the regenerator at about 6.1 cm. The subsequent rise in the ratio reflects the decreasing probability of the secondary pions to suffer multiple scattering thereby causing a bad reconstruction efficiency.

6.3 Determination of the regeneration amplitudes

To account for the variation of the regeneration amplitude Δf as a function of $K^0(\bar{K}^0)$ momentum we divide the data of both sets into five momentum intervals of 100 MeV/c width each. The asymmetry (4.2) is formed from the regeneration data separately for each momentum interval. Figure 9 shows the resulting five asymmetries. The gain in statistical precision at higher momenta is in part compensated by a loss of sensitivity caused by the decreasing evolution time of the neutral kaon before reaching the regenerator. Because of the smearing effects mentioned above it is not possible to extract the desired information by a fit to an analytical function. Instead, we perform a numerical fit, using the reference data set in the following way:

- For each momentum interval we construct the asymmetry (4.2) as for the regeneration data but now simulate the regeneration effect for a given value of Δf by applying a weight to each event. This weight is calculated individually as the ratio of the expected decay rates with and without the regenerator, taking into account the momentum and the path of the neutral kaon in the detector. The evaluation of the regeneration-corrected decay rates is based on the phenomenology presented in Section 3, in particular on the solution (3.31) of Good’s differential equations, and the neutral kaon parameters of the Particle Data Group [15]. Only coherent regeneration is taken into account as the effect of incoherent (diffractive) regeneration is found to be negligible with our method (see following Subsection).
- The simulation of the regeneration effect on the asymmetries is performed for different values of the real and imaginary parts of Δf , resulting in an array of asymmetries $A_{+-}^{\text{sim}}(\Delta f, \tau)$.
- These regeneration-simulated asymmetries $A_{+-}^{\text{sim}}(\Delta f, \tau)$ are now compared with the observed asymmetry $A_{+-}^{\text{obs}}(\tau)$ of the regeneration data by evaluating

$$\chi^2(\Delta f) = \sum_{\tau \text{ bins}} \frac{(A_{+-}^{\text{sim}}(\Delta f, \tau) - A_{+-}^{\text{obs}}(\tau))^2}{\sigma_{\text{sim}}^2(\tau) + \sigma_{\text{obs}}^2(\tau)}$$

where the σ are the statistical errors on the respective asymmetries.

- The pair $(\text{Re } \Delta f, \text{Im } \Delta f)$ that yields the smallest value for χ^2 is the result of our measurement. The fixed- χ^2 curves given by $\chi^2 = \chi_{\text{min}}^2 + s^2$ in the Δf complex plane are approximate s -

standard-deviation contours.

For most neutral kaon momenta, the inherent K_S amplitude by far outweighs the regenerated one at the time of the decay. This means that the spatial vertex distribution of $\pi^+\pi^-$ decays in the regeneration set is well approximated by the data of the reference set and the weights applied to simulate the regeneration effects are close to one. At very low momenta, however, we find that almost all K_S decay before reaching the regenerator and hence our method is not applicable. We therefore restrict the analysis to neutral kaon momenta above 250 MeV/c where the decay rates after the regenerator are still dominated by the inherent K_S amplitude.

The quantities $\langle \Delta f \rangle_{p_i}$ determined in this way are weighted averages according to the momentum distribution $\mathcal{N}(p)$ in the respective interval as found at the entrance of the regenerator (see Fig. 10):

$$\langle \Delta f \rangle_{p_i} = \frac{\int_{\Delta p_i} dp \Delta f(p) \mathcal{N}(p)}{\int_{\Delta p_i} dp \mathcal{N}(p)}$$

The differences between these spectrum-weighted means and the centre-of-interval values are small compared to our statistical errors.

6.4 Systematic uncertainties

6.4.1 K^0/\bar{K}^0 rate normalization

In the CPLEAR experiment, the tagging efficiency for \bar{K}^0 is higher than for K^0 because the strong interaction of charged kaons and pions with the detector material favour the detection of the accompanying ($K^+\pi^-$) pair over its charge conjugate. This leads to an offset (normalization factor) in the measured asymmetry which is clearly visible in Fig. 9. The factor is expected to be of the same magnitude in both the regeneration and the reference data set, i.e. the *relative* normalization factor α_{rel} should be close to one. We measured this factor by comparing the observed ratios of \bar{K}^0 and K^0 decays before the regenerator in both data sets and obtained $\alpha_{\text{rel}} = 1.0028 \pm 0.0016$, constant in phase space. Moreover we convinced ourselves by way of a Monte Carlo simulation that α_{rel} does not change significantly for decays inside and after the regenerator. In the analysis, we applied this factor as a correction to the reference data set and deduced the systematic errors by varying it in its range of statistical uncertainty. This resulted in the errors given in Table 3.

Table 3: Systematic errors on Δf due to the uncertainty in the normalization of K^0 and \bar{K}^0 rates.

mom. range MeV/c	Re Δf fm	Im Δf fm
250–550	<0.05	<0.05
550–650	0.06	0.2
650–750	0.06	0.6

6.4.2 Regenerator position

A further systematic error is caused by the uncertainty of ± 0.5 mm in the horizontal position of the regenerator, i.e. the distance between the regenerator and the $K^0(\bar{K}^0)$ production point (see Section 5.3). This uncertainty propagates to differences in the regeneration amplitudes that do not exceed 0.05 fm in both the real and imaginary parts of the amplitudes.

The errors on the vertical position and the inclination of the regenerator as evaluated in Section 5.3 turn out to be completely negligible.

6.4.3 Compatibility of the two data sets

Any difference in running conditions between the collection of the two data samples used for the analysis could constitute a further source of systematic error. In addition to ensuring that all detector and

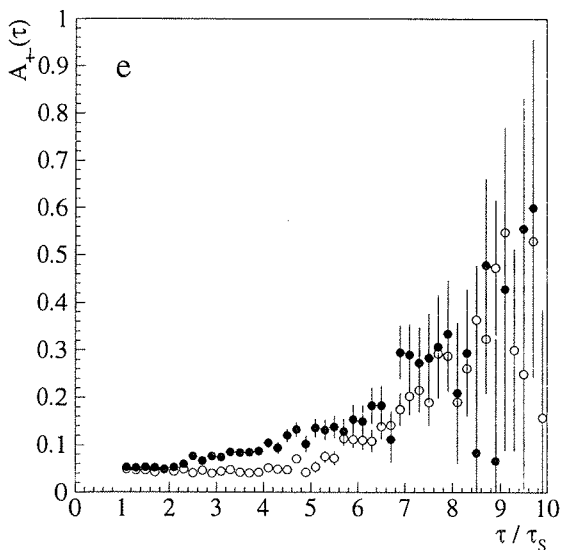
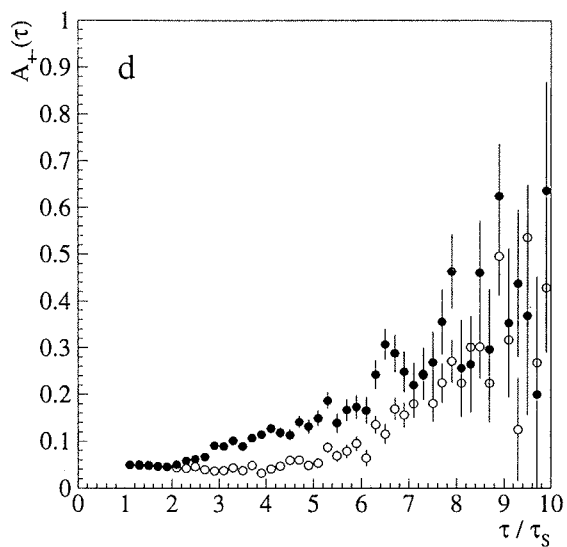
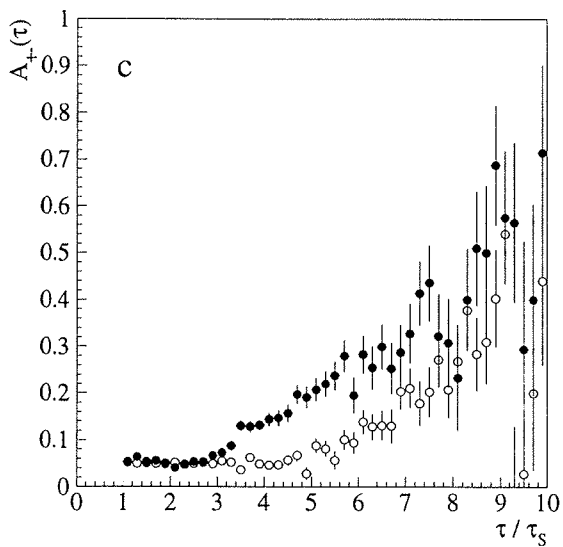
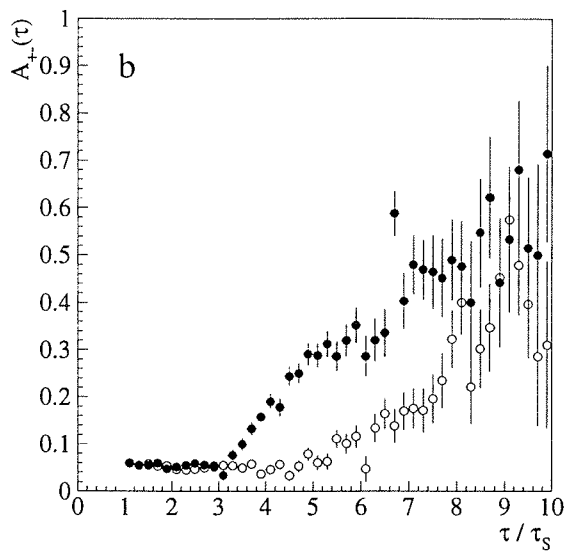
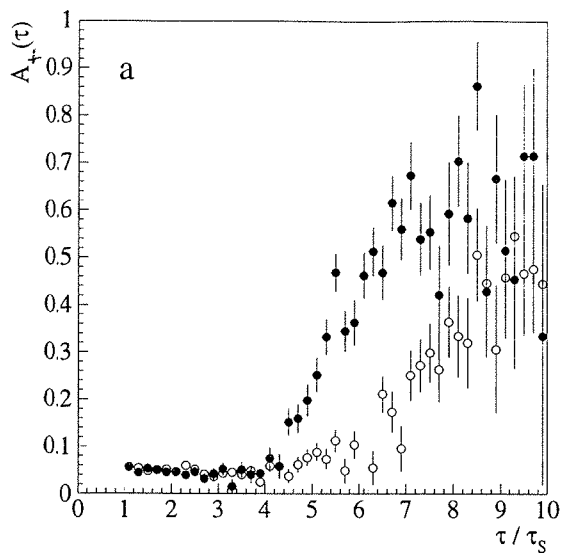


Figure 9: The measured $K^0-\bar{K}^0$ asymmetries with regenerator (full circles) and without (open circles) for the five momentum intervals centred around 300 (a), 400 (b), 500 (c), 600 (d) and 700 MeV/c (e).

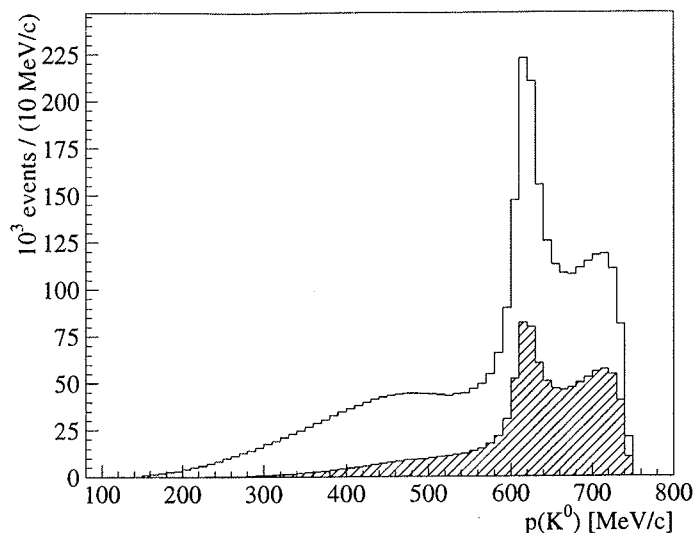


Figure 10: Momentum spectrum of the neutral kaons. The hatched part marks the spectrum at the entrance of the regenerator, i.e. the events that contribute to the measurement of the scattering amplitudes. The peak at 614 MeV/c arises from K^0 s recoiling against a $K^*(892)^0$ resonance.

trigger parameters remained the same, we verified that neither the presence of the regenerator nor the time difference of one year between the two runs affected the data in any unpredictable way. This was done by analyzing events in which no particle came close to the regenerator. The asymmetries constructed from these events are equal for the two data sets within statistical fluctuations.

6.4.4 Incoherent regeneration

We repeated the analysis allowing also for incoherent scattering in the regeneration simulation. The correction to the decay rates is calculated according to Eq. 3.40, using (3.44) as a rough estimate for the integration over the detector acceptance. The adjustments in the measured regeneration amplitudes resulting from this correction are extremely small and may be neglected. This is expected because the carbon regenerator is situated well inside the K_S -dominated decay region where coherent regeneration by far outdoes its incoherent counterpart.

6.4.5 Limitations of the asymmetry method

Apart from the systematics specific to regeneration we must also consider uncertainties arising from the asymmetry method, i.e. the systematic errors that also enter the CP violation measurement, brought about by the level of background, regeneration effects in other detector components, the decay time resolution, and the uncertainties in Δm and τ_S . These influences were studied with essentially the same tools as used in the CP violation measurement [56].

In the regeneration analysis no attempt is made to subtract background events. We checked that the introduction of a background level in the analysis and its variation within reasonable limits, as known from the CP violation analysis, has no perceptible effect on our results. Similarly, we calculated the influence of regeneration in the detector walls and convinced ourselves of its insignificance. The impact of the finite decay time resolution was studied in detail with the help of a mini Monte Carlo simulation and also found to be negligible. The neutral kaon parameters Δm and τ_S , finally, were varied in their respective ranges of accuracy according to Ref. 15, again without noticeable effects on our results for the regeneration amplitudes.

6.4.6 Further consistency checks

To further corroborate our confidence in the method of comparing simulated and measured regeneration effects we performed two additional consistency checks on the data.

In the first, we take the regeneration data set and apply the measured amplitudes to fully correct for regeneration in the carbon. Then the asymmetry formed from the corrected decay rates should arise from CP violation only. The values for the CP violation parameter η_{+-} derived from a fit to this asymmetry are indeed compatible with this hypothesis: we find $|\eta_{+-}| = (2.22 \pm 0.20) \times 10^{-3}$ and $|\phi_{+-}| = 41.6^\circ \pm 5.5^\circ$, demonstrating that the regeneration data yield a correct measurement of η_{+-} .

In the other test we split the reference data set in two and repeat the regeneration analysis, using one part as the “regeneration” data set and the other as the reference data set. The obtained “amplitudes” are compatible with zero, as expected, proving that all of the effect observed in the regeneration data must be ascribed to the presence of the carbon regenerator.

6.5 Additional constraints on $\text{Im } \Delta f$ from other experiments

The optical theorem relates total cross sections to the imaginary parts of the corresponding forward scattering amplitudes. Under the assumption of isospin invariance in kaon nucleon scattering, measurements of the difference between K^+ and K^- total cross sections may therefore be used to put further constraints on our results and possibly resolve the large correlation present in some momentum bins.

Unfortunately we know of only one such measurement that overlaps with our momentum range. Bugg et al. [62] have measured K^+ and K^- total cross sections in carbon at momenta between 655 MeV/c and 2606 MeV/c, also motivated by the study of regeneration.¹³ Applying the transmission technique they were able to determine the cross sections to a precision of 2%, limited mainly by the systematic uncertainty in the extrapolation to zero angle. We interpolated the values of Ref. 62 and weighed the resulting curves according to our momentum spectrum (Fig. 10) for better comparison. The obtained cross section difference in the momentum range 650–750 MeV, $\sigma(K^+) - \sigma(K^-) = (-145 \pm 7)$ mb, corresponding to $\text{Im } \Delta f = (-4.08 \pm 0.20)$ fm, is in excellent agreement with our error ellipse for this momentum bin. The combination of the two measurements reduces the error on the real part of Δf by more than a factor of 6 (see Fig. 11e and Table 4).

6.6 Final results

The results are summarized in Fig. 11 and Table 4 (and published in Ref. 64). They represent the first experimental data on both the real and imaginary parts of the regeneration amplitude for kaon momenta below 1 GeV/c and are in accordance with the predictions of Eberhard and Uchiyama [39] as well as with more recent calculations done for the ϕ -factory at Frascati [38].

6.7 Application to the measurement of η_{+-}

The main motivation for the regeneration measurement was the reduction of the systematic error on ϕ_{+-} , the phase of the CP violation parameter η_{+-} (2.25). Therefore it is of primary interest to see how the achieved accuracy on the regeneration amplitudes propagates to the $\pi^+\pi^-$ CP violation measurement. The procedure of correcting the decay rates for regeneration has been described in Section 4.3. It is founded on Good’s equations with the detector inventory (geometry) and the regeneration amplitudes for all materials as input. Almost two thirds of the overall regeneration effect on ϕ_{+-} stem from carbon nuclei. The remaining effect is predominantly due to nitrogen and oxygen nuclei, close neighbours of carbon in the periodic table of elements. The amplitudes for these elements are extrapolated from the Carbon amplitudes by means of a scale factor, which is derived from the work of Eberhard and Uchiyama [39] in the case of nitrogen and hydrogen. For oxygen and all other elements we obtained the scale factor from an empirical power law relating the amplitudes to the mass numbers of the nuclei where the exponent is taken from Ref. 65. The uncertainties in these scale factors, estimated from the comparison of the two methods applied to nitrogen, are negligible with respect to the errors on the carbon amplitudes.

Now we are in a position to update our regeneration correction code with the experimentally

13. Krauss et al. [63] obtained data at lower momenta but only for K^+ .

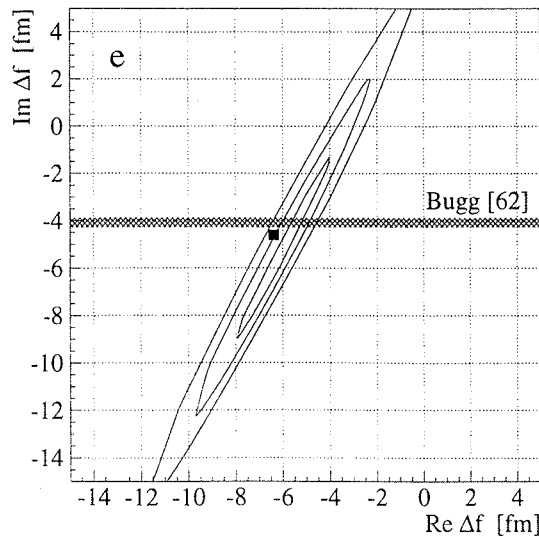
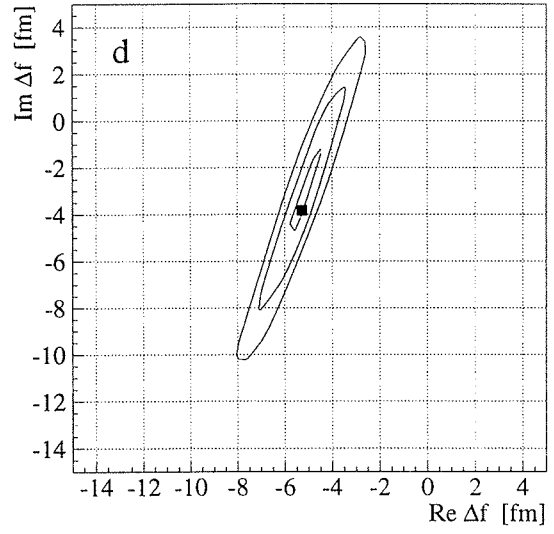
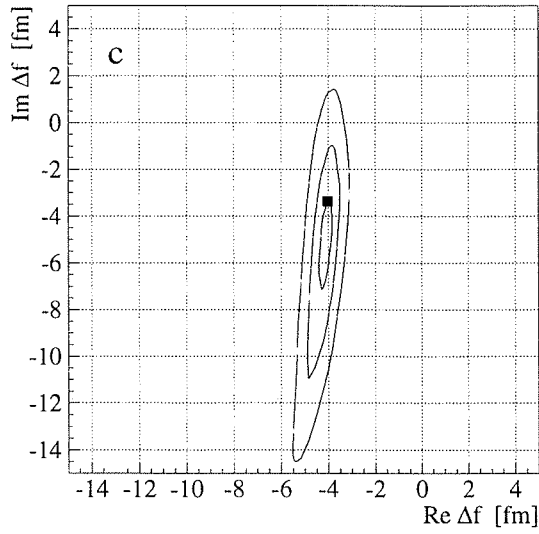
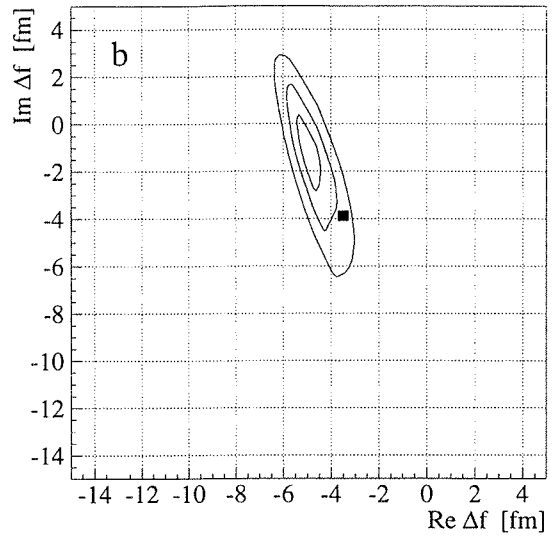
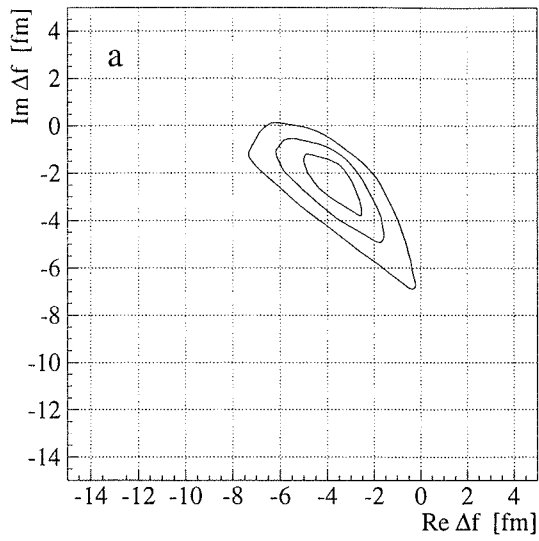


Figure 11: The Δf complex plane for the five momentum intervals centred around 300 (a), 400 (b), 500 (c), 600 (d) and 700 MeV/c (e). The curves with $\chi^2 = \chi_{\min}^2 + s^2$ are shown for $s = 1, 2, 3$, marking confidence regions that approximately correspond to 1, 2 and 3 standard deviations. The results of the optical model calculation of Ref. 39 are inserted for comparison (small squares). In (e), the total cross section measurement of Ref. 62 is also shown.

Table 4: The CPLEAR results on $\Delta f = f(0) - \bar{f}(0)$ with standard errors in the Gaussian approximation in comparison with the optical model calculations of Ref. 39 where available; in the last row the combined result of Ref. 62 and CPLEAR. The values of Refs. 39 and 62 are weighted according to the momentum spectrum of Fig. 10b.

p_{K^0} MeV/c	$\langle p_{K^0} \rangle$ MeV/c	CPLEAR			optical model [39]	
		$\langle \text{Re } \Delta f \rangle$ fm	$\langle \text{Im } \Delta f \rangle$ fm	correl. coeff.	$\langle \text{Re } \Delta f \rangle$ fm	$\langle \text{Im } \Delta f \rangle$ fm
250–350	315	-3.8 ± 1.3	-2.4 ± 1.2	-0.76		
350–450	410	-4.9 ± 0.5	-1.2 ± 1.6	-0.76	-3.48	-3.88
450–550	504	-4.2 ± 0.3	-4.9 ± 2.0	0.60	-4.03	-3.38
550–650	614	-5.1 ± 0.6	-2.8 ± 1.9	0.96	-5.26	-3.81
650–750	697	-5.7 ± 1.8	-4.3 ± 3.6	0.99	-6.38	-4.59
≈ 700		-5.5 ± 0.3	-4.1 ± 0.2			

determined scattering amplitudes and to study the propagation of the errors to the $\pi^+\pi^-$ analysis. Taking into account the result of Ref. 62 and the correlations in our measurements we find that regeneration in the detector walls shifts the fitted values for ϕ_{+-} by $-2.60^\circ \pm 0.19^\circ$ and for $|\eta_{+-}|$ by $(+0.073 \pm 0.018) \times 10^{-3}$. These shifts include contributions from incoherent regeneration of $+0.11^\circ$ and $\approx +0.003 \times 10^{-3}$, respectively.

Comparing this with the respective statistical errors of $\pm 0.54^\circ$ and $\pm 0.024 \times 10^{-3}$ we see that the goal of the regeneration experiment, as stated in Section 4.3, has been achieved. The final result on η_{+-} , to be published by the CPLEAR collaboration in 1998, is:

$$\phi_{+-} = 43.63^\circ \pm 0.54_{\text{stat}} \pm 0.23_{\text{sys}} (\pm 0.42_{\Delta m})$$

$$|\eta_{+-}| = (2.254 \pm 0.024_{\text{stat}} \pm 0.024_{\text{sys}} (\pm 0.010_{\tau_S})) \times 10^{-3}$$

These values are derived from the decay rate asymmetry shown in Fig. 12, assuming $\Delta m = (530.4 \pm 1.4) \times 10^7 \text{ } \hbar s^{-1}$ [15]. Although significantly smaller than the statistical error the regeneration-induced uncertainty remains the dominant source of systematic error for both ϕ_{+-} and $|\eta_{+-}|$. As the precision of the regeneration correction itself is limited mainly by the statistics of our measurement, we are allowed to combine the two errors, obtaining

$$\phi_{+-} = 43.63^\circ \pm 0.59^\circ (\pm 0.42_{\Delta m});$$

$$|\eta_{+-}| = (2.254 \pm 0.034 (\pm 0.010_{\tau_S})) \times 10^{-3}.$$

Figure 13 shows the CPLEAR result on ϕ_{+-} with its Δm -correlation in comparison with other recent measurements.

$$\Delta m = 5240 \pm 9.4 \pm 8.3$$

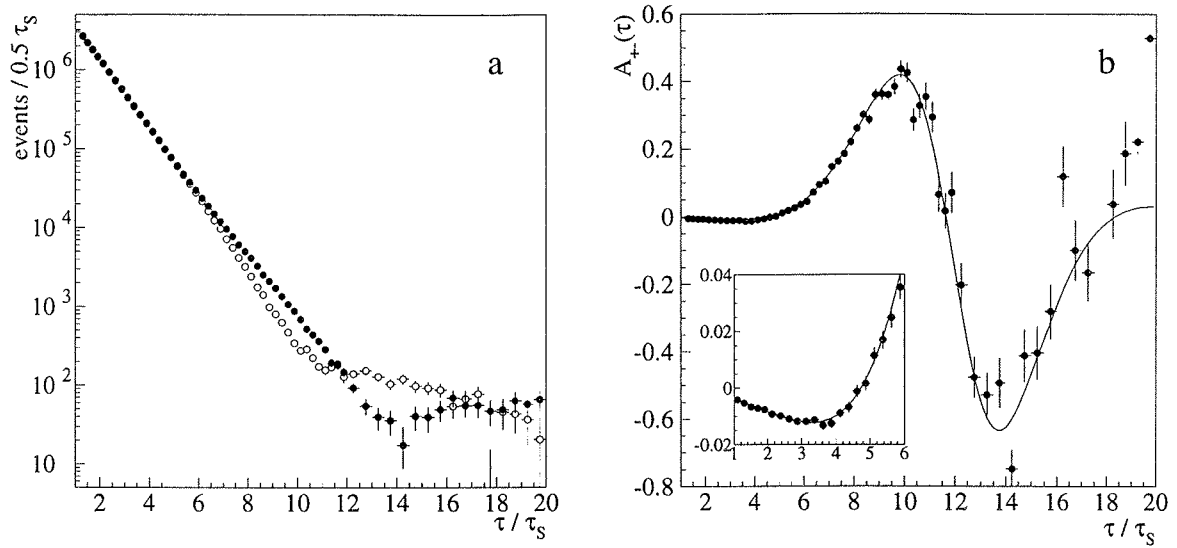


Figure 12: The decay rates of K^0 (open circles) and \bar{K}^0 (full circles) into $\pi^+\pi^-$ as measured by CPLEAR (a) and the resulting decay rate asymmetry (b). The event rates are corrected for detector acceptance, background and regeneration.

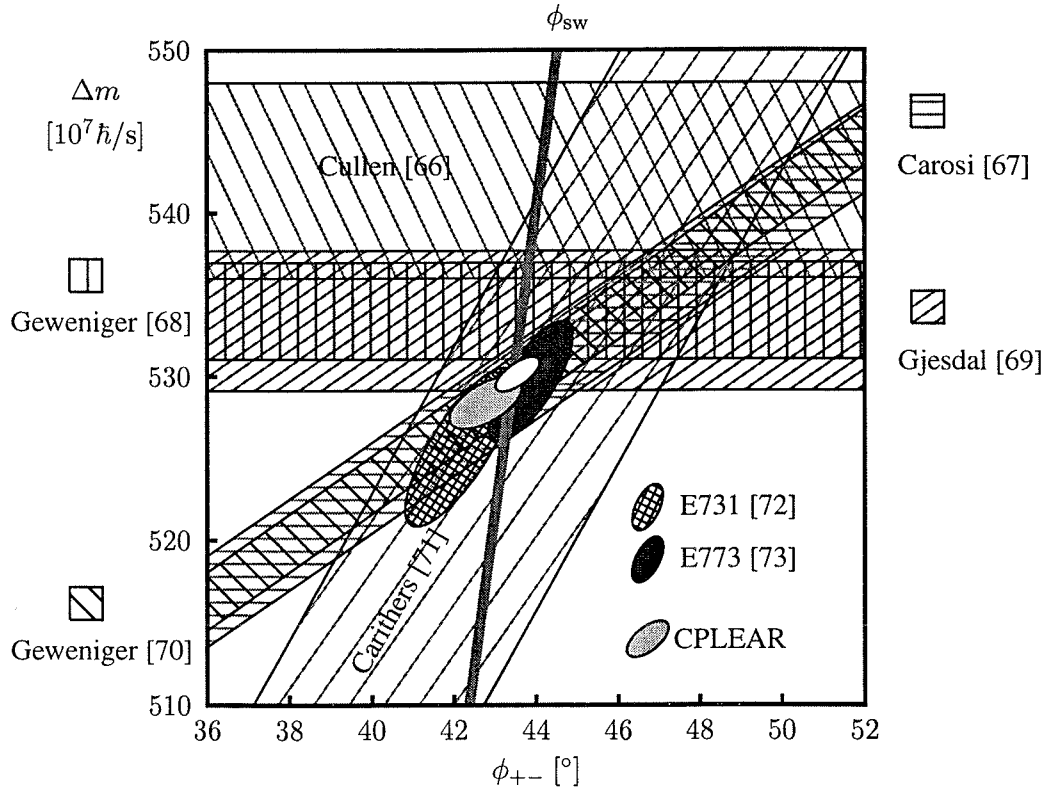


Figure 13: A comparison of recent measurements of ϕ_{+-} and Δm with the superweak phase ϕ_{sw} . The white ellipse in the centre represents the result of a global fit to all data (see also Refs. 15 and 74).

7 A DISPERSION RELATION ANALYSIS OF THE REGENERATION AMPLITUDE

Neutral kaon regeneration is not only of interest to CP violation experiments, it is also an extremely useful tool to study hadron scattering and has led to great strides in both particle and nuclear physics [75]. In this Section we compare our data on the regeneration amplitude in carbon with other, direct or indirect, measurements of this amplitude at various energies. We then combine all available experimental information with the theoretical assumptions of analyticity and Regge trajectory exchange to obtain a complete description of the amplitude as a function of beam energy. In the framework of local relativistic field theories, analyticity of the amplitude has been proven to follow from causality for KN scattering and it is therefore very natural to assume it as well for kaon scattering off nuclei. The Regge model for the description of the amplitude at high energies is very well supported experimentally [73,76].

We apply a least-squares fit of a simple dispersion relation to the available data which span an energy range of almost three orders of magnitude. More elaborate methods [77] fail because of the scarcity of the data, in particular in the low and intermediate energy range.

7.1 Selection and treatment of data

Table 5 summarizes all experimental efforts to determine the regeneration amplitude in carbon. Most regeneration experiments determined the modulus and phase of Δf from $\pi^+\pi^-$ decay rates behind a regenerator [5, 71, 73, 76, 78–82]. Two groups [83, 84] also obtained a phase measurement from the time-dependent charge-asymmetry in semileptonic decays, thus independent of the CP violation phase ϕ_{+-} .

Table 5: Carbon regeneration experiments.

group	Ref.	p_K [GeV/c]	method	measured part of Δf	χ^2/dof in fit
Christenson et al.	[5]	1.1	$K_S \rightarrow \pi^+\pi^-$	mod	0.1 / 1
Böhm et al.	[78]	2.7	$K_S \rightarrow \pi^+\pi^-$	mod	1.7 / 1
Bott-Bodenhausen et al.	[83]	4.5	$K_{L,S} \rightarrow \pi\mu\nu$	arg	1.2 / 1
	[79]		$K_{L,S} \rightarrow \pi^+\pi^-$	mod	0.0 / 1
Carithers et al.	[84]	4–10	$K_{L,S} \rightarrow \pi\ell\nu$	arg	13.0 / 13
	[71]		$K_{L,S} \rightarrow \pi^+\pi^-$	arg	8.0 / 6
	[80]			mod	6.4 / 6
Albrecht et al.	[81]	16–40	$K_{L,S} \rightarrow \pi^+\pi^-$	mod	1.3 / 6
				arg	0.4 / 3
Hladky et al.	[82]	10–30	$K_{L,S} \rightarrow \pi^+\pi^-$	mod	1.2 / 5
				arg	0.0 / 1
Roehrig et al.	[76]	30–130	$K_{L,S} \rightarrow \pi^+\pi^-$	mod	21.6 / 10
				arg	9.0 / 10
Schwingenheuer et al.	[73]	20–160	$K_{L,S} \rightarrow \pi^+\pi^-$	mod, arg ^a	0.3 / 1
CLEAR (this work)		0.25–0.75	$K^0(\bar{K}^0) \rightarrow \pi^+\pi^-$	Re, Im ^b	12.3 / 10

^a Only a fitted value for the power law exponent α is published.

^b Likelihood plots in the complex plane are given.

Owing to the isospin symmetry of the ^{12}C nucleus, K^\pm data may be used to extract information on the regeneration amplitude, if charge invariance is assumed. Then, with the use of the optical theorem, the difference between the total cross sections of K^+ and K^- is a measure of the imaginary part of Δf [62, 85–87]. One of these experiments [86] also derived values for the real part from a measurement of the differential cross section $d\sigma/dq^2$.

Table 6: Carbon K^\pm experiments.

group	Ref.	p_K [GeV/c]	measured quantities	derived part of Δf	χ^2/dof in fit
Bugg et al.	[62]	0.6–2.6	$\sigma_T(K^\pm)$	Im	17.3 / 9
Abrams et al.	[85]	1.0–3.3	$\sigma_a(K^\pm)$	Im	38.0 / 41
Gobbi et al.	[86]	1.68–2.26	$\sigma_T(K^\pm)$ $d\sigma/dq^2(K^\pm)$	Im Re	(discarded) (discarded)
Afonasyev et al.	[87]	1.8	$\sigma_T(K^\pm)$	Im	0.7 / 1
Backenstoss et al. / Seki	[89] [88]	0	$a_0(K^-)$	Im	(fixed)

Similarly, the K^-C scattering length, $a_0(K^-C)$, extracted [88] from X-ray transition data obtained with kaonic carbon [89] may be regarded as a measurement of the \bar{K}^0 scattering amplitude at zero kinetic energy. The corresponding amplitude for K^0 , having no inelastic channels open, must be purely real so that $\text{Im } \Delta f = \text{Im } a_0(K^-C)$. Table 6 lists all K^\pm experiments with carbon relevant for this analysis.

Where appropriate, the results have been adapted to the current world averages for the neutral kaon parameters, such as Δm , τ_S and η_{+-} , taken from Ref. 15. Here it is important to note that some of these averages, in particular ϕ_{+-} , are themselves influenced by regeneration measurements so that care must be taken when employing them to correct these very measurements. Such feedback effects, however, were found to be very small and may be neglected in our analysis.

The corrected data are illustrated in Fig. 14, separately for measurements of modulus, phase, and the imaginary and real parts of Δf . Fig. 14c reveals a conspicuous systematic disagreement between the total cross section result of Ref. 86 and the data of the other three experiments at the same energies. We exclude the data published in Ref. 86 from our fit, imaginary parts as well as real parts, as the latter directly depend on the former.

7.2 The dispersion relation and its parameterization

We use an unsubtracted¹⁴ dispersion relation as it is readily derived for antisymmetric amplitudes [93]. Since the precision of the data does not allow fitting several pole terms, contributions from all the poles in the complex energy plane are represented by a single effective pole:

$$\text{Re } \Delta f(\omega) = \frac{2\omega r}{\omega^2 - \omega_p^2} + \frac{2\omega}{\pi} \mathcal{P} \int_{\omega_\Lambda}^{\infty} d\omega' \frac{\text{Im } \Delta f(\omega')}{\omega'^2 - \omega^2} \quad (7.1)$$

where ω denotes the total laboratory energy of the kaon and \mathcal{P} stands for principal value. The pole term contains two parameters, position ω_p and residue r . ω_Λ marks the beginning of the unphysical cut, i.e. the energy at which production of a free Λ becomes possible, $\omega_\Lambda = 183.6$ MeV. The integration over the imaginary part starts at ω_Λ and extends all the way to infinity. To carry out the integration, a parameterization of $\text{Im } \Delta f$ is needed over this range. Guided by the data and theoretical expectations, we have chosen the following parameterization:

- The Regge model with one pole trajectory exchange [94] is applied at energies above a certain energy ω_k , giving

$$\text{Im } \Delta f(\omega) = \beta(\omega/\omega_0)^\alpha \sin\left(-\frac{\pi}{2}[\alpha + 1]\right). \quad (7.2)$$

We choose the scale $\omega_0 = 1$ MeV.

14. sometimes erroneously called “subtracted” [92]

- In the intermediate energy range around 1 GeV, the total cross section data clearly indicate a resonance. We parameterize it as a Gaussian on a background, the shape of which we describe by the same simple power law as employed at high energies, but with a different exponent:

$$\text{Im } \Delta f(\omega) = b(\omega/\omega_0)^a \sin(-\frac{\pi}{2}[a+1]) - C \exp\left(-\frac{1}{2}\left[\frac{\omega - \omega_{\text{res}}}{\sigma}\right]^2\right) \quad (7.3)$$

The transition energy ω_k follows from α , β , a and b if the function $\text{Im } \Delta f(\omega)$ is to be continuous. In the fit, we will vary ω_k in place of b as a free parameter.

- The sensitivity of the CPLEAR data to the imaginary part of the regeneration amplitude is not sufficient for a parameter fit in the energy range below the first total cross section measurement at 847 MeV. Following Refs. 95 and 96, we simply assume a linear decrease of $\text{Im } \Delta f$ from the physical threshold to 830 MeV total laboratory energy, in accordance with the data.
- At the physical threshold, we fix $\text{Im } \Delta f$ to the value corresponding to the measured K^-C scattering length. The small error on this measurement is negligible in this analysis.
- Virtually nothing is known about the behaviour of $\text{Im } \Delta f = -\text{Im } \bar{f}$ below threshold. We find that the assumption of a zero contribution from the integral between ω_Λ and m_{K^0} in Eq. 7.1 is perfectly compatible with all experimental information.

This gives $2 + 7 = 9$ parameters to be determined in the fit. It turns out, however, that the available data are quite insensitive to the pole position ω_p . We therefore fix it to the position of the Λ pole, given by the total energy needed to form a $^{12}\text{C}_\Lambda$ resonance,

$$s = m^2(^{12}\text{C}_\Lambda) = m^2(K^0) + m^2(^{12}\text{C}) + 2\omega_p m(^{12}\text{C}),$$

which gives $\omega_p = 172.3$ MeV.

Further parameters are needed for experimental reasons. As is evident from Fig. 14a, there are systematic shifts in the normalization of the moduli measured by the high energy experiments (parameter β) whereas there is good agreement on the much more relevant slope parameter α . To prevent the systematic normalization uncertainties from affecting the result on α , we allow for three additional correction factors, N_{Car} , N_{Alb} and N_{Roe} for the Brookhaven [80], Serpukhov [81, 82] and Fermilab [76] experiments, respectively, to be determined together with the other parameters in the fit. The new Fermilab collaboration [73] completely evaded the normalization problem by not publishing individual data points but only a fitted α . We directly employ this value in our fit.

7.3 Fit results and discussion

We now vary the 11 parameters defined in the preceding Subsection and compare at each data point the prediction from (7.1) with the experimental error range. Correlations between different measured quantities are taken into account where they have been reported, in particular the strong correlations between our own measurements of imaginary and real parts. Uncertainties in beam momentum/energy are neglected throughout. The weighted deviations are then summed up to a χ^2 in the usual way. Minimization of this χ^2 yields the following parameters:

$$\begin{array}{lll} r = 1.95 \pm 0.25 & \omega_k = (4570_{-330}^{+360}) \text{ MeV} & N_{\text{Car}} = 0.96 \pm 0.02 \\ C = (2.56 \pm 0.18) \text{ fm} & a = 0.61 \pm 0.03 & N_{\text{Alb}} = 1.22 \pm 0.07 \\ \omega_{\text{res}} = (1130 \pm 9) \text{ MeV} & \alpha = 0.424 \pm 0.005 & N_{\text{Roe}} = 1.07 \pm 0.03 \\ \sigma = (147 \pm 12) \text{ MeV} & \beta = (0.35 \pm 0.02) \text{ fm} & \end{array} \quad (7.4)$$

The minimized χ^2 is 133.4 for 127 degrees of freedom. The resulting fit function is inserted in Fig. 14, together with an optical model calculation [39]. Including the data of Ref. 86 in our fit hardly changes the pole residue but increases the χ^2 to 198.0 for now 133 degrees of freedom.

Perhaps the most surprising result is the pole residue r . The fit returns a positive value although theoretical considerations unambiguously lead to negative signs for the poles governing the amplitude $f(0) - \bar{f}(0)$: The sign of a pole in the unphysical region depends on the relative parity of the particles

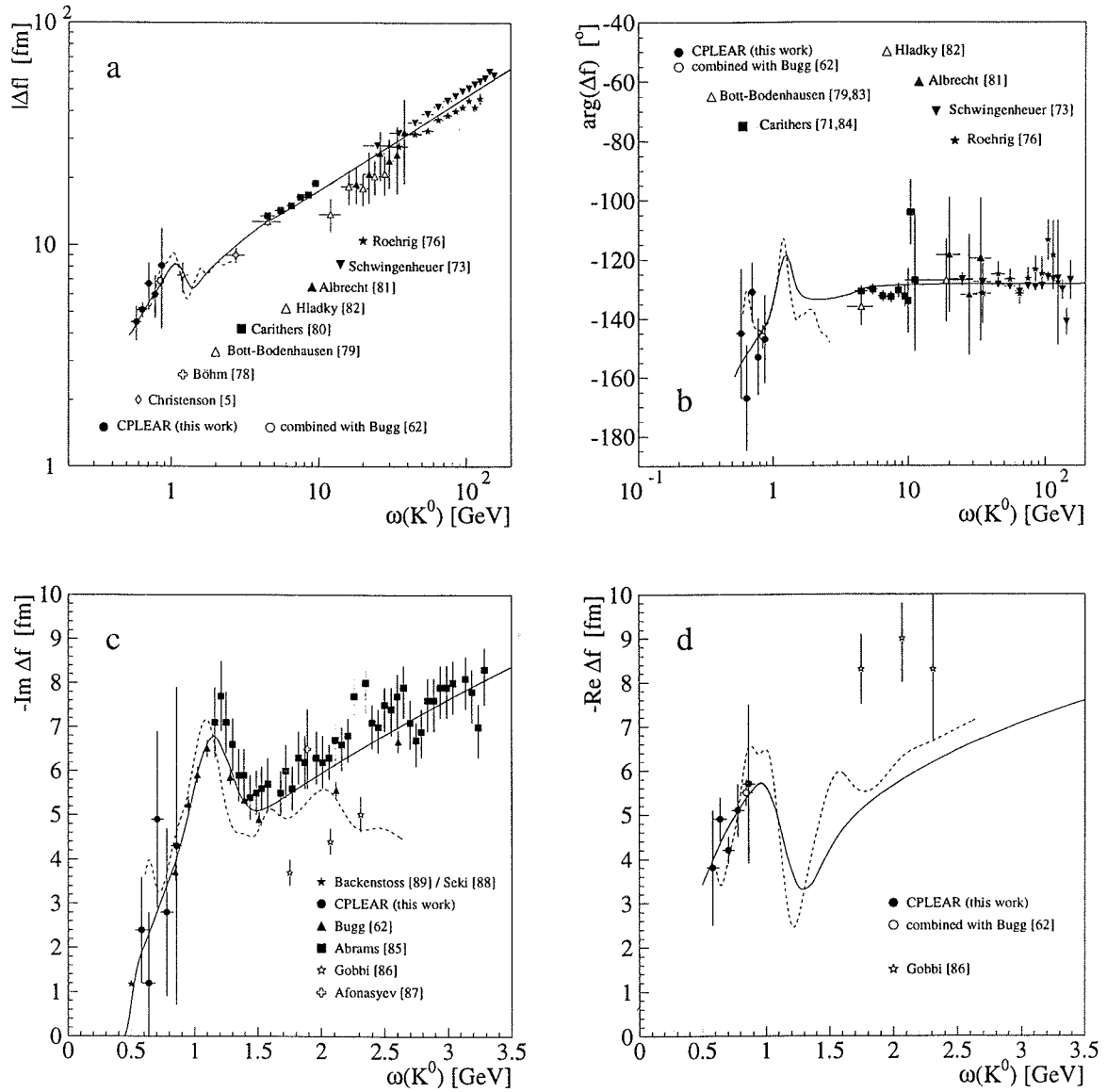


Figure 14: Modulus (a), phase (b), imaginary part (c) and real part (d) of the regeneration amplitude Δf : experimental results in comparison with our fit (full line) and the optical model calculation of Ref. 39 (dashed line). The data points of Schwingenheuer et al. are taken from Refs. 90 and 91 and are shown just for visualization (only their published value for α enters the fit). The phases of Refs. 83 and 79 as well as those of Refs. 84 and 71 have been averaged for clarity. The data of Ref. 86 are discarded in the fit. Note the different scales of the plot axes.

involved [93]. In our case we find that the direct poles appearing in the scattering of \bar{K}^0 (Λ or Σ for interaction with a neutron or a proton inside the carbon nucleus, respectively) have a positive sign whereas the corresponding exchange poles due to the K^0 component are negative. Therefore an effective pole describing the difference $f - \bar{f}$ must have a negative sign. The question arises whether there actually is a pole in the data. To see this we build the so-called discrepancy function $\Delta(\omega)$, a simple rearrangement of the dispersion relation that isolates the pole term:

$$\Delta(\omega) := \text{Re } \Delta f(\omega) - \frac{2\omega}{\pi} \mathcal{P} \int_{\omega_\Lambda}^{\infty} d\omega' \frac{\text{Im } \Delta f(\omega')}{\omega'^2 - \omega^2} = \frac{2\omega r}{\omega^2 - \omega_p^2}, \quad (7.5)$$

i.e. we look at the discrepancy between the (measured) real parts of the amplitude and the values resulting from the integration over the imaginary part, which is due to the unknown pole contributions. The Δ -values following from our data on $\text{Re } \Delta f$ are plotted in Fig. 15 together with our fit result. It can be seen that the data do not really suggest a pole but are well compatible with the one from our fit. It is therefore conceivable if not probable that our data are located in an energy range that is still dominated by resonances and not any sub-threshold poles. We must also keep in mind that our parameterization for $\text{Im } \Delta f$ is rather arbitrary: introducing structure in $\text{Im } \Delta f(\omega)$ below and above threshold leads to considerable shifts in $\Delta(\omega)$ and thus in the pole residue. Abundance and quality of the data at our disposal in the low energy range for real and imaginary parts of the amplitude are simply not sufficient to decide whether we are seeing contributions from poles or from low energy resonances, but the incompatibility of the obtained pole sign with theoretical expectation suggests the latter. Further support for this hypothesis stems from the fact that the optical model calculation of Ref. 39 shows a resonance between 600 and 700 MeV (see Fig. 14) which is not indicated by the data (but not contradicted either) and thus ignored in our fit.

Earlier attempts to determine the pole residue [95, 96] relied solely on the real parts measured by Gobbi et al. (whose data we have discarded in view of their incompatibility with all other experiments) and lead to very different results, -23.3 and -11.7 , respectively. Dumbrajs' fit, performed with essentially the same assumptions on the low energy behaviour of $\text{Im } \Delta f$, is indicated in Fig. 15. We see that, regardless of the quality of the data of Gobbi et al., it is a hopeless venture to try to learn something about the sub-threshold pole from three data points at intermediate energies! Our data below 1 GeV clearly refute his analysis.

The interpretation of our data in terms of poles and resonances is still the subject of investigation. As a preliminary conclusion it may be said that our parameterization, based on a simple dispersion relation and single Regge pole exchange (Eqs. 7.1–7.3 and 7.4), describes the current experimental information on the regeneration amplitude in carbon very well, barring the experimental normalization problems mentioned above. We must be cautious, however, when interpreting the fitted parameters and should try to avoid running into the same errors that were made in earlier analyses: probably the pole term in our parameterization just *happens* to fit the data but is not physically significant. Further data would be needed to resolve more structure, both in the unphysical (poles) and the physical region (resonances). At high energies our fit reproduces the results found by other Regge analyses [73, 76, 80, 82] (corrected for changes in the neutral kaon parameters, see Section 7.1).

7.4 Determining the regeneration phase from a dispersion relation: the example of E731/E773

A beautiful example of an application of dispersion relations to neutral kaon regeneration was given by the Fermilab E731 and E773 collaborations: they derive the regeneration phase at high energies from their measured moduli by assuming analyticity and Regge behaviour of the amplitude. A pure power law was assumed in the analysis of the E731 experiment (B_4C regenerator) leading to a systematic error of 0.5° on the regeneration phase [23, 72]. For the successor experiment E773 [73] ($CH_{1.1}$ regenerator), a more elaborate study was performed including the effects of elastic and inelastic nuclear screening, low-energy phenomena, sub-leading Regge-trajectories and electromagnetic regeneration [90]. Even so their procedure of evaluating the systematic error on the regeneration phase was sharply criticized by Kleinknecht [97], a member of the rivalling NA31 collaboration. His main argument was that breaks in the momentum power law observed with heavier nuclei at around 20 GeV/c momentum might also

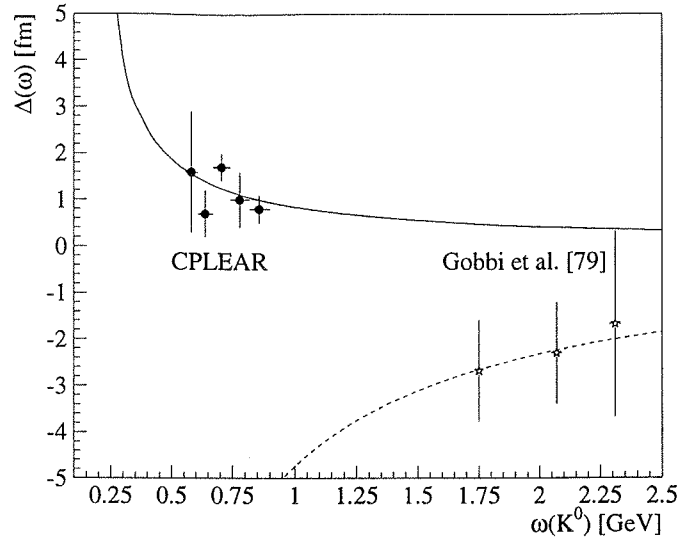


Figure 15: The discrepancy function $\Delta(\omega)$ as derived from our data (full circles) and from the data of Ref. 86 (open stars). Our pole fit yielding $r = 1.95 \pm 0.25$ is indicated as a full line. The dashed line represents the fit of Ref. 96 which gave $r = 12.2 \pm 3.0$.

occur with carbon and even reoccur at higher energies with considerable influence on the phase. Winstein and Briere of the E773 collaboration then gave convincing evidence that the mechanisms responsible for the distortions in the momentum power law for heavy nuclei are well understood and that the resulting effects are small for light nuclei like Carbon and absent anyhow at higher energies [98]. Kleinknecht remained sceptical, emphasizing the complete lack of experimental information on the modulus of the regeneration amplitude above 160 GeV/c momentum [99], and so the dispute went on [100, 101].

Unfortunately our results at low energies are not a great help in this particular case because the contributions to the dispersion integral from this energy range are localized, as pointed out in Refs. 98 and 102. Our global analysis tells us at least that all data above about 5 GeV/c momentum are compatible with a single pure power law, i.e. there is no experimental evidence for a “kink,” neither around 20 GeV/c nor at any higher momentum up to 160 GeV/c.

So to a large extent the judgement remains a matter of taste [14]. We believe that Winstein and Briere have successfully invalidated Kleinknecht’s central argument: a significant break of the momentum power law in the relevant energy range indeed seems very unlikely. On the other hand, however, Kleinknecht is perfectly right when insisting on direct, purely experimental proof in an affair of such far-reaching consequences as a test of CPT symmetry. For it is clear that if E773 actually had announced evidence for CPT violation following from this analysis then the majority of the physics community would have doubted the correctness of their regeneration phase rather than questioning CPT symmetry! The Fermilab experimenters hold out the prospect of directly measuring the regeneration phase with semileptonic decays [101].

8 SUMMARY AND CONCLUSION

In a dedicated supplementary run with a slightly modified detector the CPLEAR collaboration has successfully applied its characteristic $K^0-\bar{K}^0$ asymmetry method to determine the neutral kaon regeneration amplitude in carbon at sub-GeV energies. The experiment measures the interference between inherent and coherently regenerated K_S amplitude by comparing decay rate asymmetries recorded with and without a 2.5 cm carbon regenerator installed in the detector at a distance of 5.8 cm from the neutral kaon production point. This method yields the real and imaginary parts of the amplitudes and minimizes systematic uncertainties.

It is the first measurement of regeneration in carbon in this energy range. The obtained amplitudes are in good agreement with theoretical expectations and fit well into the picture of existing measurements at higher energies, as is demonstrated by a dispersion relation analysis taking into account all available data on regeneration in carbon. This analysis affords new insights into the behaviour of the amplitude at and below the kaon mass threshold, clearly refuting earlier studies that were based on poorer experimental input.

The primary objective of the regeneration experiment, a significant reduction of the systematic error on the CP violating phase ϕ_{+-} as measured by CPLEAR, has been achieved. This enables us to publish the world's most accurate measurement of this key parameter, an important step towards the understanding of the mechanism behind CP violation as well as an essential input for CPT tests. Apart from this most prominent result the refined regeneration correction has been used to improve many other measurements performed with the CPLEAR detector. Moreover our data will also help future low-energy neutral kaon experiments better assess the effects of regeneration in their detectors.

A PHASE CONVENTIONS IN THE NEUTRAL KAON SYSTEM

Confusion arises from the fact that many different phase conventions have been used in describing the phenomenology of neutral kaons, so that it appears appropriate to spend a few words on that subject and thereby clarify our choice of phase convention.

Apart from an overall phase factor associated with all particles we are free to choose two phases when dealing with neutral kaons, namely the phase between the strange and the non-strange sector and the phase between K^0 and \bar{K}^0 ("the relative kaon phase"). The first phase is usually fixed by demanding that the phase of the CPT operator be the same when acting on a K^0 or a two pion final state [11]. Then the remaining phase between K^0 and \bar{K}^0 may be fixed by choosing a phase *either* for one of the two-pionic decay amplitudes¹⁵ of K^0 ,

$$A_I = |A_I|e^{i\theta_I} \quad (I = 0, 2),$$

or for the CP operator acting on the state K^0 , but in general not both.

In the first case it seems natural to choose either one of the amplitudes to be real and positive. This results in the famous Wu–Yang convention [103] for $\theta_0 = 0$ or the so called quark phase convention for $\theta_2 = 0$. The two most common choices for the CP phase, both in general incompatible with either of the above-mentioned conventions, are

$$CPK^0 = \bar{K}^0, \quad (\text{A.1})$$

sometimes called the charge-parity convention, and

$$CPK^0 = -\bar{K}^0, \quad (\text{A.2})$$

which might be called the negative charge-parity convention. This choice of phases turns out to be the most natural in the framework of the standard model where everything is expressed in terms of quark fields [104, 105]. We will therefore refer to (A.2) as the SM phase convention.

We do not see any benefit in working in a completely phase independent framework and adopt the SM phase convention (A.2). In this convention the mass eigenstates are usually expressed as (cf. Eqs. 2.8 and 2.15),

$$\begin{aligned} K_{L,S} &= \frac{1}{\sqrt{|p|^2 + |q|^2}} [pK^0 \pm q\bar{K}^0] \\ &= \frac{1}{\sqrt{2(1 + |\epsilon_T|^2)}} [(1 + \epsilon_T)K^0 \pm (1 - \epsilon_T)\bar{K}^0] \end{aligned}$$

with

$$\epsilon_T = \frac{p - q}{p + q} \quad (\text{A.3})$$

where CPT symmetry is assumed. We emphasize that this T violation parameter is not identical with the decay parameter ϵ of (2.22). The ϵ defined there is (at least in principle) a measurable quantity and therefore has the same complex value regardless of any conventional phases, whereas ϵ_T does depend on our choice of phase. In the literature the phase-dependent epsilon is often labelled with a tilde ($\tilde{\epsilon}$) [105, 106] or a bar ($\bar{\epsilon}$) [107, 108], or avoided altogether [104]. The expression for ϵ corresponding to (A.3) is

$$\epsilon = \frac{p - qe^{-2i\theta_0}}{p + qe^{-2i\theta_0}} \quad (\text{A.4})$$

and illustrates how choosing a value for θ_0 fixes the phase of p/q and vice versa. From (A.3) and (A.4) follows that

$$\epsilon = \frac{1 - e^{-2i\theta_0} + \epsilon_T(1 + e^{-2i\theta_0})}{1 + e^{-2i\theta_0} + \epsilon_T(1 - e^{-2i\theta_0})} = \frac{\epsilon_T + i \tan \theta_0}{1 + \epsilon_T i \tan \theta_0} \quad (\text{A.5})$$

15. See definition in Section 2.2; θ_I does not include the strong scattering phase shift δ_I .

and we see that $\epsilon = \epsilon_T$ only holds in the Wu–Yang convention. In the SM phase convention A_0 and A_2 are only complex if there is direct CP violation (or CPT violation) in the decays to two pions, an effect that so far has escaped experimental observation and therefore must be very tiny. This means that θ_0 is very small and (A.5) may safely be written as [106]

$$\epsilon = \epsilon_T + i \frac{\text{Im } A_0}{\text{Re } A_0}. \quad (\text{A.6})$$

So, in our phase convention, ϵ_T is very nearly equal to ϵ and in circumstances where effects from direct CP violation and CPT violation may be neglected (as is the case in this work on kaon regeneration) we are left with only one parameter describing CP violation, namely

$$\epsilon \approx \eta_{+-} = 2.25 \times 10^{-3} \times \exp(i 43.6^\circ). \quad (\text{A.7})$$

REFERENCES

- [1] E.D. Commins and P.H. Bucksbaum, *Weak Interactions of Leptons and Quarks* (Cambridge University Press, Cambridge, 1983), Chapter 7.
- [2] G.D. Rochester and C.C. Butler, *Nature* 160 (1947) 855.
- [3] M. Gell-Mann and A. Pais, *Phys. Rev.* 97 (1955) 1387.
- [4] K. Lande, E.T. Booth, J. Impeduglia, L.M. Lederman, and W. Chinowsky, *Phys. Rev.* 103 (1956) 1901;
K. Lande, L.M. Lederman, and W. Chinowsky, *Phys. Rev.* 105 (1957) 1925;
M. Bardon, K. Lande, L.M. Lederman, and W. Chinowsky, *Annals Phys.* 5 (1958) 156.
- [5] J.H. Christenson, J.W. Cronin, V.L. Fitch, and R. Turlay, *Phys. Rev. Lett.* 13 (1964) 138, *Phys. Rev.* 140 (1965) B74.
- [6] V. Weisskopf and E. Wigner, *Z. Phys.* 63 (1930) 54, *ibid* 65 (1930) 18.
- [7] T.D. Lee, R. Oehme, and C.N. Yang, *Phys. Rev.* 106 (1957) 340.
- [8] N. Cabibbo, Possible consequences of the $K_S^0 \rightarrow \pi^+ + \pi^-$ decay (CP violation and other interpretations), in: *Symmetries in Elementary Particle Physics*, ed. A. Zichichi (Academic Press, New York, 1965), p. 256.
- [9] C.P. Enz and R.R. Lewis, *Helv. Phys. Acta* 38 (1965) 860.
- [10] P.K. Kabir, *The CP Puzzle* (Academic Press, London, 1968).
- [11] W.J. Mantke, CERN preprint hep-ph-9506297 (1995).
- [12] M. Kobayashi and T. Maskawa, *Prog. Theor. Phys.* 49 (1973) 652.
- [13] J.S. Bell and J. Steinberger, Weak interactions of kaons, in: *Proc. Int. Conf. on Elementary Particles* (Oxford, September 1965), eds. R.G. Moorhouse, A.E. Taylor, and T.R. Walsh (Rutherford High Energy Laboratory, 1966) p. 195.
- [14] L. Wolfenstein and T. Trippe, CP violation in K_L^0 decay, in Ref. 15 (p. 422).
- [15] Particle Data Group, R.M. Barnett et al., *Phys. Rev. D* 54 (1996) 1.
- [16] CPLEAR Collab., in preparation; see also:
A. Benelli, Ph.D. thesis, University of Liverpool (1997);
M. Danielsson, Ph.D. thesis, KTH Stockholm (1996).
- [17] H. Quinn, $B^0 - \bar{B}^0$ mixing and CP violation in B decay, in Ref. 15 (p. 507).
- [18] E. Chell and M.G. Olsson, *Phys. Rev. D* 48 (1993) 4076.
- [19] A.J. Buras, M. Jamin, and M. Lautenbacher, *Phys. Lett. B* 389 (1996) 749.
- [20] G. Buchalla and A.J. Buras, *Phys. Rev. D* 54 (1996) 6782.
- [21] L. Lavoura, *Annals Phys.* 207 (1991) 428.
- [22] V.V. Barmin et al., *Nucl. Phys. B* 247 (1984) 293, *ibid* 254 (1985) 747 (erratum).
- [23] L.K. Gibbons et al., *Phys. Rev. D* 55 (1997) 6625.
- [24] D.H. Perkins, *Introduction to High Energy Physics* (Addison-Wesley, 1987), Chapter 7.
- [25] A. Das and T. Ferbel, *Introduction to Nuclear and Particle Physics* (Wiley, New York, 1994), Chapter XII.
- [26] A. Pais and O. Piccioni, *Phys. Rev.* 100 (1955) 1487.
- [27] K.M. Case, *Phys. Rev.* 103 (1956) 1449.
- [28] M.L. Good, *Phys. Rev.* 106 (1957) 591, *ibid* 110 (1958) 550.
- [29] R.H. Good et al., *Phys. Rev.* 124 (1961) 1223.
- [30] K. Kleinknecht, *Fortschritte der Physik* 21 (1973) 57, *Ann. Rev. Nucl. Sci.* 26 (1966) 1.
- [31] G. Charpak and M. Gourdin, The $K^0 \bar{K}^0$ system, CERN 67-18, CERN, Geneva (1967).
- [32] W. Fetscher, P. Kokkas, P. Pavlopoulos, Th. Ruf, and Th. Schietinger, *Z. Phys. C* 72 (1996) 543.
- [33] M. Lax, *Revs. Modern Phys.* 23 (1951) 287; for a less rigorous treatment see also J.D. Jackson, *Classical Electrodynamics* (Wiley, New York, 1975), second edition, Section 9.14.
- [34] T.D. Lee and C.S. Wu, *Ann. Rev. Nucl. Sci.* 16 (1966) 511.
- [35] See for instance the study in Ref. 29 or H. Foeth et al., *Phys. Lett. B* 31 (1969) 544 and *B* 30 (1969) 276.
- [36] A. Böhm et al., *Phys. Lett. B* 27 (1968) 594.

- [37] R.A. Eisenstein, Kaon elastic and inelastic scattering at 800 MeV/c, in: Proc. Kaon Factory Workshop (Vancouver, August 1979), ed. M.K. Craddock (TRIUMF, Vancouver, 1979) p. 75.
- [38] R. Baldini and A. Michetti, LNF-96/008 (1996), unpublished.
- [39] P.H. Eberhard and F. Uchiyama, Nucl. Instr. and Meth. A 350 (1994) 144.
- [40] A. Michetti, Tesi di Laurea, University "La Sapienza," Rome (1993) (p. 127).
- [41] Ch. Yeche, in: Minutes of the CPLEAR $\pi^+\pi^-$ analysis meeting nr. 18 (26 May 1994), unpublished.
- [42] Ph. Bloch, CPLEAR $\pi^+\pi^-$ note nr. 11 (1997), unpublished
- [43] Th. Schietinger, CPLEAR note PPE/PS195/TS/97-02 (1997), unpublished.
- [44] E. Gabathuler and P. Pavlopoulos, Strong and weak CP violation at LEAR, in: Proc. Workshop on Physics at LEAR with Low Energy Cooled Antiprotons (Erice, 1982), eds. U. Gastaldi and R. Klapisch (Plenum, New York, 1984) p. 747.
- [45] R. Armenteros and B. French, Antinucleon-nucleon interactions, in: High Energy Physics, Vol. IV, ed. E.H.S. Burhop (Academic Press, New York, 1969) p. 237.
- [46] E. Jones, The CERN \bar{p} -complex and present status and future developments of the antiproton accumulator, in: Proc. Workshop on Physics at LEAR with Low Energy Cooled Antiprotons (Erice, 1982), eds. U. Gastaldi and R. Klapisch (Plenum, New York, 1984) p. 5.
- [47] D. Möhl, Phase-space cooling techniques and their combination at LEAR, in: Proc. Workshop on Physics at LEAR with Low Energy Cooled Antiprotons (Erice, 1982), eds. U. Gastaldi and R. Klapisch (Plenum, New York, 1984) p. 27.
- [48] M. Chanel, LEAR status, performance and developments, in: Proc. of the Third Biennial Conference on Low Energy Antiproton Physics (Bled, 1994), eds. G. Kernel, P. Križan, M. Mikuž (World Scientific Publishing Co., Singapore, 1995) p. 511.
- [49] CPLEAR Collab., R. Adler et al., Nucl. Instr. and Meth. A 379 (1996) 76.
- [50] R. Kreuger, Ph.D. thesis, Delft University of Technology (1998).
- [51] Ch. Bula, Ph.D. thesis, ETH Zurich (1992).
- [52] M. Dejardin, J. Derre, J.L. Faure, C. Guyot, and G. Marel, Nucl. Instr. and Meth. A 283 (1989) 484.
- [53] R. Rickenbach, Ph.D. thesis, University of Basel (1989).
- [54] CPLEAR Collab., A. Angelopoulos et al., Nucl. Instr. and Meth. A 311 (1992) 78.
- [55] CPLEAR Collab., R. Adler et al., Nucl. Instr. and Meth. A 390 (1997) 293.
- [56] CPLEAR Collab., R. Adler et al., Phys. Lett. B 363 (1995) 243.
- [57] See for instance A.C. Kak and M. Slaney, Principles of Computerized Tomographic Imaging (IEEE Press, New York, 1987).
- [58] M. Wolter, Ph.D. thesis, ETH Zurich (1996).
- [59] CPLEAR Collab., R. Adler et al., Phys. Lett. B 363 (1995) 237.
- [60] C. Thibault in: Proceedings of the 41st CPLEAR Collaboration Meeting (Geneva, April 1998), CERN PS195/CM-41/10, unpublished.
- [61] CPLEAR Collab., A. Apostolakis et al., Phys. Lett. B 422 (1998) 339.
- [62] D.V. Bugg et al., Phys. Rev. 168 (1968) 1466.
- [63] R.A. Krauss et al., Phys. Rev. C 46 (1992) 655;
see also R. Weiss et al., Phys. Rev. C 49 (1994) 2569.
- [64] CPLEAR Collab., A. Angelopoulos et al., Phys. Lett. B 413 (1997) 422.
- [65] A. Gsponer et al., Phys. Rev. Lett. 42 (1979) 13.
- [66] M. Cullen et al., Phys. Lett. B 32 (1970) 523.
- [67] R. Carosi et al., Phys. Lett. B 237 (1990) 303.
- [68] C. Geweniger et al., Phys. Lett. B 52 (1974) 108.
- [69] S. Gjesdal et al., Phys. Lett. B 52 (1974) 113.
- [70] C. Geweniger et al., Phys. Lett. B 48 (1974) 487.
- [71] W.C. Carithers et al., Phys. Rev. Lett. 34 (1975) 1244.
- [72] L.K. Gibbons et al., Phys. Rev. Lett. 70 (1993) 1199.
- [73] B. Schwingenheuer et al., Phys. Rev. Lett. 74 (1995) 4376.
- [74] CPLEAR Collab., R. Adler et al., Phys. Lett. B 369 (1996) 367.

- [75] V.L. Telegdi, K_S -regeneration: an interplay of nuclear and particle physics, in: AIP Conf. Proc. No. 26 (International Conference on High-Energy Physics and Nuclear Structure, Santa Fe and Los Alamos, June 1975), eds. D.E. Nagle et al. (AIP, New York, 1975) p. 289.
- [76] J. Roehrig et al., Phys. Rev. Lett. 38 (1977) 1116, *ibid* 39 (1977) 674 (erratum).
- [77] J. Antolín, Phys. Rev. D 43 (1991) 1532, J. Math. Phys. 31 (1990) 791;
J. Antolín and A. Cruz, J. Math. Phys. 27 (1986) 104, J. Phys. G: Nucl. Phys. 12 (1986) 297.
- [78] A. Böhm et al. (1966) unpublished, cited in K. Kleinknecht, Fortschritte der Physik 21 (1973) 57 (p. 71); K. Kleinknecht, private communication.
- [79] M. Bott-Bodenhausen et al., Interference between K_L and K_S amplitudes in the $\pi^+\pi^-$ decay mode, in: Proc. Topical Conference on Weak Interactions (Geneva, January 1969), CERN 69-7 (Geneva, 1969) p. 329.
- [80] W.C. Carithers et al., Nucl. Phys. B 118 (1977) 333.
- [81] K.-F. Albrecht et al., Nucl. Phys. B 93 (1975) 237.
- [82] J. Hladký et al., Czech. J. Phys. B 26 (1976) 1290.
- [83] M. Bott-Bodenhausen et al., Phys. Lett. 24B (1967) 438.
- [84] W.C. Carithers et al., Phys. Rev. Lett. 34 (1975) 1240.
- [85] R.J. Abrams et al., Phys. Rev. D 4 (1971) 3235.
- [86] B. Gobbi, W. Hakel, J.L. Rosen, and S. Shapiro, Phys. Rev. Lett. 29 (1972) 1278, 1281.
- [87] V.N. Afonasyev et al., Yad. Phys. 47 (1988) 1656.
- [88] R. Seki, Phys. Rev. Lett. 29 (1972) 240.
- [89] G. Backenstoss et al., Phys. Lett. 38B (1972) 181.
- [90] R.A. Briere, Ph.D. thesis, University of Chicago (1995).
- [91] R.A. Briere, private communication (1997).
- [92] N.M. Queen and G. Violini, Dispersion Theory in High-Energy Physics (Macmillan, London, 1974).
- [93] T.E.O. Ericson and M.P. Locher, Nucl. Phys. A 148 (1970) 1.
- [94] N. Cabibbo, Phys. Lett. 22 (1966) 212.
- [95] K. Arai, I. Endo, and M. Kikugawa, Prog. Theor. Phys. 56 (1976) 1345.
- [96] O. Dumbrajs, Nuovo Cimento 54 A (1979) 155, see also: Kaon-nucleus scattering, regeneration and analyticity, in: Proc. Low and Intermediate Energy Kaon-nucleon Physics (Rome, March 1980), eds. E. Ferrari and G. Violini (D. Reidel, Holland, 1981) p. 187.
- [97] K. Kleinknecht and S. Luitz, Phys. Lett. B 336 (1994) 581.
- [98] R.A. Briere and B. Winstein, Phys. Rev. Lett. 75 (1995) 402, *ibid* 75 (1995) 2070 (erratum).
- [99] K. Kleinknecht, Phys. Rev. Lett. 75 (1995) 4784.
- [100] R.A. Briere and B. Winstein, Phys. Rev. Lett. 75 (1995) 4785.
- [101] Contributions to round-table discussion on regeneration phase measurement by A. Martin, K. Kleinknecht and B. Winstein, in: Proc. of the Workshop on K Physics (Orsay, 1996), ed. L. Iconomidou-Fayard (Editions Frontières, Gif-sur-Yvette Cedex, 1997) p. 329–342.
- [102] R.A. Briere, CPT tests from E773 and the regeneration phase, in: Proc. of the Workshop on K Physics (Orsay, 1996), ed. L. Iconomidou-Fayard (Editions Frontières, Gif-sur-Yvette Cedex, 1997) p. 321.
- [103] T.T. Wu and C.N. Yang, Phys. Rev. Lett. 13 (1964) 380.
- [104] E. Leader and E. Pedrazzi, An Introduction to Gauge Theories and Modern Particle Physics (Cambridge University Press, 1996), Chapter 19.
- [105] E. de Rafael, Chiral Lagrangians and kaon CP-violation, in: CP violation and the limits of the Standard Model, Proc. of the 1994 Theoretical Advanced Study Institute in Elementary Particle Physics (Boulder, Colorado, May–June 1994), ed. J.F. Donoghue (World Scientific, Singapore, 1995) p. 15.
- [106] L. Wolfenstein, Section 13 in Ref. 15 (p. 102).
- [107] Y. Nir, The CKM matrix and CP violation, in: Perspectives in the Standard Model, Proc. of the 1991 Theoretical Advanced Study Institute in Elementary Particle Physics (Boulder, Colorado, June 1991), eds. R.K. Ellis, C.T. Hill and J.D. Lykken (World Scientific, Singapore, 1992) p. 339.
- [108] M.C. Bañuls, J. Bernabéu, Phys. Lett. B 423 (1998) 151.

ACKNOWLEDGEMENTS

The past three years have been a magnificent time for me, professionally as well as personally. I have felt very privileged to experience both the amicable atmosphere of the Basel physics institute and the ineffable excitement of working at the world's largest research facility. I would like to thank everyone who contributed to this work in one way or another. In particular I wish to express my appreciation and gratitude to:

- Ludwig Tauscher for entrusting me with the job of measuring regeneration with the CPLEAR collaboration and for giving me all the liberty to pursue this challenging task. I have much profited from his subtle yet firm guidance and enjoyed many a discussion with him which always are refreshing experiences thanks to his crystal-clear opinion on whatever subject.
- René Rickenbach for teaching me a lot about physics, statistical methods and many other things more or less useful in life as well as for his (fruitless) efforts to develop a taste for grappa in me.
- Noulis Pavlopoulos for a warm welcome into CPLEAR, for the enormous confidence he placed in me from the start, and for being a good boss to all of us.
- Guido Polivka for the gratifying cooperation within CPLEAR, for his help in countless computing problems, and for not smoking too often in the office.
- Wulf Fetscher, Panos Kokkas, and Thomas Ruf for their help in the earlier stages of this work. Without their efforts in the preparation of the regeneration experiment the measurement would never have gone so smoothly.
- Maria Fidecaro for all the energy and dedication she has put into CPLEAR ensuring a high scientific standard in our collaboration, and for initiating me into Italian literature.
- Philippe Bloch for his many intelligent suggestions and comments on my work.
- John Ellis, Nikolaos Mavromatos and Milan Locher for their assistance in the dispersion relation analysis; special thanks to Nik for the hospitality at Oxford.
- my cernmates (in alphabetical order): Pedram Bargassa, Olaf Behnke, Angela Benelli-Maley, Frédéric Blanc, Rob Kreuger, and Bernd Pagels, for the good times at CERN and elsewhere.
- the rest of the Basel gang (in reverse alphabetical order): Maneesh Wadhwa, Sotirios Vlachos, Michael Steinacher, Fabian Leimgruber, Beat Henrich, Daniel Haas, and Pablo García-Abia, for the pleasant atmosphere in our group and for sharing their experience and knowledge at numerous occasions.
- all other members of the CPLEAR collaboration for designing, constructing and operating this marvellous experiment which I proudly was part of.
- Michael Dröge and Daniel Guyon for their technical support.
- Andres Laib (and his colleagues at IBT Zurich) for performing the computer tomography of the regenerator—and for a lot more than that!
- Martin Dickopp for his valuable contribution to the photon conversion analysis.
- Esther Meyer and Nathalie Grüb for taking care of all the administrative tasks at the Basel Institute and at CERN, respectively, and for being around and helpful whenever needed.
- Paul Maley for carefully reading and correcting the manuscript, drawing my attention to some of the finer subtleties of the English language.

Above all though, I am indebted to my parents for their great support and encouragement throughout the years. And then I also wish to thank *my first, my last, my everything*, Annette Widmer, for her love, support, and understanding.

CURRICULUM VITAE

Thomas Martin Schietinger, citizen of Basel, Switzerland:

8 May 1969 born in Basel.

1975–1985 schools in Binningen (BL)

1985–1988 Gymnasium Oberwil (BL), Matura (type B)

1988–1994 ETH Zurich, physics diploma

diploma thesis: *Measurement of Charm Production in the H1 Detector at HERA*

supervisor: Ralph Eichler

1995–1998 University of Basel, care of students, and

CERN, research within the CPLEAR collaboration

The following lecturers have contributed to my academic education: A. Anselm, E.H. Berninger, G.C. Branco, J. Brunner, R.E. Bühler, A. Cohen, J.-P. Egger, R. Eichler, L.R. Evans, F.L. Fabbri, W. Fetscher, P. Franzini, J. Fröhlich, H.-J. Gerber, C. Guaraldo, K. Hepp, W. Hunziker, V.G. Kadyshevsky, K. Kajantie, O.E. Lanford, J. Lang, P. Läuchli, E. Leader, H.J. Leisi, C.H. Llewellyn Smith, W. Lukosz, M. Mangano, J. Marti, G. Martinelli, A. Masiero, T. Nakada, H. Nussbaumer, K. Osterwalder, H.R. Ott, P. Pavlopoulos, D. Perret-Gallix, M.E. Peskin, A. Pich, M. Preger, E. de Rafael, T.M. Rice, R. Rickenbach, G. Rostoker, D. Schaile, C. Schmid, H.-J. Schötzau, A.Yu. Smirnov, M. Spiro, L. Tauscher, E. Trubowitz, and G. Wüstholtz.

ZUSAMMENFASSUNG

In einem Zusatzexperiment mit leicht modifiziertem Detektor hat die CPLEAR-Kollaboration die ihr eigene $K^0-\bar{K}^0$ -Asymmetrie-Methode mit Erfolg angewandt, um die K_L-K_S -Regenerationsamplitude in Kohlenstoff bei Energien unter einem GeV zu bestimmen. Das Experiment mißt die Interferenz zwischen ursprünglicher und regenerierter K_S -Amplitude durch Vergleich der Zerfallsasymmetrien, welche einmal mit dem Kohlenstoffregenerator im Detektor und einmal ohne denselben aufgezeichnet worden sind. Der Regenerator hat eine Dicke von 2.5 cm und befindet sich in einer Entfernung von 5.8 cm vom $K^0(\bar{K}^0)$ -Produktionspunkt. Diese Methode ermöglicht die Messung von Real- und Imaginärteil der Amplituden und minimiert systematische Fehler.

Es handelt sich hier um die erste Messung von Kaon-Regeneration in Kohlenstoff in diesem Energiebereich. Die erhaltenen Amplituden stimmen gut mit theoretischen Erwartungen überein und passen auch gut in das Bild bisheriger Messungen bei höheren Energien, wie eine Dispersionsanalyse unter Berücksichtigung aller verfügbaren Daten über Regeneration in Kohlenstoff zeigt. Diese Analyse gewährt neue Einblicke in das Verhalten der Amplitude in der Nähe der durch die Kaonmasse gegebenen Schwelle und widerlegt eindeutig ältere Arbeiten, welche auf Daten von geringerer Qualität beruhen.

Das primäre Ziel des Regenerationsexperimentes, eine deutliche Verringerung des systematischen Fehlers der von CPLEAR gemessenen CP-verletzenden Phase ϕ_{+-} , wurde erreicht. Dies erlaubt uns nun die Publikation der weltweit genauesten Messung dieses bedeutsamen Parameters – einerseits ein wichtiger Schritt im Bemühen um die Entschlüsselung des Rätsels der CP-Verletzung, andererseits aber auch eine Verbesserung vieler CPT-Tests. Neben diesem wohl bedeutendsten Ergebnis konnten auch viele andere mit dem CPLEAR-Detektor durchgeführten Messungen von der verbesserten Regenerationskorrektur profitieren. Darüberhinaus werden unsere Daten wohl auch zukünftigen niederenergetischen Kaon-Experimenten helfen, die Regenerationseffekte in deren Detektoren besser abzuschätzen.